"Structural biology of Schistosome:

Glutathione Peroxidase and Thioredoxin Glutathione Reductase

from a human parasite"

Docente guida   Coordinatore

Prof. Maurizio Brunori   Prof. Marco Tripodi

Dottoranda

Daniela Dimastrogiovanni

XXIII CICLO

ACKNOWLEDGEMENTS

CONTENTS

Contents

1. INTRODUCTION

1.1 Schistosomiasis: a water-born disease

Schistosomiasis, also known as "Bilharziasis" from the name of the German pharmacist Theodor Bilharz who described the illness in 1851, is a human parasitic disease still affecting more than 200 million people especially in tropical and subtropical countries [1]. The control programmes adopted in the last twenty years have changed to some extent the worldwide distribution of the disease, but Schistosomiasis still remains a real scourge in more than 74 endemic countries (Fig. 1, [2]). Asia, South-America and sub-saharian Africa count about 200,000 deaths per year, 85% of them belonging to the African continent [2, 3].

almost eliminated
ongoing large-scale control
limited or no control
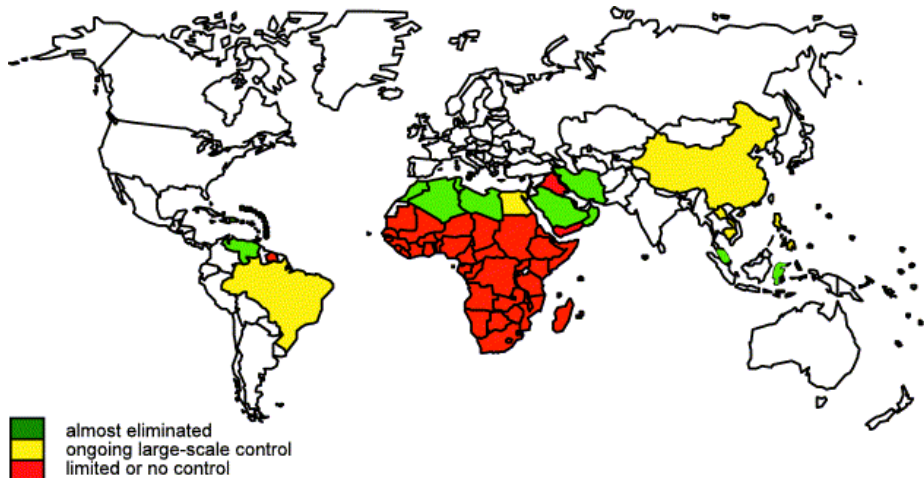
Fig. 1: Geographical distribution of Schistosomiasis (adapted from [2]).

A flatworm parasite of the genus Schistosoma (see section 1.2.1) is the causing agent of the disease (Fig. 2). The worm spends part of his life cycle in the freshwaters using a snail as intermediate host before being ready to infect humans.

Thus it is not surprising that the earliest infection from the parasite was detected in 1914 in Egypt in people working for the construction of the first great dam across the Blue Nile river. The project, the so-called "Gezira Scheme", was a real commercial success but the rapid growth of artificial water canals created soon an ideal habitat for the snails and provided the basis for the diffusion of Schistosomiasis. The infected people were treated with tartar-emetic but the spread of the disease was unavoidable. During the 20th century lots of projects resembling the "Gezira Scheme" caused the dramatic spread of the disease in the developing countries [4].

Fig. 2: A couple of paired worms (*Schistosoma mansoni*). The male is holding the female in the gynecophoral canal, a longitudinal groove down his body.

Nowadays Schistosomiasis is second only to malaria for prevalence and number of deaths. The reasons for the difficulty of eradication of Schistosomiasis are various but we can say that, besides the difficulties in finding an effective pharmacological solution and the extremely easy transmission of the parasite in endemic areas, poverty itself is certainly both a cause and a consequence of the disease spreading. The access to clean water is still rare in the poorest countries, this increases the probability for local people to be affected by Schistosomiasis and other water-born diseases. Moreover, being these infections often chronic and really

disabilitating, they augment undernutrition and reduce people productivity, with the final result of ever-increasing poverty [5].

1.2 Infection and progression of the disease

1.2.1 The parasite

As mentioned above human Schistosomiasis results from the infection by a bloodfluke worm, a platyhelminth of the genus Schistosoma. The adult parasites are white, approximately 1 cm long and 0.11 cm wide and, differently from the other trematode species, schistosomes have separate sexes. Females have a cylindrical body, they are longer and thinner than males and can be hosted in a groove, the gynaecophoric channel, present in the body of the male worm. Once paired the two partners live permanently coupled within the venous system of the human host, feeding themselves with erythrocytes. The localization of the adult schistosomes inside the human body depends on the infecting species. *Schistosoma mansoni* and *S. japonicum*, cause hepato-intestinal Schistosomiasis as they migrate into the mesenteric circulation once matured to the adult stage, while *S. haematobium* is responsible for the genito-urinary form of the disease, being localized in the venous system which surrounds the human bladder. Minor species with limited geographical distribution are *S. intercalatum* and *S. mekongi* (Fig. 3).

The parasites can remain in the human host for a period that varies from three to thirty years, and in the meantime the adult females are able to produce 100-300 eggs per day. Some of the eggs are able to reach the lumen of the intestine (*S. mansoni* and *S. japonicum*) or of the bladder (*S. haematobium*) and are then excreted through feces or urines (Fig. 4). Once in contact with the freshwater the eggs hatch releasing miracidia, which represent the first larval stage of the parasite. Each miracidium searches for its intermediate host, a snail of the genus *Biomphalaria* (for *S. mansoni*), *Bulinus* (for *S. haematobium*) or *Oncomelania* (for *S. japonicum*), and penetrates it. The snail is required by the parasite to proceed through a series of asexual reproductions. A single snail can release in the freshwater thousands of

swimming larvae, the cercariae, which finally recognize and penetrate the human skin using their bifurcated tails.
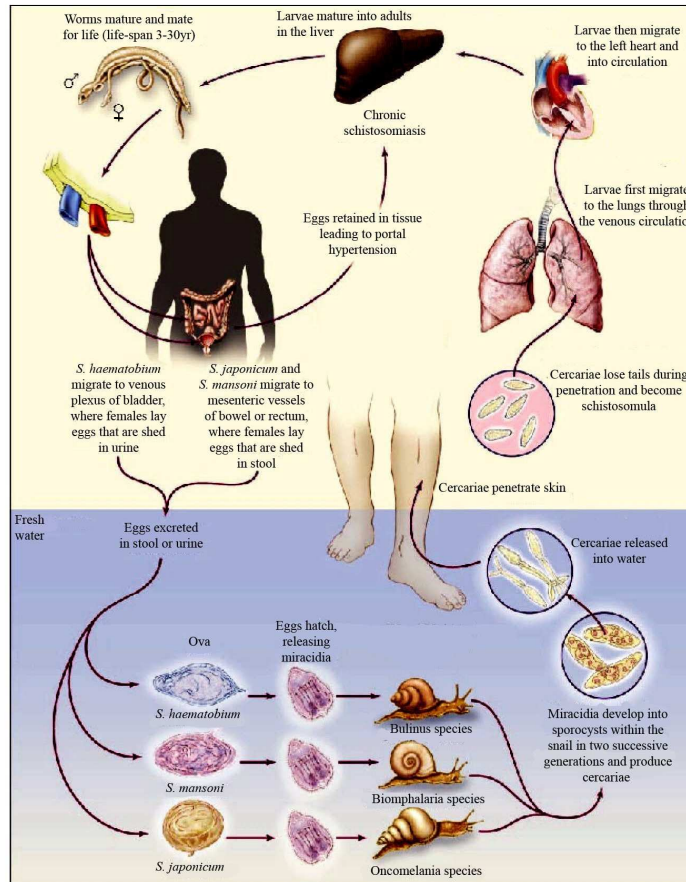
Fig. 3: The life cycle of the three most infective species of schistosoma (*S. mansoni, S. haematobium and S. japonicum*) [1].

Fig. 4: *S. mansoni* egg. The schistosome eggs have terminal or lateral spines trough which they can penetrate the host tissues.

The head of the cercaria transforms into an endoparasitic larva, the schistosomula, which lives for a few days under the skin before being ready to enter the lymphatic and venous circulation. The larvae migrate to the lungs and from here to the heart reaching finally the hepatoportal circulation, where schistosomulae develop into sexually mature worms within 4-6 weeks. Schistosome couples reach their definitive district in the human body according to the parasite species, females begin to produce eggs and the parasite life cycle starts again (Fig. 4).

1.2.2 Immunopathogenesis
A number of eggs produced during the schistosome permanence inside his definitive host are not released outside the human body, but are permanently entrapped in the host tissues. Thus it is not surprising that the main symptoms of chronic schistosomiasis develop at the sites of major accumulation of eggs, i.e. the intestine and the liver (*S. mansoni* and *S. japonicum*) or the genitourinary apparatus (*S. haematobium*). Many studies have been carried out in animal models of Schistosomiasis in order to clarify the involvement of the immunitary system in the pathogenesis of the disease. Independently from the parasite species and from the infected organism, it is now clear that the eggs' antigens induce a strong $CD4^+$ T-cell mediated response that directs a granulomatous reaction. The formation of granulomas proceeds from the early accumulation of macrophages, which take up the secreted eggs' antigens. These mononuclear cells both present the antigens on

their surface and secrete limphokines that attract different immune cells around the deposited egg: especially CD4$^+$ T-cells, B-cells, neutrophils and eosinophils. In the latest stages of the granuloma formation epitheloid cells and fibrocytes accumulate at the periphery of the lesion, finally becoming predominant over the other cell types. As the granuloma matures the egg is disintegrated and become calcified, while the fibrocytes mediate the massive deposition of collagen, which finally leads to fibrosis and to a progressive decay of functionality of the organs interested by the granulomatous reactions (Fig. 5).

A   **B**
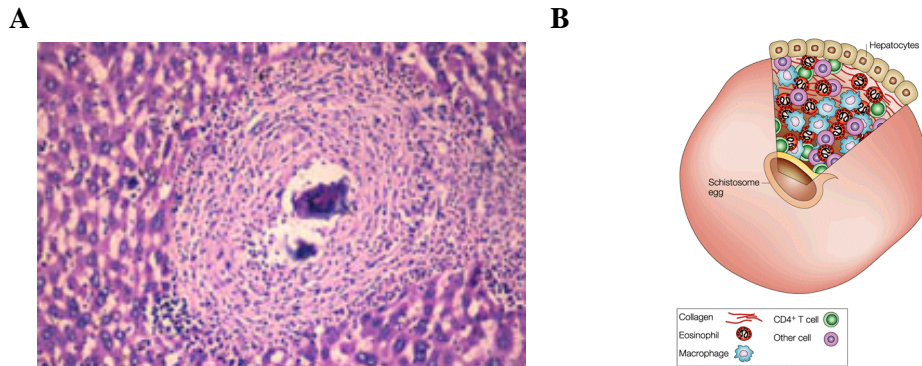
Fig. 5 Panel A: granuloma in the liver due to *Schistosoma mansoni*, the *S. mansoni* egg is at the center of the granuloma. **Panel B**: representation of an hepatic granuloma showing its cellular composition (adapted from [6]).

It is clear that the severity of the disease correlates better with the alteration/modulation of the host immune response, rather than with the parasite burden inside the host. Results obtained from the study of the murine form of the disease have demonstrated that a T helper-1 (Th1) mediated immune response dominates the earlier stages of the disease. When the parasite is sexually mature and starts to produce eggs the T helper-2 (Th2) response becomes dominant on the former. The Th2 prolonged action seems to be directly involved in the granuloma formation. Some cytokines released during this secondary response, among them IL-

4 and IL-13, have been demonstrated to have a fibrogenic role, as mice deprived of IL-13 do not develop fibrosis as a consequence of Schistosoma infection. These molecules should induce the expression of the enzyme arginase inside macrophage and should activate the biosynthetic pathway that leads to the synthesis of the aminoacid proline, an essential precursor for the production of collagen [6, 7]. Unfortunately the specific pattern of immune cells and chemical signals that are activated as a consequence of the Schistosoma infection in humans is not completely elucidated yet. However the progression of the infection is accompanied also in humans by a change from Th1 to Th2 mediated immune response, and IL-13 seems to be the main fibrogenic cytokine in humans too, while IL-4, IL-10 and INF-γ could play an important role in controlling morbidity [6, 8].

1.2.3 Clinical features

The clinical symptoms of Schistosomiasis are different depending either on the number of exposures of the patient to the parasite or on the particular infecting species. A distinction between acute and chronic disease may be easily drawn. Usually travellers, who are subjected to a single contact with the worm, present the typical manifestations of acute Schistosomiasis: cercarial dermatitis and katayama fever. The former is characterized by a pruritic rash which results from the IgE-mediated immune response to the cercaria penetration; the latter manifests 14-84 days after the infection and determines fever, headache, myalgia, cough, general malaise, sometimes accompanied by abdominal pain as a result of the migration of juvenile worms through the human body [6]. The chronic form of Schistosomiasis, involving mainly the endemic populations, is more dependent on the infecting species which localize, as above mentioned, in typical anatomic districts of the mammalian host. Abdominal pain, loss of appetite and rapid weight loss, diarrhoea, vomit, together with portal hypertension, splenomegaly, ascites, gastrointestinal bleeding and periportal fibrosis in the late stages are usually associated with the development of granulomatous lesions consequently to *S. mansoni* and *S. japonicum* migration to the hepatic and intestinal districts. Anaemia may accompany these

symptoms causing wasting in adults and growth retardation in children. The infection with *S. haematobium* instead involves the genitourinary apparatus and has as major symptoms renal colics, fibrosis and calcification of the bladder and ureters where the parasite eggs are accumulated, leading to a gradual renal failure. A series of co-infections sometimes may complicate the clinical prospect of patients affected by Schistosomiasis. It has been pointed out that hepatitis C (HCV) and B (HBV) viruses have a crucial role in increasing morbidity due to *S. mansoni* infection, as they accelerate progression of the disease towards liver fibrosis and cirrhosis. On the other hand it is not so uncommon that women affected by genitourinary Schistosomiasis are subjected to infertility if the parasite reaches the uterus, tubes or ovaries, and usually they have a higher tendency to the transmission of sexually transmitted infections such as HIV, because of the development of ulcerative lesions in the genital tract as a consequence of the egg deposition in this district. In addition to the above-described variants of Schistosomiasis, the lung district and the CNS may be also damaged by the parasite infection although with fewer incidence. Neuroschistosomiasis, mainly caused by *S. mansoni*, has not been extensively studied yet but preliminary evidences suggest a pathogenesis similar to the hepatic-intestinal and genitourinary form of the disease. Eggs trapped in the CNS tissues should evoke an immune response probably Th2-mediated, with the consequent development of granulomatous lesions and serious damaging of the host nervous tissues [6, 9].

1.3 Prevention and morbidity control

1.3.1 Prevention strategies

Schistosomiasis morbidity and mortality have been underestimated for years and the spreading of the disease has made urgent the finding out of effective and preventive control measures.

The water-based diffusion of Schistosomiasis suggested that a regular provision and use of safe water and an appropriate health education, together with specific environmental management programs aimed at reducing the contamination

of water resources, might represent a good strategy to promote hygiene and sanitation and eventually to reduce the morbidity in some areas. Even if these initiatives have had only limited success till now, it is indeed general opinion that, given the high rate of reinfection in endemic areas such interventions, aimed to break the parasite transmission routes, could be extremely useful though far from representing the final solution for Schistosomiasis [5, 10].

A vaccine applicable to humans could represent a key step towards the definitive eradication of the disease, but a vaccine production has proved to be rather tricky. The main reason for that can be found in the ability of schistosomes to survive for decades in the human bloodstream, evading the host immune defenses through different highly effective mechanisms: (i) they mask themselves through the absorption of some host serum proteins; (ii) they evade the immune attack by producing antigens with epitopes similar to those of the host; (iii) they modulate the human immune response in order to reduce the parasite-specific immunity and assure their life-maintenance into the host [11, 12].

In spite of the ability of the parasite to elude the human defenses, some experimental evidences demonstrate that the development of a successful vaccine is a realistic prospective: (i) the immunization of mice with irradiated cercariae conferred them 50-70% protection, and (ii) the repetitive exposition of people living in endemic areas to schistosome infection finally results in the natural development of a partial protection [13]. Based on these premises in the last decade various molecular candidates for the design of a vaccine against Schistosomiasis have been proposed; glutathione-S-transferase [14], paramyosin [15], triose phosphate isomerase [16], fatty acid binding protein (FABP, [17]), Sm23 ([18]), glyceraldehyde-3-phosphate dehydrogenase (GAPDH, [19]) are among them. Recent evidences suggest also that DNA-mediated vaccination with antioxidant enzyme, such as superoxide dismutase (SOD) confers a certain degree of protection against schistosome infection [20, 21]. According to the WHO directions, which established that an effective vaccine should induce at least 40% protection in mice infected, some of the discovered antigens, SOD among them, are ready to enter the

human clinical trial phase. However most of the current schistosome vaccine candidates do not confer more than 50% protection in animal models, thus further efforts are needed either to develop adjuvant molecules, which can enhance protection levels, or to find out new more effective parasite antigens [13].

1.3.2 Chemotherapeutic approaches and current therapy

Because of the unavailability of an effective human vaccine a huge amount of schistosomicidal compounds have been employed in the last century to counteract the spread of the disease [22]. The main compounds proposed as drugs against Schistosomiasis are listed in Fig. 6.

In the early 1900s the first schistosome contagions were treated with an antymonial salt, namely **tartar emetic** (or potassium antymonium tartrate). The drug unfortunately proved to be toxic, as the excretion of the metal from human tissues could take several weeks and in the meantime a number of serious side effects appeared. Several years later, **oltipraz** and **artemether** were proposed as valid chemotherapeutic alternatives. Oltipraz, a dithiole thione derivative, is no longer employed in the clinic of schistosome infections because of its serious dose-related side effects, such as paresthesiasis and loosening or detachment of fingernails [23].

Still rather promising antischistosomal drugs seem to be represented by **metrifonate**, **oxamniquine and artemether**. Metrifonate, an organophosphorous compound, was demonstrated to be an acetylcholinesterase inhibitor, with a strong activity against *S. haematobium* species. Today it is still one of the WHO recommended drugs for the treatment of urinary Schistosomiasis [22]. On the other hand the therapy of *S. mansoni* infections has been based for many years on the employment of oxamniquine, a tetrahydroquinoline derivative, which is easily administered orally to patients and has no relevant side effect. Much is known about its mechanism of action: the drug is activated by a schistosome sulphotransferase enzyme, the active metabolite is able to alkylate DNA, causing cellular damage and finally leading to the death of the worm [23, 24]. Artemether, an artemisinin derivative, is a very well tolerated compound, demonstrated to be active against the

juvenile stages of all three main species of schistosome infecting humans [25]. Artemisinins are at the moment widely used in the treatment of malaria, thus their employment as antischistosomal agents is forbidden especially in areas where the two parasitic diseases are co-endemic, in order to avoid the development of Plasmodium strains resistant to the drug.

Unfortunately the species- and stage-specificity of these drugs have limited till now their employment in the large scale treatment of Schistosomiasis, thus the current chemotherapy is mostly based on **praziquantel**, a drug discovered in the mid-1970s and administered to several millions people for more than 20 years (Fig. 6). Praziquantel is a pyrazino-isoquinoline derivative, commercially available as a very low cost drug, easily administered through a single oral dose. It is effective against all species of schistosomes infecting humans, though the juvenile stages are less susceptible then the adults to the drug, and lacks both short-term and long-term relevant side effects [23]. At the moment the drug is commercially available as a racemic mixture of L- and D-praziquantel, but only the L-optical isomer is active, and its mechanism of action is actually still puzzling. It is known that the administration of praziquantel causes the disruption of the worm tegument and enhances the muscular contraction, but it is neither clear if this last effect is mediated by an increase of the intracellular concentration of Ca^{2+}, involving the action of the drug on the parasite voltage-gated Ca^{2+} channels, nor if praziquantel induced tegumental damaging may lead to the exposure of the schistosome antigens, which finally elicit the host's immune responses against the parasite [22]. Recently a new study suggested that the drug might act as an inhibitor of nucleoside uptake by the parasite, a relevant effect since the schistosome is unable to synthesize purine nucleosides *de novo* [26]. Besides its uncertain molecular target praziquantel has been administered to several millions people, giving a large contribution to reduce the worm burden in endemic areas and to limit the disease spreading. However it must be pointed out that the massive use of this unique drug is resulting in the emergence of schistosome strains resistant or less susceptible to the drug [27], which makes urgent the search for valid therapeutic alternatives.

1.4 Main tracks of current bio-medical research

1.4.1 Discover new drug combinations

The use of a single drug in the treatment of Schistosomiasis, with the actual resulting problem of resistance, puts the current chemotherapy under danger and shows how pressing the need for more effective drugs is. In the last years interesting chemical compounds have emerged for their schistosomicidial effect (Fig. 6). In particular a high-throughput screening identified oxadiazole 2-oxides and phosphinic amides as the more effective compounds, for their ability to inhibit the activity of thioredoxin glutathione reductase (TGR), an enzyme essential for the parasite survival into the human host. The toxicity of these proposed antischistosomal drugs is not very different from that of praziquantel, and some of these compounds, **furoxan** among them, are able to reduce the worm burden in mice infected with the parasite by more than 80% [28]. Such values exceed the WHO criteria for the selection of drugs to employ in the treatment of the disease, thus the research work is still in progress to generate effective derivative compounds to be used in the clinic of human Schistosomiasis.
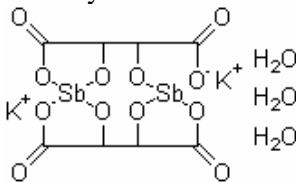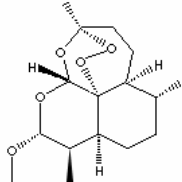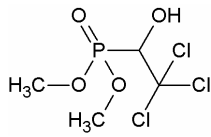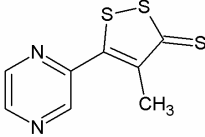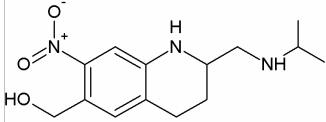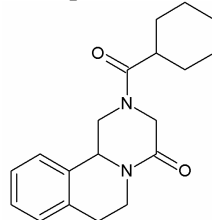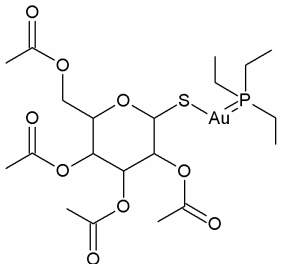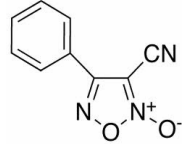
Potassium antimony(III) tartrate hydrate	Arthemeter	Metrifonate
Oltipraz	Oxamniquine	Praziquantel
Auranofin		Furoxan (4-phenil-3-furoxan carbonitrile)

Fig. 6: List of the main chemotherapeutic compounds employed in the treatment of human Schistosomiasis since the early 1900s and recently proposed schistosomicidial compounds.

An alternative approach to the finding out of new chemotherapeutic candidates relies in the attempt to employ old drugs already in clinical use for other human diseases. This is the case of **auranofin** ([AuI(PEt3)(thioglucose)]), a gold-containing compound used to cure rheumatoid arthritis for 25 years, and which has been recently demonstrated to be highly effective as schistosomicidial drug [29] (Fig. 6). Finding new uses of clinically established drugs, which have a well-known and quite safe toxicity profile, represents a clever strategy of drug discovery considering the drastic reduction in times and costs [30]. These considerations become of extreme importance especially when we are dealing with research on neglected diseases such as Schistosomiasis that have a limited financial market, being not attractive for the funding providing organizations.

1.4.2 Identify drug targets and vaccine candidates

In the last decade a series of schistosome proteins has been selected for their potential interest in the treatment of Schistosomiasis. Some of them, suggested either as potentially "druggable" proteins or as vaccine candidates, are grouped below:

• *Enzymes required in the different stages of schistosome infection*: (i) proteolytic enzymes, involved both in the early stages of cercarial penetration [31] and in the adult life of the parasites when, especially cysteine proteases, seem to be involved in the suppression of the human Th1-mediated response in order to assure the parasite survival into its host [32]; (ii) phenol oxidases (tyrosinase 1 and 2), copper-containing glycoenzymes, which play a key role in the eggshell formation and production [33]. Their inhibition is likely to be crucial for the prevention of the egg-induced inflammatory reactions, which open the road to the development of the chronic disease symptoms.

• *Factors crucial for the parasite life-maintenance*: (i) protein kinases, which are involved in intracellular signaling pathways in adult worms. One of them, cAMP-dependent protein kinase A (PKA) has recently proved to be essential for the parasite viability *in vitro* [34]; (ii) cyclophillins, enzymes with a

peptidyl prolyl isomerase activity, involved in protein folding and chaperoning mechanisms. Their interest as potential drug target has increased when recently a cyclophillin from *S. mansoni* has been demonstrated to be efficiently inhibited by cyclosporine [35], a compound with a proved antiparasitic effect [36]; (iii) voltage-gated calcium channels [37], whose modulation may determine an increase of the calcium influx into the worm with the resulting muscle contraction and paralysis, one of the proposed and discussed effects of praziquantel; (iv) enzymes required for the parasite redox homeostasis (discussed in detail in section 1.4.3).

• *Proteins localized at the host-parasite interface*: lots of surface-exposed tegumental proteins have been recently identified, among them transport proteins, heat shock proteins and tetraspanins. It is clear that, being the worm tegument directly involved in the mechanisms of evasion of the host immune response, its protein components could be extremely useful in the future design of a human vaccine [38].

1.4.3 The Schistosoma thiol-detoxification pathway: a promising target

Adult Schistosomes spend their entire life in the bloodstream of the human host, where they are constantly subjected to oxidative stress determined by the reactive oxygen species (ROS) that come both from their own aerobic metabolism and from the immune response of the host phagocytes to the parasite infection. Macrophages as well as neutrophil, eosinophil or basophil granulocytes, in fact, contain several enzymes which produce free radicals in order to fight the infectious agent [39, 40]. All aerobic organisms require protection against ROS; reactive species such as superoxide anion radicals ($O^{2-\cdot}$), hydrogen peroxide (H_2O_2), and hydroxide radicals ($OH^{\cdot}$), are able indeed to trigger radical reactions which may result in severe cellular damage through the oxidation of protein, lipids and nucleic acids.

Mammals possess two main systems devoted to the detoxification of these highly damaging compounds: the thioredoxin (Trx) and the glutathione (GSH)

systems (Fig. 7) [42]. Two redox cascades are headed by Thioredoxin Reductase (TR) and Glutathione Reductase (GR) enzymes respectively. TR and GR are homodimeric flavoenzymes, belonging to the family of pyridine nucleotide disulfide oxidoreductases, involved in various cellular processes crucial for cell function and proliferation, besides their key role in redox homeostasis and antioxidant defense [43]. Crystallographic evidences proved the high structural similarity between TR and GR. The two proteins share the main structural fold and the arrangement of the binding sites for NADPH and FAD. Indeed the main difference between TR and GR resides in the C-terminal segment of the polypeptidic chains, where the former protein presents a selenocysteine (Sec) residue located in a Gly-Cys-Sec-Gly tetrapeptide, essential for the full catalytic activity and absent in GR (Fig. 8) [43, 44]. Both enzymes are able to shuttle reducing equivalents from NADPH to peroxidated substrates, by means of a series of thiol-/selenol-mediated redox exchange reactions involving intermediate enzymatic and non-enzymatic partners (Fig. 7). Trx peroxidases (Tpx) in addition to Trxs are the other components of the Trx system, while the GSH system involves GSH Peroxidase (Gpx) and Glutaredoxin (Grx), an oxidoreductase acting on S-glutathionylated substrates [45, 46].

All species of Schistosoma (e.g. *japonicum*, *mansoni*, *haematobium*) have evolved an enzymatic mechanism quite different from their mammalian host in order to protect themselves by oxidative damage. It is based on a single multifunctional oxidoreductase, namely Thioredoxin Glutathione Reductase (TGR), which transfers reducing equivalents to both GSH and Trx systems (Fig. 7) [39]. A recent analysis of the platyhelminth genomes and transcriptomes has found out that, while free living Plathyhelminths (class Turbellaria) possess the three types of antioxidant enzymes (TR, GR and TGR), platyhelminth parasites (*Schistosoma*, *E. granulosus*, *T. solium*, *F. hepatica*) have lost the genes coding for TR and GR as a result of their adaptation to the endoparasitic life, and depend on the single TGR enzyme to control redox homeostasis [47]. The peculiarity of the parasite detoxification system, relying

on the unique TGR enzyme, explains why this pathway currently provides excellent enzymatic targets in the search for new antischistosomal drugs.

The main components of Schistosoma linked thioredoxin-glutathione detoxification system are represented in Fig. 7, though the correct positioning and relations betweens some of them inside the pathway have not been fully clarified yet. TGR is the hub enzyme, able to exploit the three enzymatic activities of thioredoxin reductase, glutathione reductase and glutaredoxin, through the unique fusion of a TR with a glutaredoxin (Grx) domain. It is because of its peculiarity that TGR has been recently proposed and partially validated as one of the most promising drug targets against Schistosomiasis [29, 48]. A more detailed description of Schistosoma TGR and a review of the recent concerning literature will be provided in section 1.6.

The intermediate thiol-exchange reactions, that precede the reduction and detoxification of peroxides, involve Trx and GSH as direct substrates of TGR. Schistosoma thioredoxin is a 12 KDa monomeric protein, containing a redox-active site with the conservative motif CXXC [49]. When this cysteine couple is recycled to its reduced state by TGR, Trx is able to provide reducing equivalents to its substrates, such as ribonucleotide reductase and thioredoxin peroxidase (TPx). On the other hand TGR can supply electrons to the oxidized tripeptide γ-L-Glutamyl-L-cysteinylglycine (GSSG), which once reduced may act as the substrate of other enzymes, e.g. Glutathione Peroxidase (Gpx), though it is still controversial if Gpx is maintained in its reduced state by GSH or by an enzymatic partner. The parasite Gpx is classified as a phospholipid hydroperoxide glutathione peroxidase enzyme, being able to reduce peroxides of phospholipids and cholesterol more efficiently than H_2O_2 and other organic peroxides [50, 51]. Its direct role in the protection of the parasite membranes from oxidation and its localization on the tegument of the worm make Gpx a potential target either for the development of drugs or for the design of vaccine against Schistosomiasis [20]. Further details about the parasite Gpx will be provided in section 1.5.

The detoxification pathway of the worm comprises also the parasite Peroxiredoxins (Prx), which have been recently proved to be the major family of antioxidant enzymes involved in the detoxification of H_2O_2 in Schistosomes. This result is compatible with the observation that parasites lack catalase, which usually works as H_2O_2-scavenger, and express high levels of superoxide dismutase (SOD), whose $O^{2-\cdot}$-detoxifying activity results in the release of hydrogen peroxide. Taking into account the fact that the parasite Gpx has a poor reactivity towards H_2O_2 if compared with lipid peroxides, it is clear that the role of Prx is crucial for the parasite survival. It has been demonstrated in *S. mansoni* the existence of at least three Prx enzymes, belonging to the class of 2-Cys Prxs: Prx1, Prx2, Prx3. The three proteins are highly effective in the reduction of H_2O_2 using reducing equivalents provided by Trx, but Prx2 and Prx3 seem to be more efficient in accepting electrons from the GSH system [52]. *In vitro* experiments of RNA interference, performed incubating schistosomulae with Prx1 double-stranded RNA, have proved that also this enzyme is essential for the parasite survival and can be thus classified among the promising target of antischistosomal therapy [53].

A
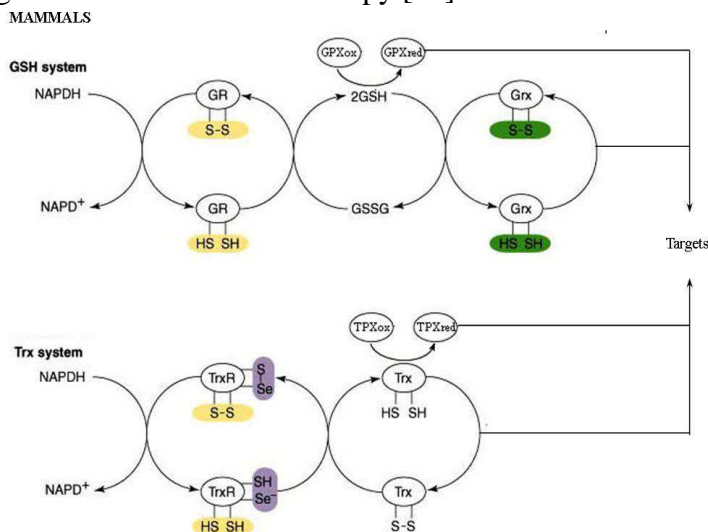
B
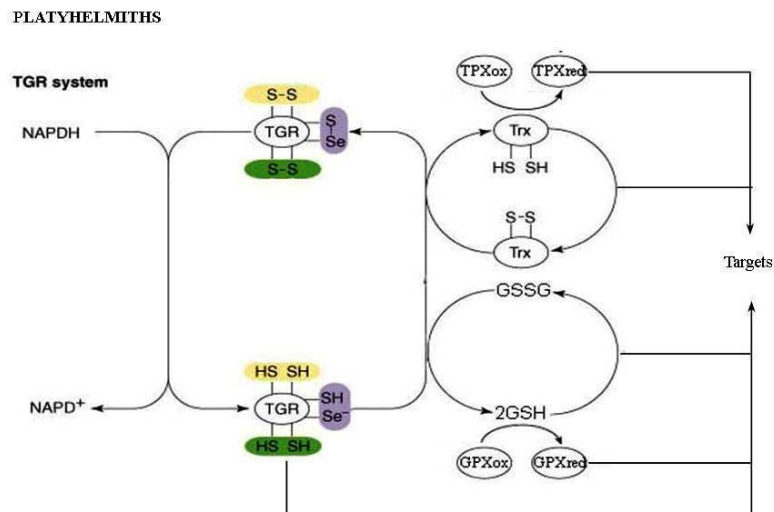
Fig. 7: Antioxidant detoxification pathways in mammals and platyhelminths (adapted from [41]). The electron flow in the Trx and GSH systems of mammals and TGR system of platyhelminths is shown. **Panel A**: In mammals, NADPH donates electrons to both TrxR and GR; TrxR shuttles electrons to Trx, which directly reduces TPX and various oxidized targets, such as ribonucleotide reductase. GR converts oxidized glutathione (GSSG) to its reduced form (GSH). GSH donates electrons to Gpx, Grx and other oxidized targets. Gpx and Grx are able to reduce peroxides and GSH-mixed disulphides respectively. **Panel B**: Platyhelminths have a single hub enzyme, TGR, which exploits the functions of either mammalian GR, TrxR and Grx. In both pathways the Grx redox site is shown in green, the FAD redox site in yellow, and the C-terminal tetrapeptide GCUG in violet.
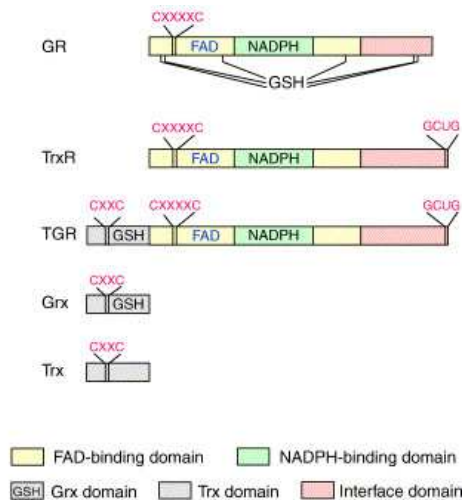
Fig. 8: Primary structure of TGR, TR, GR, GRX and TRX enzymes. The NADPH and FAD binding domains on TGR, TR, and GR is shown, with the close cysteine couple contained in a CXXXXC motif. The C-terminal GCUG tetrapeptide is present in TR and TGR but absent in GR. The CXXC motif containing the catalytic cysteine couple on the Grx domain of TGR is shown [39].

1.5 The Schistosoma Glutathione Peroxidase (Gpx)

1.5.1 The Gpx family: an overview

Glutathione peroxidase (Gpx) is the general name given to a family of antioxidant enzymes that catalyze the reduction of hydrogen peroxide and organic hydroperoxides to water or the corresponding alcohols, usually using reduced glutathione (GSH) as electron donor, according to the following reaction:

$$ROOH + 2GSH \rightarrow ROH + H_2O + GSSG$$

where ROOH is an organic or inorganic peroxide (including H_2O_2).

The variety of existing Gpx isozymes, showing various molecular organizations, cellular localizations and substrate specificities, reflected so far in the difficult efforts to give a definitive classification to the Gpx family [54]. In spite of this complexity, at the moment it is possible to identify at least six classes of enzymes: cytosolic or classical (Gpx1); gastrointestinal (Gpx2); plasma secreted Gpx (Gpx3); Gpxs with specificity for phospholipid hydroperoxides substrates (PhGpx or Gpx4); Gpxs localized in the epididymal (Gpx5) and olfactory epithelium (Gpx6) [54-56]. Recently a philogenetic analysis has proved Gpx4 to be the ancestor among Gpx isozymes. It seems likely that, by a first duplication event, the ancestral gene of Gpx4 lead to the formation of two groups of genes: the first coding for intracellular Gpx1 and Gpx2 isozymes, and the second coding for the secreted Gpx3, Gpx5 and Gpx6 [55].

All Gpx isozymes except Gpx5 and Gpx6 are selenium-containing proteins, having a selenocysteine residue (Sec) in their active site. The Sec residue, referred to as the 21st amino acid, is encoded by a UGA codon, which is otherwise usually recognized as a stop codon during protein synthesis. In the presence of a stem loop structure (SeCys element) in the transcribed mRNA, located either downstream the UGA codon or at the 3'-end of the gene in prokaryotes and eukaryotes respectively, accessory proteins may mediate the binding of the cellular Sec-tRNA to the UGA codon and the incorporation of the selenocysteine residue in the nascent peptide [57-59]. Both *in vivo* and *in vitro* experiments have demonstrated that the Sec residue,

when present in the active site of glutathione peroxidases, is strictly required for the full catalytic activity of the enzymes [60, 61].

A few crystallographic data on Gpxs from different classes have elucidated some aspects of their macromolecular assembly and clarified the nature of their catalytic sites. With the exception of Gpx4, the other isozymes appeared in the tetrameric form [62-64] and all of them share the same basic mechanism of action. In this respect a detailed computational study recently suggested a model for the catalytic mechanism of all selenium-containing enzymes belonging to the Gpx family. It is based on a ping-pong mechanism, where the reduction of peroxides by Gpx is coupled to the oxidation of the catalytically active form of the enzyme, represented by the selenolate anion (E-Se$^-$), to selenenic acid (E-SeOH). Then, in a second step two reducing equivalents, usually supplied by two glutathione molecules, should recycle the enzyme to its active form passing through a selenosulfide intermediate (E-Se-S-G) [65] (Fig. 9).
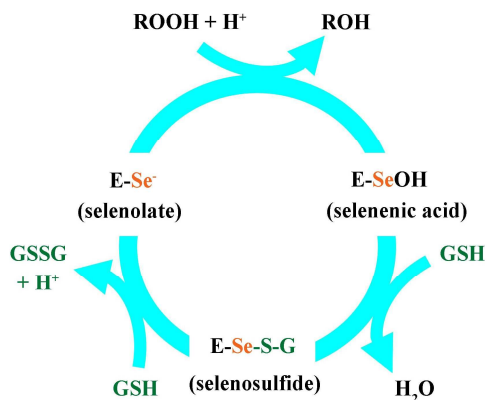
Fig. 9: Proposed mechanism for the catalytic cycle of glutathione peroxidase. The enzyme shuttles between the reduced form E-Se$^-$ (selenolate anion) and the oxidized one (selenenic acid). The peroxide reduction is accompanied by the oxidation of the selenolate to the selenenic acid. Then the oxidized enzyme is recycled back to the active reduced form reacting with two molecules of GSH and passing through an intermediate selenosulfide adduct (E-Se-SG).

The active site of Gpxs from all classes presents some highly conserved aminoacidic residues, which may explain the similar mechanism of action. Apart from the reactive Sec, a Gln and a Trp residues are also highly conserved, and recently it has been demonstrated that an additional Asn residue plays an essential role in the catalytic reaction [66].

1.5.2 The parasite Gpx and its interest for antischistosomal therapy

The first gene coding for a monomeric Sec containing Gpx (SmGpx-1) was cloned in *S. mansoni* more then ten years ago [67, 68], but a recent analysis of the parasite genome lead to the identification of an additional Gpx gene, encoding a 178 aminoacid protein (SmGpx-2). It shares with the previously discovered SmGpx-1 an in-frame UGA codon, coding for the active site Sec residue, and a SECIS element in the 3'-non-coding region of the corresponding mRNA, essential for the insertion of the Sec residue by the cellular translation apparatus [53]. Both SmGpx-1 and SmGpx-2 belong to the class-4 of Gpxs, as proved by the fact that the predicted aminoacid sequence of SmGpx-2 has 55% and 48% identity with SmGpx-1 and HsGpx-4, but less then 36% identity with other classes of human Gpxs. Indeed the main difference between the two Schistosoma enzymes seems to rely in their cellular localization. Slight modifications in the sequences of the two proteins, related both to aminoacidic substitutions in the C-terminal segment and to the presence of an additional N-terminal cleavable peptide in the sequence of SmGpx-2, could explain the different cellular targeting of SmGpx previously demonstrated by immunolocalization experiments [67, 69]. Thus, though extremely similar, SmGpx-1 could be directed mainly to the egg vitelline cells of female worms, while SmGpx-2 should be a secreted enzyme directed to the tegument and gut epithelium [53].

Apart from this still questionable difference in the cellular localization, a functional characterization of the Schistosoma Gpx has clarified that the enzyme has a great similarity with the human Gpx-4 (HsGpx-4), a 20 KDa monomeric enzyme highly reactive towards phospholipids and cholesterol hydroperoxides rather than towards inorganic peroxides, such as hydrogen and cumene hydroperoxides [50, 51].

Its substrate specificity and the evidence of an association of SmGpx with the tegument in adult worms [69], have proved the exclusive role of the Schistosoma enzyme in the protection of biological membranes from oxidative damage, making on the one side this enzyme a potential druggable target, and on the other hand a promising candidate for the design of a vaccine against Schistosomiasis, being localized at the host-parasite interface. In this respect preliminary vaccination of mice with DNA constructs coding for SmGpx resulted in a worm burden decrease of more than 40% if compared with a control group [20], but further efforts are still needed in order to localize SmGpx epitopes and/ or to find out specific chemotherapeutic drugs.

1.6 The Schistosoma Thioredoxin Glutathione Reductase (TGR)
1.6.1 Different roles of mammalian and parasite TGRs

As mentioned above, Thioredoxin Glutathione Reductase (TGR) is a flavoprotein belonging to the TR family of pyridine nucleotide oxidoreductases. Both mammalian and Schistosoma TGR are homodimeric enzymes, sharing the same domain organization but having a very different physiological role. The protein results from the fusion of different domains: a big pyridine-disulfide oxidoreductase domain, containing both binding sites for FAD and NADPH cofactors and a thiol-redox active couple; a small glutaredoxin domain at the N-terminal end; a dimerization domain in the C-terminal portion of the polypeptide chain, at the end of which is located the Gly-Cys-Sec-Gly terminal tetrapetide [70].

The mammalian TGR has a tissue-specific localization, being overexpressed only in testis after puberty, though low levels of the enzyme can be found also in other tissues. The main activity of TGR in mammals seems to be a disulfide isomerase/reductase: the enzyme catalyzes the isomerization of disulfide bonds in proteins, promoting the formation of structural components of sperm [70]. In parasites, on the contrary, TGR acts above all as antioxidant enzyme, exploiting a key role in redox homeostasis and parasite life-maintenance into the host. A few TGR isoforms have been identified in different human parasites, such as *T.*

crassiceps and *E. granulosus,* all sharing a similar domain organization if compared with the mammalian enzyme: a Grx domain fused with a TR domain, which can work either coupled or independently from each other. It has been proved in fact, for *E. granulosus,* that the Grx domain can accept reducing equivalents directly by the TR domain or by GSH, while the TR domain can shuttle electrons either internally to the Grx domain or externally to Trx [71, 72].

The first functional characterization of a TGR from *S. mansoni* (SmTGR) definitively demonstrated that the enzyme completely replaces TR and GR enzymes in the parasite, thus stating the peculiarity of the worm detoxification pathway relying on a unique multifunctional oxidoreductase and its divergence from the human counterpart [48]. The catalytic mechanism of SmTGR has not been fully elucidated yet, though a hypothesis already exists for the mouse TGR. The NADPH-dependent activities of the enzyme seem to be dependent on the penultimate Sec residue located at the C-terminal segment of the protein. It is clear in fact that the depletion of selenium from diet has a negative effect on the expression of TGR in mice and mutations in the C-terminal Sec residues cause a significant decrease in the catalytic efficiency of the enzyme [73]. A comparative modeling study on SmTGR has recently localized the putative binding sites of substrates and cofactors to the enzyme, suggesting a catalytic mechanism that implies some conformational transitions during the electron transfer which follows the binding of NADPH to the enzyme [74]. In this respect the crystallographic analysis of SmTGR, in both its unligated form and in complex with its physiological substrates, have provided a pattern of more specific information about the active sites of the enzyme and its catalytic mechanism, as will be discussed in detail in chapter 3 [75, 76].

1.6.2 Inhibitors of SmTGR as antischistosomal drugs

TGR is an essential enzyme for Schistosoma, as highlighted by its particular role in the redox homeostasis. There is evidence that its suppression or inhibition highly compromises the parasite survival. In fact RNA interference experiments, in which a dsRNA was added to schistosomula in vitro in order to silence TGR

expression, resulted in the death of 90% of the cultured worms within 4 days and a decrease by more than 60% of SmTGR activity after 3 days of treatment. The existence of a strict connection between the parasite survival and the catalytic activity of TGR enzyme was confirmed by further inhibition assays. Auranofin, a potent TGR inhibitor, besides being able to increase the effect of RNAi on worm viability, caused unpairing of female and male Schistosomes after 1h and up to 100% of worm mortality within 9h if added to a concentration of 10μM to cultured worms. It is necessary to point out that mammalian cells may tolerate up to 100μM of AF for 5 days, while worm death was obtained in 24h at a concentration of 5μM of AF. It was also demonstrated that, besides auranofin, SmTGR activity is strongly affected by oltipraz and antimonium potassium tartrate, two schistomicidial drugs used in the past to fight the infection, suggesting that the enzyme is the main target of these compounds [29].

Taken together these observations have contributed to raise the interest in TGR as a potential target of antischistosomal drugs and recently a quantitative high-throughput screening of ~71000 compounds was performed to isolate new lead compound with schistosomicidal activity. Among them phosphinic amides and oxadiazoles 2-oxides were demonstrated to be active against *S. mansoni* antioxidant pathway. The activity of several derivatives of these lead compounds were tested for their effect on Schistosoma TGR, on live cultured worms, and *in vivo* on mice infected with the parasite. The most active compound, which even surpassed the criteria stated by the WHO for potential lead compound for Schistosomiasis, was represented by 4-phenyl-1,2,5-oxadiazole-3-carbonitrile-2-oxide, able to inhibit both the TR and GR activity of TGR in the low nanomolar range. Moreover *S. mansoni* parasites cultured in the presence of 10 μM of the inhibitor resulted in 100% worm death after 24 h, while the administration of the compound by intraperitoneal injection to infected mice resulted in a substantial reduction both in worm burden and in hepato- and splenomegaly. Because of its protective effect, low cytotoxicity in mice, and high effect on the three major species of Schistosoma infecting humans

and on the different parasite life cycle stages, furoxan is at the moment considered a promising lead compound for the development of antischistosomal drugs [28, 77].

Besides the huge number of chemical compounds discovered for their schistosomicidal activity, for most of them further research is needed in order clarify their mechanism of action and to assess their possible safe employment in the treatment of human Schistosomiasis. A few steps towards a better understanding of the drug action have been made in the case of furoxan. It has been hypothesized that the release of NO by this compound plays a crucial role in its mechanism of action Furoxan acts as a NO donor in the presence of TGR, NO may react with the active thiols of the enzyme and thus the consequent inhibition could be the result of the covalent S-nitrosilation of the active site cysteines and/or selenocysteines. The release of NO by furoxan has been also directly related to the worm killing as the employment of NO scavengers decreased the activity of the drug [28]. More detailed information has been presented for auranofin, at the moment one of the most promising antischistosomal drugs. *In vitro* experiments demonstrated that different cultured parasites (*Taenia*, *Echinococcus* and *Schistosoma*) are killed by auranofin [29, 78], which has been suggested to be a selective inhibitor of Sec-containing oxidoreductases. Indeed the gold-compound has a strong effect on TR and TGR activities if used at stoichiometric amounts, whereas 1000-fold higher concentrations are required to inhibit GR, which lacks the C-terminal Sec residue, over the same time regime of TR [79]. These observations suggested that Sec is crucial for the inhibition of reductases by AF, as it has been recently proved by our recent structural and kinetic analyses. The C-terminal Sec residue of TGR should facilitate the undressing of gold from its ligands in AF (the thioglucose and the triethylphosphine) given its higher nucleophilic power than sulphur. The gold atom (Au^{+1}) binds at first to the final Sec-Cys redox center of the enzyme and then it is transferred to the other couples of reactive cysteines leading to formation of gold-protein thiols adducts, which finally inhibit the catalytic activities of the enzyme [80].

2. AIM OF THE WORK

Targeting the Schistosoma antioxidant detoxification pathway is among the topics of current researches for new antischistosomal therapies. This pathway is responsible for the detoxification of reactive oxygen species produced by the host in response to the parasite invasion, and it is thus essential for the survival of Schistosomes into the human host. This work is aimed to characterize two enzymatic components of the worm detoxification pathway, i.e.: Glutathione Peroxidase (SmGpx) and Thioredoxin Glutathione Reductase (SmTGR).

Glutathione peroxidases (Gpx) are a family of sulfur or selenium-dependent isozymes sharing the ability to reduce peroxides using the reducing equivalents provided by glutathione or possibly by small proteins such as thioredoxin. SmGpx is one of the frontline antioxidant defenses of the parasite, being localized in the worm tegument, the outermost defense layer. A few structures of oligomeric Gpxs already exist from different organism but less is known about the class 4 monomeric Gpxs, whom the Schistosoma enzyme belongs to. In this work the first crystal structure of two recombinant SmGpxs, carrying the active site mutations U43C and U43S respectively, will be presented. The geometry of the active site of the U43C SmGpx and the organization of residues surrounding the catalytic cysteine will be explored, based on the details provided by an atomic resolution crystal structure of the U43C mutant. Moreover a comparison with the human Gpx4 (HsGpx4) recently characterized will allow to investigate the peculiar reactivity of the parasite enzyme, whose active site Cys undergoes spontaneous oxidation to sulfonic acid, not reported for the same Sec/Cys mutant of HsGpx4. To test whether the oxidation of Cys43 to the bulkier sulphonic acid altered the structure of SmGpx, the structure of the U43S mutant will be solved as well. Indeed the U43S mutant of SmGpx maintains the same 3D structure of the U43C mutant, thus strongly suggesting that the oxidation of Cys43 does not perturb significantly the native structure of the enzyme. Given the absence of any structure of Gpx in its ligated form, a combined analysis of the static and dynamic clefts close to the catalytic C43 in the U43C mutant will be performed,

by mean of the CASTp algorithm and the molecular dynamic simulations, respectively. The functional relevance of the identified clefts and the conformational changes relevant to catalysis will be discussed in order to give some hints about the putative binding site for glutathione and phospholipid hydroperoxides, the substrate of choice for SmGpx, being the enzyme membrane-associated and involved in the detoxification of lipid peroxides more than H_2O_2 and inorganic peroxides.

Thioredoxin glutathione reductase (SmTGR) is a key flavoenzyme expressed by Schistosomes and derived from the peculiar fusion of a glutaredoxin domain with a thioredoxin selenocysteine (Sec)-containing reductase domain. It basically links two detoxification pathways (the glutathione and the thioredoxin pathways), both essential for the protection of the worm from oxidative stress. The silencing of the gene coding for SmTGR has been demonstrated to seriously compromise the parasite life-maintenance inside the mammalian host, hence this enzyme has become one of the most appealing drug targets against Schistosomiasis. A characterization of SmTGR by mean of X-ray crystallography will be here presented highlighting the structural basis for the multienzymatic function of this enzyme, which is able to exploit either thioredoxin reductase, glutathione reductase and glutaredoxin-like activities, thus fully replacing TR, GR and Grx mammalian enzymes. Two mutants have been employed in this work, the former lacking the two last residues (U597 and G598), belonging to the C-terminal G-C-U-G tetrapeptide, and the latter carrying the U597C mutation in the C-terminal segment. The C-terminus of SmTGR, as already pointed out for TR enzymes from different organisms, has a key role in the catalytic activity of the enzyme, thus the comparison between the functional properties of the two recombinant enzymes will give some hints in this respect. It is already known that, similarly to mammalian TR, SmTGR is able to accept reducing equivalents from NADPH, and electrons then will flow through the enzyme and will reach either the GSH reducing site, the glutaredoxin domain or the SmTrx reducing site. The U597 mutant has been crystallized in different redox states (i.e.: the oxidized form; the NADPH- and GSH-bound forms; and a species showing the entire and ordered C-terminus of one subunit fully reduced) in order to obtain insights into the

structural changes associated with the progression of the enzyme through the catalytic cycle. These structural observations combined with two models showing SmTGR in the act of transferring electrons to SmTrx and to the Grx domain, will assign a critical role to the C-terminus of the protein, which mediates the interdomain communication in SmTGR and seems to act as a flexible arm able to switch between different positions while transferring electrons either to the Grx domain of SmTGR or to the external SmTrx substrate. The possible function of this peculiar parasitic enzyme, which is absent in the free-living non-pathogenic species of the same platyhelminth phylum, will be finally discussed.

3. MATERIALS AND METHODS

I part: Glutathione peroxidase from *S. mansoni* (SmGpx)

3.1 Mutagenesis

The U43C SmGpx gene, with codons optimized for *E. coli* expression (GeneArt AG, Germany), was cloned between BamHI and XhoI restriction sites of a pGex4T-1 expression vector (GE Healthcare) to obtain a GST-fusion protein. In order to obtain the second recombinant mutated protein U43S, a mutagenesis experiment was carried out using the QuickChange Site-Directed Mutagenesis Kit (Stratagene). The U43C SmGpx expression vector was used as template and the following oligonucleotides containing the mutated serine codon AGC were synthesized (Primm srl, MI-Italy) and used as primers:

For: 5'-CGTGGCGTGCAAAAGCGGCGCGACCG-3'
Rev: 5'-GCACCGCACGTTTTCGCCGCGCTGGC-3'

3.2 Protein expression

The plasmids containing the genes coding for both the GST-fused U43C and U43S mutant of SmGpx were used to transform *Escherichia coli* BL21(DE3) cells (Novagen), which were then plated onto LB/Agar plates containing 100μg/ml ampicillin (Amp). One colony was used to inoculate 5ml LB/Amp, grown overnight at 37 ℃ with shaking. This culture was used to further inoculate 1lt LB/Amp, which was incubated at 37 ℃ with shaking until an optical density of 0.5 Abs at 600 nm was reached. The expression of the soluble protein was obtained after the addition of 0.5 mM IPTG and overnight incubation at 25 ℃ with shaking.

3.3 Protein purification

Two methods were used for the purification of recombinant U43C SmGpx, so after centrifugation the cells were divided into two stocks. Lysis buffer composed of 20mM Tris/HCl, 0.2M NaCl, 5mM TCEP, 0.1% TrytonX-100, DNase, 1mM PMSF,

1mM EDTA, pH 7.4 was added to one of the two samples before sonication. U43C SmGpx was purified from the soluble fraction through affinity chromatography using a GSH-Sepharose column (GE-Healthcare), and GST was cleaved with bovine thrombin (Sigma). The second protein sample was purified by ionic exchange chromatography. The purification was performed adding 10mM GSH to the lysis buffer to assure the maintenance of a reduced environment both during cell lysis and protein purification. To purify the protein, after sonication, the soluble fraction was applied on a HiTrap SP FF column (GE-Healthcare) equilibrated with the starting buffer 20mM Tris/HCl, 20mM NaCl, 5mM TCEP, 5mM GSH, 1mM EDTA, pH 7.4. U43C protein was eluted by continuous salt gradient using a second buffer with a higher ionic strength (100mM Tris/HCl, 0.5M NaCl, 5mM TCEP, 5mM GSH, 1mM EDTA, pH 7.4). The eluted protein was then cleaved with bovine thrombin. Recombinant U43S protein was purified through GST-affinity chromatography, as described previously for U43C SmGpx. For each purification the purity of the protein was assessed through overloaded SDS-PAGE, showing a single band corresponding to 19.4 KDa. The purified protein was then dialyzed in 20mM Tris/HCl, 0.1M NaCl, 1mM DTT, 0.5mM EDTA, pH 7.4, concentrated by ultrafiltration (Amicon) and stored at -20°C.

3.4 Size exclusion chromatography

U43C SmGpx assembly was assayed by gel filtration in HPLC with a Superdex75^{TM} column (GE Healthcare). The protein was concentrated up to 5mg/ml and a sample volume of 100µl was applied to the column, which was run at 0.4 ml/min flow. The following buffer was used 20mM Tris/HCl, 0.1M NaCl, 1mM DTT, 0.5mM EDTA, pH 7.4.

3.5 Enzymatic assays

The activity of U43C and U43S SmGpx was assayed in a coupled reaction with yeast glutathione reductase (GR; Sigma), measuring the decrease of A_{340} as a

consequence of the reduction of the hydroperoxide by U43C protein. The assay mixture, composed of 1µM U43C SmGpx, 0.2mM NADPH, 3mM GSH, 1 unit of GR, in 20mM Tris/HCl, 0.1M NaCl, pH 7.4, was incubated for 5 minutes at 25 °C. The reaction started with the addition of 100µM *tert*-butyl-hydroperoxide or hydrogen peroxide.

3.6 Protein crystallization
3.6.1 Basic procedure

Vapor diffusion is the most frequently used technique for protein crystallization and basically consists in allowing a slow and controlled precipitation of the protein in order to obtain ordered crystals instead of amorphous precipitate. An equal volume of protein solution and crystallization solution (reservoir), containing the appropriate precipitant at a concentration just below that necessary to precipitate the protein, are mixed to form a drop (Fig. 10). The drop containing the protein/reservoir mix is allowed to equilibrate in a closed container with a large volume of reservoir solution (Fig. 10). Being the [precipitant] in the drop equal to 50% of the [precipitant] in the reservoir solution vapor diffusion (evaporation and condensation) results in the net transfer of water molecules from the drop to the reservoir, until the equilibrium is reached. At this point both the [protein] and the [precipitant] in the drop have increased and the first nuclei of crystallizations form in the drop (nucleation region in Fig. 11). In a perfect system as the crystal grow the [protein] gradually decreases and the conditions move towards those of the "growth" region (growth region in Fig. 11) allowing the formation of a big crystal.

Vapor diffusion can be obtained through two different methods depending on the position of the protein/precipitant drop with respect to the reservoir solution: the hanging drop and the sitting drop. In hanging drop, the drop is suspended on a cover slip over a sealed reservoir, containing the crystallization solution; in sitting drop, the drop is held in a microbridge in the centre of the reservoir (Fig. 10). In both cases vapor diffusion occurs between the drop and the reservoir solution until an equilibrium is reached, during which one hopes to bring the protein to

supersaturation and hence crystallization conditions (Fig. 11). Protein purity, [protein] and [precipitant], as well as pH of the protein/reservoir solution and temperature are among the variables that determine the success of a crystallization experiment.
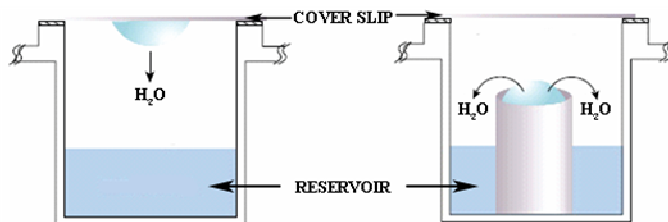
Fig. 10: Vapor diffusion by: (a) hanging drop and; (b) sitting drop crystallization. The reservoir contains the crystallization buffer and the precipitant; the drop hanging from the cover slip or sitting on the microbridge contains the protein/reservoir solution.
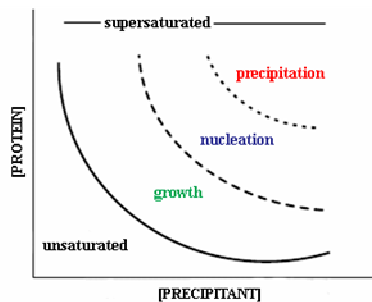
Fig. 11: Phase diagram for crystallization mediated by a precipitant. In the undersaturated zone the solution is not saturated with the protein so neither nucleation nor growth may occur. Inside the supersaturated zone the regions in which the [protein] and [precipitant] are optimal for nucleation and growth of protein crystals are shown. Conditions inside the precipitation zone lead to the formation of amorphous precipitate rather than ordered protein crystals.

3.6.2 Crystallization of U43C and U43S SmGpx

Crystals of SmGpx were grown by vapor diffusion according to sitting drop methods. A solution of 15 mg/ml U43C or U43S SmGpx was used to screen the crystallization conditions by mean of an automated robotic system (Phenix, Art Robbins). Refinement of the crystallization conditions was done by hand in sitting drop vapor diffusion 24-well plates, with symmetric drops of 1 µl each of protein solution and reservoir After 4 days crystals of U43C mutant were obtained in the drops with the following well solution: 0.2M LiSO$_4$, 0.2M Na Acetate, 24% PEG 8000, pH 4.5. A longer time of 7 days was required to obtain good crystals of U43S SmGpx using a well solution of 0.2M NaH$_2$PO$_4$, 0.1M MES, 32% PEG-MME 5000, pH 6.0.

3.7 Data collection, processing and refinement

X-ray data collection was performed at the synchrotron beamline ID29 at ESRF (Grenoble, France) with an ADSC Q315R detector for U43C SmGpx, while data collections of U43S crystals were performed at the synchrotron beamline ID14.2 at BESSY (Berlin, Germany) with a MARCCD detector. All data were indexed with Mosflm and processed with programs of the CCP4 Suite [81]. U43C mutant crystallized in a $P2_12_12_1$ space group with cell dimension of a= 41.40 Å, b=60.62 Å, c=62.54 Å, $\alpha=\beta=\gamma=90°$, and 1 molecule in the asymmetric unit.

The structure was solved by molecular replacement using human HsGpx4 as model (PDB code: 2OBI, [63]). U43S mutant showed the same space group but slightly different cell dimensions of a=39.91 Å, b=51.17 Å, c=90.62 Å, $\alpha=\beta=\gamma=90°$. In this case the structure of U43C SmGpx was used as model for the molecular replacement. Molrep and Refmac programs were used respectively for the molecular replacement and the successive refinements [81]; the structures were built using COOT [82]. Figures were produced with CCP4mg [83]. The quality of the models was assessed with MolProbity [84] and ProCheck [85]. Data collection and refinement statistics are summarized in tab. 1. The structures were deposited at

RCSB Protein Data Bank (U43C SmGpx PDBcode: 2v1m; U43S SmGpx PDBcode: 2wgr).

3.8 Sequence alignment

The ClustalW2 [86] server was used to obtain a multiple alignment between SmGpx1-2, HsGpx1-4 and BtGpx1 sequences, extracted from NCBI protein sequence database. The alignment files obtained with ClustalW have been visualized with ESPript [87].

3.9 Surface analysis

In order to look for static cleft and/or cavities to detect GSH and phospholipids binding sites the deposited coordinates were analyzed with the online program CASTp (http://sts-fw.bioengr.uic.edu/castp/index.php), using the server default value of 1.4 Å as probe radius.

3.11 Docking

Molecular docking was performed using the PatchDock algorithm [91]. Two files of coordinates, for SmGpx (2v1m) and for the phosphatidylcholine (CPL), enriched with hydrogen atoms, were used as input for the program. After setting the RMSD to 9, PatchDock output was a list of potential protein-ligand complexes, among which we choose the solution with the highest geometric shape complementarity score.

3.10 Molecular Dynamic (MD) simulations

The MD simulations, included in this thesis for sake of completeness, have been performed by Dr M. Anselmi and Prof. A. Di Nola of the Dep. of Chemistry of the University of Rome "Sapienza".

The starting coordinates employed for the simulations were taken from the x-ray structure at 1.0 Å resolution of the U43C mutant of *S. mansoni* Gpx, replacing the sulfonic SO_3^- group with the Se^- or SeOH group. Thus the selenocysteine (Sec)

in reduced wild type Gpx was modeled as deprotonated, while selenenic derivative (SeOH) in oxidized Gpx was considered as protonated. In order to determine the partial charges of Sec and its selenenic derivative (SeOH) we performed the quantum chemical calculations on the isolated ethyl selenolate ($CH_3CH_2Se^-$) and methyl selenenic acid (CH_3SeOH), respectively. Density functional calculations, Becke's three parameters exchange [92], and Lee, Yang, Parr correlation (B3LYP) [93] were performed using the Ahlrichs VTZ basis set [94]. All quantum chemical calculations were carried out using the Gamess US package [95]. Partial charges were obtained from the CHELPG algorithm [96]. The same calculations were performed on analogues, as ethanol or ethanthiol, in order to test the reliability of the procedure, obtaining partial charges in agreement with the force field used. The following set of partial charges were chosen: for selenolate group of Sec, -0.85 e for the Se atom and -0.15 e for the C_β atom, while for selenenic group of the Sec derivative, 0.2 e for the Se atom, -0.65 e for the O atom and 0.45 e for the H atom. Non-bonded parameters for selenium were set to $\sigma = 0.458$ nm and $\varepsilon = 1.154$ kJ/mol [97]. The force constants of bonded interactions for selenium were taken to be identical to those for sulfur while the equilibrium values were changed. In particular we set the C-Se bond to 1.95 Å, the Se-O bond to 1.82 Å, the C-C-Se angle to 108°, the C-Se-O angle to 97° and Se-O-H angle to 116°.

Each protein was solvated in a box with explicit SPC water molecules [98]. Three Cl^- for Gpx(Se$^-$) and four Cl^- for Gpx(SeOH) were added, in order to provide a neutral simulation box. For all systems, the solvent was relaxed by energy minimization followed by 50 ps of MD at 293 K, while restraining protein atomic positions. The systems were then minimized without restraints and their temperature brought to 293 K in a step-wise manner, before starting the production runs of 30 ns. MD simulations were performed with the Gromacs software package [99] using GROMOS96 force field [100]. Simulations were carried out at constant temperature of 293 K. The Lincs algorithm [101] to constrain bond lengths and the rototranslational constraint algorithm [102] were used. The temperature was held constant by the isothermal algorithm [103]. The Particle Mesh Ewald (PME) method

[104] was used for the calculation of the long-range interactions. A time step of 2 fs was used. We used the essential dynamics technique [102] to characterize the dynamical behaviour of the protein. The package SURFNET [105] was used for detecting the clefts on the protein surfaces and estimating their volumes. Cavity volumes were evaluated without taking into account the presence of water molecules.

II part: Thioredoxin Glutathione Reductase from *S. mansoni* (SmTGR)

3.12 Mutagenesis

The gene for the full-lenght SmTGR with the mutation U597C (U597C SmTGR), was obtained starting from the gene of truncated SmTGR (SmTGRtr) lacking the last two amino acids Sec597-Gly598 optimized for *E. coli* expression (GeneArt AG), with appropriate DNA primers.

For: 5'-GATCGGATCCCCGATGCCGCCGGCAGATGGC-3'
Rev: 5'-ACTCGCCGACGACGCCGATTATTGAGCTCGCC-3'

Both genes were cloned in a pGEX4T-1 commercial vector (GEHealthcare) between BamHI and XhoI restriction sites.

3.13 Protein expression and purification

Both the SmTGRtr and the U597C SmTGR mutant were expressed in BL21(DE3) *E. coli* cells (Novagen). The best results, in terms of solubility and protein yield, were obtained upon induction at 22°C with 1 mM IPTG in the presence of 1 mM FAD for SmTGRtr, while the soluble full-length SmTGR was obtained at 20°C overnight with 50μM FAD, without IPTG induction. In both cases successful expression was confirmed by SDS-PAGE, highlighting a band at about 90 kDa. The protein was purified by standard affinity chromatography; the GST tag was cleaved by thrombin (Sigma) and removed according to manufacturer's instructions. Protein purity was >98% as assessed by SDS-PAGE, and concentration

was determined from the FAD absorption peak ($\varepsilon 463 = 11.3$ mM^{-1} cm^{-1}). Both proteins were dialyzed in 20 mM Tris-HCl pH 7.4, 50 mM NaCl, 100μM FAD (to saturate the enzyme), concentrated up to 10 mg/mL using an Amicon Ultra centrifuge filter device (Millipore) and stored at -80°C.

3.14 Protein crystallization
3.14.1 Truncated SmTGR

Crystallization conditions were initially screened by Phoenix nanolitre dispensing robot (ArtRobbins, USA) and then refined according to standard hanging drop methods. Crystals of SmTGR grew over 2 days in a drop composed of 1 lL protein (15 mg/mL) and 1 lL well solution (22% (w/v) PEG 3350, 0.1M Hepes pH 7.2, 0.2M NaNO3, 5 mM DTT, or b2ME).

3.14.2 Oxidized U597C SmTGR (Structure 1)

A crystal of U597C SmTGR, grown in Hepes 0.1M pH7.4, 20% PEG 3350, KI 0.2M and β-mercaptoethanol 5mM, was picked up and incubated in the same well solution with 2μM CuSO4 and without β-mercaptoethanol. After 48h, the crystal was frozen under liquid nitrogen, after adding 30% PEG 200 as cryoprotectant.

3.14.3 U597C SmTGR-NADPH complex (Structure 2)

120μM of purified U597C SmTGR in 20 mM Tris, pH 7.4, 100 mM NaCl was initially incubated for 24 hours with 300μM plumbagin (SIGMA), 400μM NADPH, in anaerobiosis condition. The mixture was then concentrated to 10mg/mL before crystallization trials set up. The protein solution was mixed with an equal amount of the reservoir solution containing 0.1 M Hepes at pH 7.0, 20% PEG 3350, 0.2M KSCN, and 5 mM GSH. Crystal grew in 1 month in standard sitting drop method and were cryoprotected with the same reservoir solution adding 30% PEG 200.

3.14.4 U597C SmTGR with reduced C-terminal end (Structure 3)

Crystallization conditions were initially screened by the Phoenix nanoliter dispensing robot (ArtRobbins) and then manually refined. Crystallization was achieved at 293 K by the sitting drop vapor diffusion technique. 10 mg/mL protein sample were equilibrated in 1mM NADPH in 20 mM Tris-HCl, 100mM NaCl pH7.4. Drops of 2μL were mixed with an equal amount of the reservoir solution containing 0.2M Mg-formiate, 20% PEG 6000, 0.1M Hepes at pH 7.0-7.5 plus 5mM β-mercaptoethanol. Crystals grew in 1-2 weeks and were cryoprotected with the same reservoir solution adding 30% PEG 200.

3.14.4 U597C SmTGR-GSH complex (Structure 4)

Crystals were grown by sitting drop vapor diffusion. Crystals grew in conditions similar to those of oxidized U597C SmTGR (See above). 5mM GSH replaced β- mercaptoethanol. Crystals grew in 1 week and were cryoprotected with the same reservoir solution containing 30% PEG 200.

3.15 Data Collection, Processing and Refinement
3.15.1 Structure 1, Structure 2 and Structure 4

The best data sets for the oxidized and for the NADPH-bound form and for the of SmTGR(U597C) have been collected at BESSY (Berlin, German) at 100K at 1.9 and 2.3Å resolution, respectively; while for the GSH-bound form the best dataset was collected at ESRF at 1.9Å resolution. Data analysis was performed with HKL2000 suite [106] indicating that all crystals belonged to the C2 space group. Difference Fourier method was used to solve all structures and refinements were performed using REFMAC5 [81]. When present, NADPH and GSH were excluded from the first rounds of refinement and added only after convergence of R and R_{free} factors. COOT [82] was used to build all the models of protein and ligands. The quality of the model was assessed with ProCheck [85]. Data collection and refinement statistics are summarized in tab. 4. The structures were deposited at

RCSB protein data bank (PDB codes: 2X8G for the oxidized form; 2X99 for the NADPH complex; and 2X8H for the GSH complex).

3.15.2 Structure 3

Diffraction data were collected at 3.1Å resolution at Bessy (Berlin, Germany) and analyzed using the HKL2000 suite [106]. The 3D structure was solved by molecular replacement [81] using as a search model one protomer of truncated SmTGR structure (PDB code: 2v6o) [75]. The structure was refined using REFMAC5 and fit to the generated electron density maps using Coot [82]. Refinement was performed until a final R/R_{free} of 22.0% and 29.3% respectively was reached. The final model showed one dimer in the asymmetric unit with a FAD molecule bound to each subunit. The quality of the model was assessed with ProCheck [85]. The statistics of crystallographic data collection and model refinement are shown in tab. 4. The structure was deposited at RCSB protein data bank (PDB code: 2X8C).

3.16 Modeling
3.16.1 Model 1: the C-terminus of U597C SmTGR onto the Grx domain

The C-terminal residues, C597 and G598, visible in *Structure 3*, were superimposed to the Cys and Gly residues of the GSH bound to the Grx domain in the GSH-bound form of the SmTGR (*Structure 4*). The model was obtained mainly by rotation of the C-terminal arm at the level of K586 psi angle. Small adjustments of the main chain were performed in order to obtain the best superposition of the last two residues of the protein with the analogue residues of the bound GSH, avoiding clashes between amino acid side chains. Idealization of the model (Refmac5, [81]) was done at the end to ensure the absence of unfavourable contacts between atoms. The model, after optimization, was evaluated with PROCHECK [85].

3.16.2 Model 2: the SmTGR-SmTrx complex

A model of a plausible complex between the structure of SmTrx (pdb code: 2XBI) and *Structure 3* of U597C SmTGR (pdb code: 2X8C) was obtained using a rigid body method with shape complementarity. The structures were used as input for the SUMMA server [107]. The server has calculated the best complementary surface and was told to freely perform energy minimization only on SmTGR C-terminal arm (residues 509-598) and on the active site stretch of SmTrx (residues 33-38). Idealization of the model was automatically performed at the end to ensure the absence of unfavourable contacts between atoms. A S-S bond was built between SmTrx C34 and SmTGR C596 with rotamers compatible with the reduced SmTrx protein.

3.17 Kinetic measurements

3.17.1 TR activity

Both the 5,5'-dithio-bis (2-nitrobenzoic acid) (DTNB) reduction assay and the insulin reduction assay were performed. For the DTNB assay [108] SmTGR (0.5 μM) was added to a mixture of 100 mM potassium phosphate pH 7.0, 10 mM EDTA, 0.2-5 mM DTNB and 300 μM NADPH at 25°C. The increase in absorbance at 412 nm was monitored (ε_{412}= 13.6 mM^{-1}cm^{-1}). For the insulin assay the absorbance at 650 nm was measured after addition of U597C SmTGR (0.5 – 2.5 μM) to a reaction mixture composed by 50 mM K-phosphate pH 7.0, 200 μM NADPH, 1 mg/ml insulin, and 9 μM of SmTrx. Stock solutions of insulin were prepared as previously described [109]. Insulin precipitation after reduction by Trx was followed spectrophotometrically according to [109]. As control, the precipitation of insulin was performed using dithiothreitol (DTT) as the reducing agent. The time for the start of precipitation, defined as an increase by 0.02 at A_{650} over a stable base-line recording, was determined. The second parameter calculated was the rate of precipitation at 650 nm, defined as the maximal increase ΔA_{650}/min in the interval between 0 and 1.0 in absorbance at 650 nm.

3.17.2 GR activity

A classical assay was performed [110]. 1ml assay mixture contained 150mM potassium phosphate pH 7.0, 5 mM EDTA, 300 µM NADPH, and variable GSSG (250 µM-5 mM). The reaction was initiated by addition of 2.5 µM U597C SmTGR and the decrease in absorbance at 340 nm was followed at 37°C.

3.17.3 Grx activity

The assay was performed as described (by monitoring absorbance at 340 nm, at 25°C, [111]). The mixed disulfide formed by hydroxyethyl-disulfide (HED) and GSH was reduced by U597C SmTGR to produce GSSG, which in turn is reduced by GR with consumption of NADPH. The reaction mix contained 1 mM GSH, 300 µM NADPH, 5 mM EDTA, and variable HED with or without 6 U/ml of yeast GR. The same assay has been performed in the absence of yeast GR to evaluate the ability of the mutated C-terminus to internally transfer reducing equivalents to the Grx domain.

3.17.2 Reductive half-reaction of U597C SmTGR

Stopped-flow experiments were carried out using an Applied Photophysics (Leathered, UK) in aerobic conditions at 25°C.

The stopped-flow apparatus allows the rapid mixing of two reactant solutions (Fig. 12). The mixed solution is then forced through an observation cell and a stopping syringe. The flow fills the stop-syringe, until the plunger hits the trigger-switch. This simultaneously stops the flow and starts the data acquisition. The sample is illuminated by light at fixed wavelength, and the outcoming radiation is collected and amplified by a photomultiplier. The reaction may be monitored using a suitable spectroscopic probe, such as absorbance or fluorescence. The change in the spectroscopic signal as a function of time is recorded.
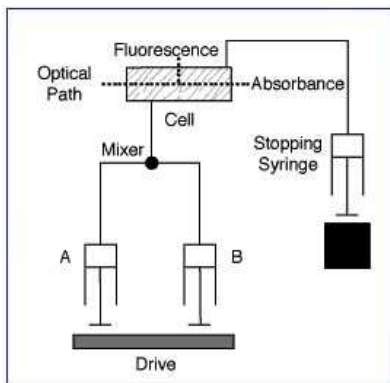
Fig. 12: Schematic representation of a stopped-flow apparatus.

In the case of the reaction of reduction of SmTGR by NADPH, time dependent spectra were followed using the diode array detector and single-wavelength kinetic traces were recorded with a photomultiplier. Solutions of SmTGR (2.5 and 7.5 μM) in 0.1 M NaCl, 0.1 M Tris pH7.4 and EDTA 1mM were mixed with several NADPH solutions, ranging between 3.3 μM and 20 μM.

3.17.3 Oxidative half-reaction of U597C SmTGR

SmTGR (3.0 μM, 5 μM and 10 μM) were anaerobically reduced with 2 equivalents of NADPH to produce the EH4 species, at 25C° in 0.1 M NaCl, 0.1 M Tris pH 7.4, EDTA 1 mM. The reduced enzymes were then mixed with 2 equivalents of SmTrx and the reactions were followed until completion.

4. RESULTS AND DISCUSSION

I part: Glutathione peroxidase from S. mansoni (SmGpx)

4.1 Expression and purification of two mutants of SmGpx

SmGpx in its native form is a selenoenzyme, presenting a SeCys residue (U43) in the active site. For this study two mutants of SmGpx have been employed, which present a Sec/Cys (U43C) and a Sec/Ser (U43S) aminoacidic substitution respectively. This strategy was mainly dictated by the fact that the synthesis of recombinant selenoproteins does not assure a good yield especially if it deals with the expression of eukaryotic proteins in bacteria. A brief description of the mechanism of selenoprotein synthesis will clarify this statement. The insertion of a Sec residue in a protein sequence during translation in eukaryotic cells requires the presence of a stem-loop secondary structure (SE-CYS element) in the 3'-UTR region of the mRNA, besides a pattern of accessory proteins and specific tRNA molecules, which are able to recognize the UGA codon as coding for a SeCys residue. Differently from eukaryotes, in bacteria the SE-CYS element must be located directly downstream the UGA codon for the Sec residue. Thus, the heterologous expression of a eukaryotic gene in bacterial cells strictly requires a modification inside its coding sequence, which seriously compromises the yield and the purity of the protein product [58, 59, 70]. Therefore with the aim to obtain large amounts of recombinant protein for crystallization studies we decided to synthesize the U43C mutant. The gene of U43C SmGPX was inserted, between BamHI and XhoI restriction sites, into a pGex4T-1 expression vector, which allows the addition of a thrombin-cleavable N-terminal GST tag. After the thrombin cleavage the protein contains two additional residues at the N-terminus (Gly-Ser) that constitute part of the cleavage site (Fig. 13).

A point-mutagenesis on the U43C construct allowed us to obtain the gene coding for the U43S SmGpx (see Chapter 3). The expression of both mutants of SmGpx in E. coli BL21(DE3) strand was evaluated by SDS-page, showing a clear

band around 19.4 KDa (after the thrombin cleavage), which corresponds to the expected molecular weight of the pure protein (Fig. 14).
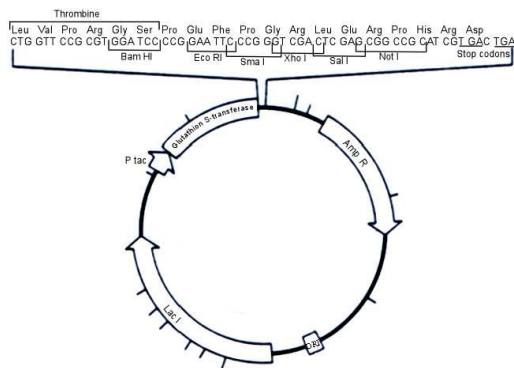
Fig. 13: Map of the pGex4T-1 expression vector. The thrombin cleavage site, placed downstream the GST gene, is shown.
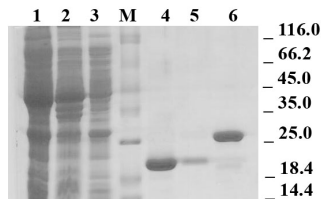
Fig. 14: SDS-Page showing the expression of U43C SmGpx after the IPTG induction. Lanes 1: supernatant after sonication of the cell extract; 2: pellet after sonication; 3: flow through containing the material unbound to the GST-affinity column; 4: U43C SmGpx eluted by the GST-affinity column after thrombin cleavage; 5: U43C SmGpx after the benzamidine column, which is required to remove thrombin; 6: elution from the GST-affinity column with 10 mM GSH, the amount of the GST band around 26 KDa is comparable to the eluted SmGpx in lane 4. The eluted U43C SmGpx has a M.W. of 19.4 KDa and is well purified from contaminants in the final step (lane 5). The molecular weights of the protein markers (lane M) are shown on the right side of the gel.

4.2 Structural characterization of U43C and U43S SmGpx

The following sections will describe the overall structure of two SmGpx mutants (U43C and U43S), with insights into the interaction sites of the enzyme with its substrates. A few structures of isozymes from the Gpx family are available, the most of them belonging to the class 1 and 3 of tetrameric Gpxs [62, 64]. A Sec/Cys mutant of the human Gpx4 (HsGpx4), the unique member of the Gpx4 class to be structurally characterized [63], will be here used as a comparison model in order to highlight and explain some special features of the parasite enzyme.

4.2.1 Analysis of the primary structure of SmGpx

The multiple sequence alignment between SmGpx and Gpxs from all four main classes highlights some peculiarities of the schistosoma enzyme. Though SmGpx retains the catalytic residues known to be invariant in the other Gpxs (Sec43, Gln78, Trp132, and Asn133, [66]), it lacks the conserved residues apparently involved in GSH binding (Arg57, Arg185, and Met147 in bovine Gpx, [62]) and presents two large gaps corresponding to the intersubunit interaction sites of the tetrameric mammalian Gpx1-3 (i.e.: residues 94-98 and 136-153 in HsGpx1) (Fig. 15). These features of the primary structure, consistently with gel-filtration and analytical ultracentrifugation measurements (data not shown), confirmed the monomeric nature of the schistosoma enzyme, clearly assigning it to the class 4 of Gpx family. Sayed *et al.* proposed that *S. mansoni* has a second variant of SmGpx enzyme, called SmGpx2 [53] (see section 1.5.2). The sequence alignment of SmGpx with SmGpx2 shows that the two proteins share the same above mentioned sequence features, thus proving that the parasite finally possesses only a type-4 Gpx isozyme (Fig. 15).

```
SmGpx     1   ..............|.........|...MSSSHKSWN...........SIYEFTVKDING.VDVSLEK
SmGpx2    1   .MFDRFTSLLSLI|IF........LANSEACMRSPASG........KIYDFTVTDIDG.NEVQLKK
HsGpx4    1   MSLGRLCRLLKPALLCGALAAPGLAGTMCASRDDWRCA........RSMHEFSAKDIDG.HMVNLDK
HsGpx1    1   ..............MCAAR...LAAAAAAQS.................VYAFSARPLAGGEPVSLGS
HsGpx2    1   ..............|.........|.MAFIAKS.............FYDLSAISLDG.EKVDFNT
HsGpx3    1   ........MARLLQASCLLSLLLAGFVSQSRGQEKSKMDCHGGISGTIYEYGALTIDGEEYIPFKQ
BtGpx1    1   ..........MCAAQRSAAALAAAAPRT................VYAFSARPLAGGEPFNLSS

SmGpx    32   HVCLIVNVACKUGATDKNYRQLQEMHTRLVGKGLRILAFPCNQFGGQEPWAEAEIK.....KFVTEK
SmGpx2   51   KVCIIVNVATEUGLAGTNYPQLQRLYTQYSENGFRILAFPCNQFRGQEPGTDQEIK.....QRVLAK
HsGpx4   62   FVCIVTNVASQUGKTEVNYTQLVDLHARYAECGLRILAFPCNQFGKQEPGSNEEIK.....EFAAG.
HsGpx1   38   KVLLIENVASLUGTTVRDYTQMNELQRRLGPRGLVVLGFPCNQFGHQENAKNEEILNSLKYVRPGGG
HsGpx2   29   RAVLIENVASLUGTTTRDFTQLNELQCRF.PRRLVVLGFPCNQFGHQENCQNEEILNSLKYVRPGGG
HsGpx3   62   KYVLFVNVASYUGLTG.QYIELNALQEELAPFGLVILGFPCNQFGKQEPGENSEILPTLKYVRPGGG
BtGpx1   41   KVLLIENVASLUGTTVRDYTQMNDLQRRLGPRGLVVLGFPCNQFGHQENAKNEEILNCLKYVRPGGG

SmGpx    97   QFDMFSKIKVNGSDADDLYKFLKSRQHG...................TLTNNIKWNFSKFLVDRQGQ
SmGpx2  116   TFDLFHKIDVNGENAIPLYKFLKQSISS...................WFSRDIEWNFVKFLVDRNGT
HsGpx4  126   KFDMFSKICVNGDDAHPLWKWMKIQPKGKG..................ILGNAIKWNFTKFLIDKNGC
HsGpx1  108   NFMLFEKCEVNGAGAHPLFAFLREALPAPSDDATALMTDPKLITWSPVCRNDVAWNFEKFLVGPDGV
HsGpx2   98   TFTLVQKCEVNGQNEHPVFAYLKDKLPYPYDDPFSLMTDPKLIIWSPVRRSDVAWNFEKFLIGPEGE
HsGpx3  131   NFQLFEKGDVNGEKEQKFYTFLKNSCPPTS....ELLGTSDRLFWEPMKVHDIRWNFEKFLVGPDGI
BtGpx1  111   NFMLFEKCEVNGEKAHPLFAFLREVLPTPSDDATALMTDPKFITWSPVCRNDVSWNFEKFLVGPDGV

SmGpx   148   RYSPTTAPYDIEGDIMELLEKK........
SmGpx2  167   RYSSITPPNSMES..|.............
HsGpx4  179   RYGPMEEPLVIEKDLPHYF...........
HsGpx1  178   RYSRRFQTIDIEPDIEALLSQGPSCA....
HsGpx2  168   RYSRTFPTINIEPDIKRLLKVAI.......
HsGpx3  197   RWHHRTTVSNVKMDILSYMRRQAALGVKRK
BtGpx1  181   RYSRRFLTIDIEPDIETLLSQGASA.....
```

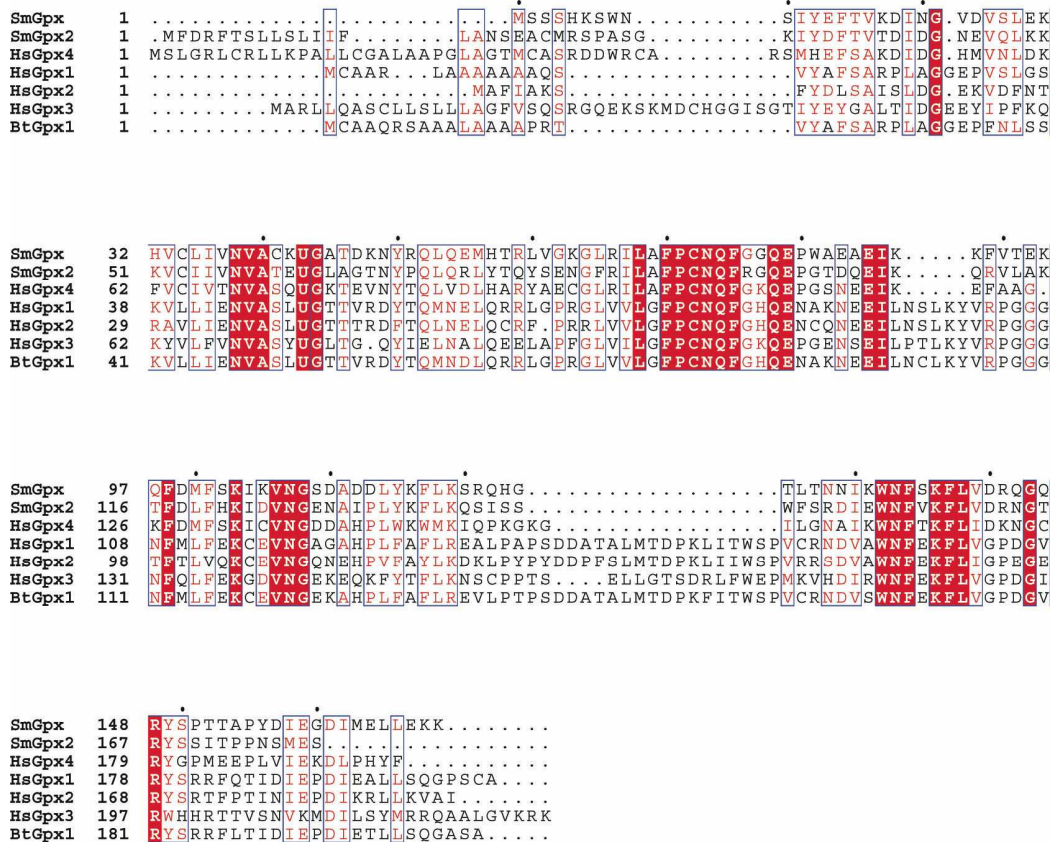**Fig. 15:** Sequence alignment of SmGpx with Gpx of all classes. Identical residues are boxed in red, conserved residues are shown in red character. Sm, Schistosoma mansoni; Hs, Homo sapiens; Bt, Bos taurus.

4.2.2 Overall 3D structure of U43C and U43S SmGpx mutants

The crystal structure of U43C SmGpx was solved by molecular replacement (see Chapter 3) using the structure of human Gpx4 (HsGpx4) as model (PDB code:

2OBI; [63]). A summary of the crystallographic parameters is presented in tab. 1. The diffraction data, collected up to 1.0 Å resolution, were refined to the final R_{factor} and R_{free} values of 17.5% and 18.4%, respectively. The validation programs [84, 85] showed a very good final geometry and density fit, with all residues lying in the preferred regions of the Ramachandran plot. The flexibility of the molecule is extremely limited and only nine side chains are placed in alternative conformations. The average B-factor is 6.29 $Å^2$, with slightly higher values restricted to the ill-defined side chains of a few superficial Lys. The high resolution made easier the identification of the correct positioning of great part of the polypeptide chain, with the exception of the N-terminal region, where a weak electron density map prevented us from adding the first six residues to the model.

U43C SmGpx appears in a monomeric form and shows only a few differences with the typical Trx fold, characterized by 4 β strands flanked by 3 α helices [112]. U43C SmGpx presents, in fact, a N-terminal extension including two more β strands and an insertion with one more β strand and one α helix. For the sake of consistency, these secondary structure elements are named β1a, β1β, β2a and α1a. A comparison between the topological diagrams of a typical Trx and SmGpx is presented in Fig. 16. The central β sheet of U43C SmGpx contains four β strands: two of them (β3, β4) are antiparallel and connected to the C-terminal helix α3 to form the typical ββα Trx motif; the other two parallel strands (β1, β2) flank helix α1 to form a βαβ structural motif. Helix α2, perpendicular to α1 and α3, connects β2 and β3 strands through a linking region containing the additional α1a and β2a motifs. Far from the central core and closer to the N-terminal region, the topological diagram shows the last structural motif of U43C SmGpx composed by two antiparallel β strands (β1a, β1b) (Fig. 16 and 17A).
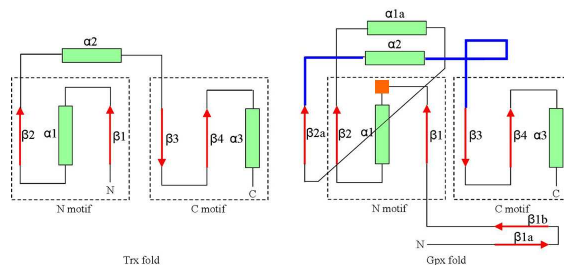
Fig. 16: Topological diagrams for Trx fold (left) and Gpx fold (right), redrawn from [112]. The blue lines indicate the loops preceding and following helix α2, related to the fluctuations of the putative GSH binding site (see section 4.2.4); the orange box indicates the position of OCS43.

| Data collection	U43C SmGpx	U43S SmGpx
Space group	P2$_1$2$_1$2$_1$	P2$_1$2$_1$2$_1$
Cell dimensions		
a, b, c (Å)	41.40, 60.62, 62.54	39.91, 51.17, 90.62
α, β, γ (°)	90, 90, 90	90, 90, 90
Resolution (Å)	41.38/1.00 (1.05/1.00)*	45.31/1.70 (1.79/1.70)*
R_{sym} or R_{merge}	0.098 (0.313)*	0.077 (0.159)*
$I / \sigma I$	17.8 (2.4)*	17.3 (9.3)*
Completeness (%)	100 (95.32)*	99.7 (100)*
Redundancy	6.3 (4.9)*	5.3 (5.4)*
Refinement		
Resolution (Å)	41.38-1.00	90.54-1.70
No. reflections	100817	112663
R_{work} / R_{free}	0.17/ 0.18	0.18/ 0.21
No. atoms	1616	1482
Protein	1387	1333
Ligand/ion	14	9
Water	215	140
B-*wilson*	4.13	12.7
B-*overall*	6.29	10.6
R.m.s deviations		
Bond lengths (Å)	0.022	0.015
Bond angles (°)	1.958	1.406

Table 1: Crystallographic data collection and refinement statistics for U43C and U43S SmGpx.
*Highest resolution shell is shown in parenthesis.

The structure of the U43C mutant evidences the presence of a few loops, one of which, connecting β1 to α1, hosts the catalytic cysteine (Cys43), which was here

found oxidized to sulphonic acid (Ocs43, SO_3^-) (Fig. 17A). The possibility that the oxidation of Cys43 could result in a local distortion of the active site structure, in order to accommodate the bulky sulphonic acid, seems unlikely, given that the superposition of the U43C SmGpx with the reduced U73C mutant of HsGpx4 does not show any macroscopic difference in the 3D structure of the two proteins (Fig. 17B and section 4.2.3). However, to demonstrate this point, the U43S mutant was purified and crystallized as well. The crystal structure was solved by molecular replacement using the U43C SmGpx structure as the model (PDB code: 2v1m). Data were collected up to 1.7Å resolution and refined to the final R_{factor} and R_{free} values of 18.2% and 21.2%, respectively (Tab. 1). The validation programs [84, 85] showed also for this second model a very good final geometry and density fit, with all residues lying in the preferred regions of the Ramachandran plot. The quantitative comparison of U43S with U43C SmGpx did not show any significant structural difference neither in the stereochemistry of the residues into the active site nor in the 3D structure of the protein at large ($RMSD_{main\ chain}$=0.38 Å; $RMSD_{side\ chain}$=1.21 Å). This finally leads to the conclusion that U43S SmGpx maintains the same 3D structure of the U43C mutant, strongly suggesting that the easier oxidation of Cys43 does not perturb significantly the native structure of the enzyme. An additional proof in support of this statement came from the molecular dynamic (MD) simulations on SmGpx, where the in silico replacement of the SO_3^- group with functional Se^- or SeOH groups did not determine any significant perturbation of the enzyme structure (see Chapter 3).
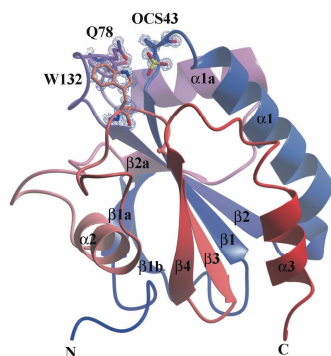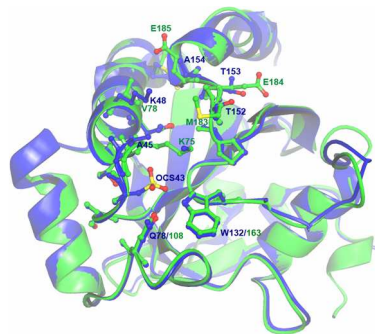
A   **B**

Fig. 17 Panel A: Ribbon representation showing the overall 3D structure of U43C SmGpx. Colour blending from N-terminus (blue) to C-terminus (red). The active site residues, including sulfonated catalytic Cys (OCS43), Gln 78, Trp 132, are shown as ball and stick and contoured with 2Fo-Fc electron density map at 1σ. **Panel B:** Superposition of U43C SmGpx (blue) and HsGpx4 (green). View of the two proteins from the top looking into the cleft surrounding the catalytic triad; residues different among the two are shown as ball and stick.

4.2.3 Insight into the catalytic site of SmGpx

The complexity of the Gpx superfamily, including different enzymes with various substrate specificity and cellular localization, does not result in a similar heterogeneity in the active site organization. It has been already demonstrated, for example, that bovine and human Gpx_s display a highly similar pattern of catalytic residues, though classified as cytosolic (Gpx1) and extracellular (Gpx3) enzymes respectively. Two conserved amino acids, Gln and Trp, are crucial for the enzymatic activity of Gpx_s, being localized at hydrogen bonding distance from the catalytic Sec; but recent results suggest that also the conserved Asn residue closer to Trp may play a role during catalysis [62, 64, 66].

SmGpx does not differ significantly from this pattern of active site residues: Q78, W132 and N133 are conserved in SmGpx (Fig. 15, 17A) and located at H-bond

distance from Ocs43 (Tab. 2), consistently with their presumed role in the stabilization of the reduced form of the native enzyme (R-Se⁻) during catalysis.

SmGpx			HsGpx4		
Atom 1	Atom 2	Distance	Atom1	Atom2	Distance
43OCS/O	45 ALA/N	3.11	73CYS/O	75 LYS/N	3.12
	46 THR/OG1	3.03		76 THR/OG1	3.03
	46 THR/N	**3.04**		**76 THR/N**	**3.01**
	61 HOH	**3.12**			
43OCS/N	41 CYS/O	3.78	73CYS/N	71 SER/O	3.79
	46 THR/OG1	**3.03**		**76 THR/OG1**	**3.12**
43OCS/SG	44 GLY/N	3.39	73CYS/SG	75 LYS/N	3.48
	132 TRP/NE1	3.84		181 TRP/NE1	3.92
	74 HOH	3.75		164 ASN/ND2	3.63
43OCS/OD1	78 GLN/NE2	3.86			
	132 TRP/NE1	3.49			
43OCS/OD2	44 GLY/N	3.11			
	132 TRP/NE1	3.08			
	133 ASN/ND2	**2.91**			
	74 HOH	**3.09**			
43OCS/OD3	44 GLY/N	3.22			
	45 ALA/N	**2.79**			
	46 THR/N	3.89			
	74 HOH	3.27			

Table 2: Inter residue contacts around the active Ocs43/ Cys73 in U43C and human HsGpx4 respectively. Distances shown are between each residue and the catalytic Ocs43/Cys73. Putative H-bonds (in bold) have been identified choosing a bond length cut-off of 3.10 Å [136] and allowing for an experimental error of 0.05 Å. Moreover, their bond angles have been checked and demonstrated to be compatible with the expected linear geometry. To describe how the angles were determined, we schematically represent the H-bond as X─D─H···A, where D is the donor atom and A is the acceptor. In our maps the H atom is not detected, thus the linear arrangement of atoms D─H···A cannot be checked directly. However, linearity can be safely assumed if the D─A distance is below the threshold and X─D─A angle is compatible with the known hybridization of D.

The structural superimposition of the U43C SmGpx with the U73C mutant of the HsGpx4 leads to an overall r.m.s.d of 0.68 Å. In particular the residues belonging to the SmGpx active site (C43, Q78, W132, N133) show an average displacement of 0.17 Å with respect the corresponding residues in the human enzyme. Hence the geometry of the active site is strictly conserved, the most obvious difference between the two enzymes being the redox state of the mutated catalytic cysteine, which is fully reduced in HsGpx4, while over-oxidized in SmGpx (Fig. 17B).

All attempts to obtain a reduced U43C SmGpx, through different purification protocols employing several reducing agents, including TCEP, DTT, β-Mercaptoethanol and GSH (see Chapter 3), were unsuccessful. The over-oxidized state of the catalytic C43 unfortunately compromised all the measurements of the enzymatic activity. Hence the enzyme was proved to be totally inactive, as well as the U43S mutant, at every stage of the purification and with the different substrates tested (see Chapter 3). The loss of activity was expected for the U43S mutant but not in the case of the U43C SmGpx, as the homologous HsGpx4 carrying the same point mutation and the same structural features was proved to be active [63].

The reason for the major tendency to auto-oxidation of the schistosome enzyme if compared with the human Gpx4 cannot be unequivocally assigned, but a more detailed comparison between the active site environments of the two enzymes gives some hints in this respect. Indeed superposition between SmGpx and HsGpx4 with SSM methods (secondary-structure matching) shows a few point mutations involving residues surrounding the catalytic Cys: A45, K48, T153 and A154 in SmGpx are respectively mutated to K, V, E and E, in the human enzyme (Fig. 17B). A specific role for these residues is not immediately apparent, though the charge distribution around the catalytic Cys might be changed by the following substitutions: C41 of U43C SmGpx to S in HsGpx4 and A45 to K. The analysis of the surface charge distribution confirms that the active site pocket of U43C SmGpx has a strong positive charge, while in HsGpx4 the pocket is less positive and more hydrophobic (Fig. 18A-18B). Thus the most obvious difference between the human

and the schistosoma enzyme seems to lie in the greater polarity of U43C SmGpx active site, which could favour access to water and possibly metal ions that could exert a catalytic role and promote the oxidation of C43 to sulphonic acid.

4.2.4 Static and dynamic clefts on SmGpx and their functional relevance

With the aim to provide details about the catalytically relevant regions of SmGpx involved in the binding of specific substrates, such as glutathione (GSH/GSSG) and phospholipid hydroperoxides, the CASTp algorithm has been used to analyse the protein clefts (see Chapter 3). Two topologically equivalent cavities, close to the catalytic residue, have been identified in U43C SmGpx and in HsGpx4, having different areas and volumes: 140Å^2/ 94Å^3 for U43C SmGpx and 93Å^2/ 72Å^3 for HsGpx4, respectively. A contribution to the greater extension of SmGpx pocket may be attributed to the lack of the H-bond between E158 and Q52, which in the human enzyme partially close the pocket shielding the catalytic C73 from direct access to the solvent.

The SmGpx cavity (yellow surface in Fig. 18C) is delimited by hydrophobic, polar and aromatic residues, which are close to the catalytic Ocs43 and in some cases form H-bonds with it (Tab. 2-3). Therefore, we refer to this cavity as the active-site cleft. CASTp also identifies a secondary crevice in SmGpx, centred on K131, having area and volume of about 107 Å^2 and 57 Å^3, respectively (magenta surface in Fig. 18C). This secondary cleft has limited access to C43, it is smaller than the active site one but has a greater density of positive charges (Fig. 18A and Tab. 3). The two clefts are divided by a ridge that hosts C43, whose volume is increased because of oxidation and which seems to act as a flexible barrier in between. Elimination of sulphonic acid by mutation of C43 to S or by computational methods, does not change significantly this condition, except that the physical barrier between the two half-clefts is less prominent.
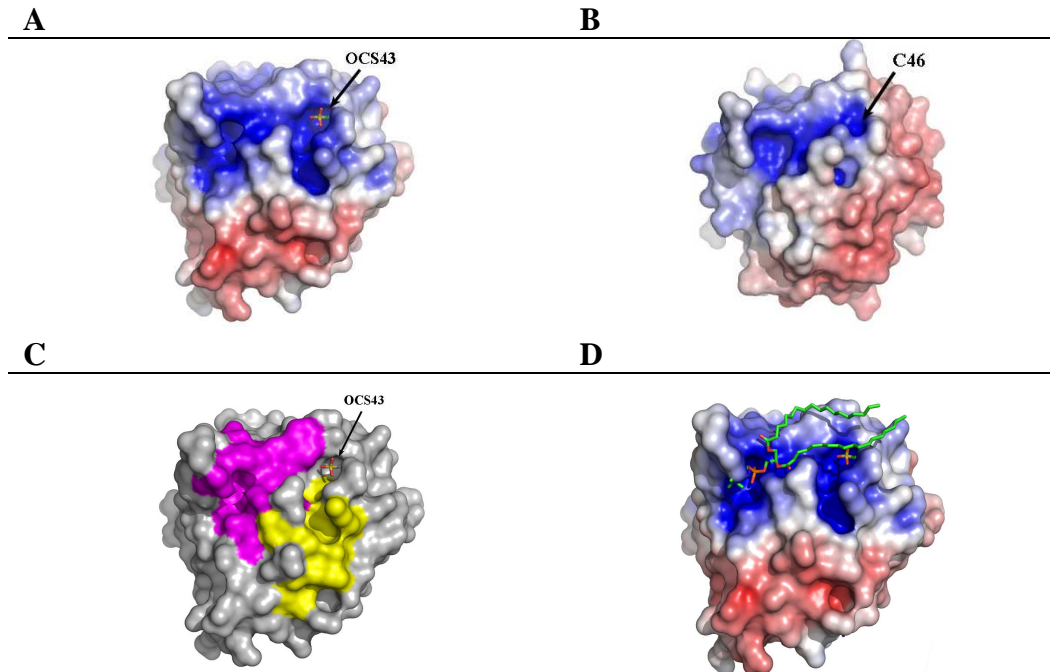
Figure 18 Panel A and Panel B: Representation of the electrostatic potential on SmGpx and HsGpx4, respectively. The higher density of positive charges surrounding the catalytic C43 in the parasite enzyme is evident. The two proteins are in the same orientation of SmGpx in panel C. In both proteins the position of the catalytic cysteine is pointed by an arrow. Electrostatic-potential maps were calculated with APBS [88], using the PDB2PQR server [89] and visualized with PyMOL [90]. Deep red corresponds to an electrostatic potential of -7 kT/e; deep blue corresponds to +7 kT/e. **Panel C**: Representation of the clefts detected by CASTp and MD analysis in SmGpx. Yellow: active site cleft; magenta: secondary cleft (putative GSH binding site). The catalytic Cys residue placed between the two clefts is shown as sticks. **Panel D**: Docking of phosphatidylcholine (PDB code CPL) on the active site cleft. The phosphorous atom is located in the negative pocket hosting a sulfate anion in the crystal structure, and the two fatty acid chains lie on top of the hydrophobic surface just above OCS43.

	CASTp on U43C crystal structure	MD simulation on SmGpx
Residues in the active site cleft	OCS43	Sec43
	Ala45	
	Lys48	**Lys48**
	Asn49	**Asn49**
	Gln52	**Gln52**
	Trp132	**Trp132**
		Phe134
	Lys 136	Lys136
	Pro151	
	Thr152	**Thr152**
	Thr153	**Thr153**
	Ala154	**Ala154**
	Pro155	**Pro155**
		Tyr156
		Glu159
		Ile162
Residues in the secondary cleft (putative GSH binding site)		Gly124
		Thr125
		Asn129
	Ile130	**Ile130**
	Lys131	**Lys131**
	Trp132	**Trp132**
	Ser135	**Ser135**
	Arg148	**Arg148**
		Tyr149
		Ser150
		Pro151

Table 3: Residues lining the clefts identified by the static and dynamic analysis of SmGpx. The active site cleft is delimited by hydrophobic, polar and aromatic residues; the secondary cleft (smaller than the active site one) has a greater density of positive charges. Residues detected in both static and dynamic analysis are shown in bold.

The results obtained from CASTp analysis are supported by the observations coming from MD simulations performed on SmGpx in different redox states (see

Chapter 3). During the simulations, transiently formed cavities with volumes ranging from 10 to a few hundreds Å^3 are detected on the surface, close to residue C43. The volume distributions of such cavities, reported in Fig. 19A (upper panel) for reduced (Se⁻) and oxidized (SeOH) SmGpx, are by-and-large independent of the oxidation state of Sec. Dynamic analysis identified also a secondary positively charged cleft close to K131 which is detected for a fraction of time of 80-85% for both reduced and oxidized SmGpx (Fig. 19A bottom panel). In reduced SmGpx the volume distribution is characterized by a large single peak with a maximum at about 200 Å^3, while in oxidized SmGpx it is significantly broader and almost flat, with values ranging from 100 to 300 Å^3. The motions of two loops, preceding and following helix α2 (β2a-α2 loop: residues 104-112, and the α2-β3 loop: residues 122-134, Fig. 16), are specifically correlated to the fluctuations of the secondary cleft, as detected by essential dynamics (ED) analysis ([102] and Chapter 3), performed on the backbone of amino acids 104 to 140. In Fig. 19B the extreme configurations corresponding to the opposite values of the projection on the first eigenvector as determined from the simulations of SmGpx(Se⁻) and SmGpx(SeOH) respectively, are reported. The approximate position of the cavity is highlighted by a sphere. The principal motions of the two loops, β2a-α2 and α2-β3, are correlated in both oxidation states. Therefore, MD simulation shows that in SmGpx(SeOH) the displacement of the β2a-α2 loop towards the active site is coupled with a displacement of the α2-β3 loop away from the β4 strand and thereby an increase of the cleft volume. On the other hand, in SmGpx(Se⁻) the coupling between the two loops is anti-correlated, since, when the β2a-α2 loop moves towards the active site, the distance between the α2-β3 loop and the β4 strand decreases and the cleft volume shrinks (Fig. 19B). The list of the main residues lining both the static and dynamic clefts (Tab. 3) shows that the core of both the active site and the secondary cleft detected by CASTp is superimposable to the pattern of residues lining the dynamic clefts. Therefore MD suggests that both clefts detected by CASTp may undergo transient expansion. This area/volume changes may be functionally

relevant, since the cleft's volume from the static crystal structure appears too small to accommodate either substrate (i.e. the organic hydroperoxides or GSH).
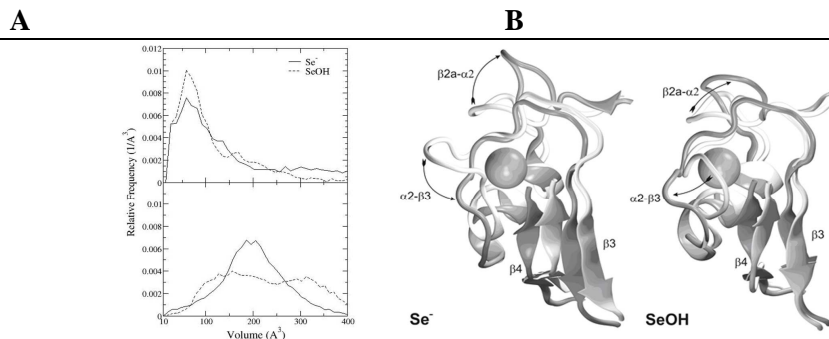

Figure 19 Panel A: Relative frequency of the volume distributions of the active site cleft (upper panel) and of the secondary positively charged cleft (bottom panel), shown for the reduced (Se⁻, solid lines) and the oxidized (SeOH, dashed lines) states of SmGpx. **Panel B**: Extreme configurations from the most different eigenvalues for each simulation of reduced (Se⁻) and oxidized (SeOH) SmGpx. The directions of motion of the loops (β2a-α2, α2-β3 preceding and following helix α2 are shown. The approximate position of the secondary cleft limited by the two loops is highlighted by a sphere.

Although it is difficult to assign a specific functional role to each cleft identified in U43C SmGpx, mainly because the attempts to crystallize the enzyme in the presence of its substrates did not gave any positive result, the information coming from the crystal structure here presented and from the surface analysis allowed to hypothesize a binding region for both phospholipid hydroperoxides and GSH/GSSG on SmGpx.

Functional studies have proved that class 4 Gpx$_s$ prefer phospholipid hydroperoxides as substrates over-and-above H_2O_2 or other organic hydroperoxides [50]. Moreover it is known that schistosomes, being unable to synthesize de novo fatty acids, upload these compounds from the host and that adult worms usually use the host oleate (18:1) and elongate the chain to eicosenoate (20:1), which is

incorporated predominantly in the phosphatidylcholine molecule together with palmitate (16:0) [113]. An automated docking procedure (see Chapter 3, [91]) has been here employed in the attempt to identify a possible binding site for phosphatidylcholine (PC) in U43C SmGpx in the proximity of C43 (Fig. 18D). In spite of the high flexibility of the substrate PC, under the assumption that the phosphate (P) of PC occupies the same site of the sulphate or pyrophosphate anion present in U43C SmGpx and U43S SmGpx respectively, a plausible PC binding site was identified, comprising: (i) the residues surrounding the active site cysteine (43-45 and 74-77) (the Cys residue should act on the peroxidatic double bond of the phosphatidylcholine hydroperoxide fatty acid chains) and (ii) those surrounding the strongly positive pocket ($57\mathring{A}^3$) next to the catalytic Cys hosting a sulfate/pyrophosphate anion (residues 123-133 and 148-151). MD simulations had already shown that such a pocket undergoes relevant expansions in solution, enabling it to accommodate larger substrates (Fig. 19A). The program Patchdock optimized the position of the substrate, with the following constraint: P to R148 distance=3.9 $\mathring{A}$. Although this procedure is somewhat arbitrary, it is useful to suggest a possible orientation of a highly flexible substrate. It is possible that when the phosphate group of the phosphatidylcholine is located in the pocket containing the sulfate or pyrophosphate anion, the two fatty acid hydrophobic chains may lodge on top of a large hydrophobic surface located above the catalytic cysteine, positioning C43 close to C_9-C_{10} double bond of the eicosenoic acid. This observation may have a functional relevance as it is known that over-oxidation of unsaturated fatty acids occurs usually on a double bond located around C_{10} yielding similar oxidation products for monoene-, diene- and triene- fatty acids [114] (Fig. 20). With respect to the GSH binding site on Gpx enzymes, the unique information available in literature comes from the work of Epp et al., who proposed a model based on differences in the electron density maps between the oxidized and GSH reduced wild type bovine cellular enzyme (PDB code: 1GP1, [62]). They concluded that three residues (R57, R184 and M147) are involved in GSH binding. Sequence alignment and structural superposition allowed us to trace the equivalent positions in

U43C SmGpx. This putative GSH binding site overlaps with the secondary cleft in the schistosoma enzyme, even though the residues that should interact with GSH are different. In fact, while the putative role of R57 could be played in U43C SmGpx by K48, R184 is mutated to P150 and an equivalent of M147 is absent. The latter observation is consistent with the fact that SmGpx is a monomeric enzyme, while bovine Gpx1 is tetrameric: in the bovine enzyme M147 is localized in a loop of residues involved in the dimerization of oligomeric Gpxs which is absent in the monomeric enzymes, such as SmGpx (Fig. 15). In view of these differences, the hypothesis that the functional role of the secondary cleft is to provide the actual GSH binding site must be considered with caution, though the high concentration of positive charges in this cleft together with its dynamic volume fluctuations, occurring when the enzyme passes through the two redox state of its catalytic cycle (from R-Se$^-$ to R-Se-OH), makes it plausible.
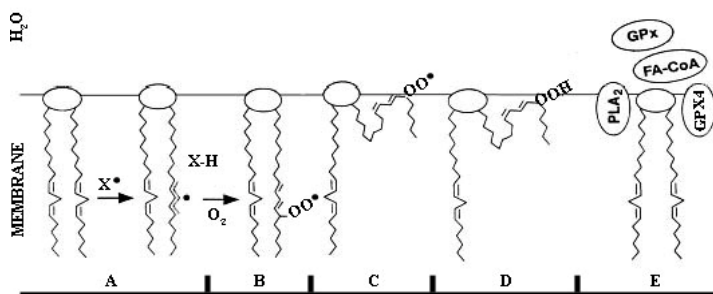

Fig. 20: Main steps of membrane lipid peroxidation: (A) initiation of the peroxidation process by an oxidizing radical X·, by abstraction of a hydrogen atom; (B) oxygenation to form a peroxyl radical and a conjugated diene; (C) peroxyl radical moiety partitions to the water-membrane interface; (D) peroxyl radical is converted to a lipid hydroperoxide; (E) the enzymes phospholipase A2 (PLA2), glutathione peroxidase 4 (GPX4), glutathione peroxidase (GPx) and fatty acyl-coenzyme A (FA-CoA) cooperate to detoxify and repair the oxidized fatty acid chain of the phospholipid (adapted from [115]).

II part: Thioredoxin Glutathione Reductase from *S. mansoni* (SmTGR)

4.3 Expression and purification of two mutants of SmTGR

The gene coding for a GST-fused SmTGR, lacking the last two amino acids Sec597-Gly598, cloned into a pGEX-4T1 vector, was expressed in BL21(DE3) E. coli cells upon induction with IPTG, in order to obtain the truncated form of the enzyme (SmTGRtr) (see Mat. & Met.). The gene coding for SmTGRtr was used as a template to synthesize the U597C mutant gene for full-lenght TGR (see Chapter 3). The expression of this construct in BL21(DE3) *E. coli* cells without IPTG induction gave the best results in terms of protein yield. For both mutants the SDS-PAGE analysis confirmed the presence of a band at about 90 kDa corresponding to the molecular weight of the GST fused with a monomer of SmTGR. The protein purity was >98%, after the thrombin cleavage and removal of the GST tag by affinity chromatography.

The two SmTGR mutants showed the typical UV-VIS spectrum of flavoenzymes having an absorption peak at 280 (due to both the protein and its FAD cofactor) and another peak at 460 nm (representative of the FAD) which has been used to estimate the protein concentration (see Chapter 3 and Fig. 21).

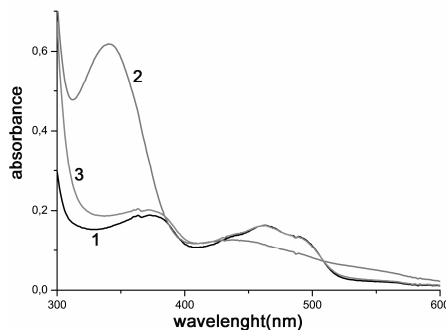**Fig. 21:** absorption spectra of SmTGRtr in different redox states. *Spectrum 1*: 15 μM of oxidized SmTGR ($\varepsilon_{460} = 11,300$ M^{-1} cm^{-1}). *Spectrum 2*: SmTGR reduced with 4 equivalents of NADPH ($\varepsilon_{340} = 6220$ M^{-1} cm^{-1}), 1 min after the addition of reductant. *Spectrum 3*: SmTGR reoxidized by 1 mM GSSG, 1 min after the addition of oxidant.

Both the truncated and U597C SmTGR have been employed in crystallization experiments and their structures have been solved (PDB codes: 2V6O, 2X8C, 2X8G, 2X8H, 2X99). However, given the absence of relevant structural changes between the SmTGRtr and the oxidized form of U597C SmTGR, the former will be excluded from the structural description reported below.

4.4 Structural characterization of intermediates of the catalytic cycle of SmTGR

As described in section 1.6, SmTGR is a homodimeric flavoprotein belonging to the class of the pyridine nucleotide oxidoreductases, which includes also thioredoxin reductase (TR) and glutathione reductase (GR) [48]. The structural characterization here presented explains how the peculiar domain organization of the parasite's SmTGR makes it able to exploit the functions which normally compete to both TR and GR in the mammalian hosts, being involved in the transfer of reducing equivalents from NADPH to both the GSH and Trx antioxidant systems, in order to finally permit the reduction/detoxification of hydrogen peroxide and organic peroxides to H_2O_2 and hydroxides respectively. The active cysteine couples located in different domains of the protein (i.e.: the C-terminal Gly-Cys-Sec-Gly tetrapeptide, the FAD binding site, and the N-terminal glutaredoxin domain) are at the base of the reducing activity of SmTGR (Fig. 22).

Several structures of TR and GR from different organisms have been solved [44, 116-118], but the absence of details about the 3D organization of TGRs has prevent the elucidation of its catalytic mechanism. Furthermore the demonstration that TGRs from different parasites (Schistosoma among them) are targets of choice for the development of new drugs, because of their key role in the life-maintenance of the parasites inside the human host, has made more and more interesting the elucidation of the macromolecular organization and of the mechanism of action of such enzymes [29, 71, 119].

In this respect the following sections will provide a detailed description of TGR from Schistosoma mansoni, with insight into the main structural changes

which accompany the redox transformations occurring during the catalytic cycle. The U597C mutant of SmTGR has been crystallized in different redox states: (i) a fully oxidized form [*Structure 1* (1.9 Å)]; (ii) a partially reduced form, obtained either in the presence of NADPH and reduced glutathione (GSH) [*Structure 2* (2.3 Å)] or (iii) with GSH alone [*Structure 4* (1.9 Å)]; (iii) and a species having the fully reduced C-terminal tetrapeptide [*Structure 3* (3.1 Å)], whose relevance for the catalysis will be further explained below. The statistics of the diffraction and refinement data for each of the four structures are summarized in Tab. 4.

	Structure 1	**Structure 2**	**Structure 3**	**Structure 4**
Data collection				
Space group	C2	C2	$P2_12_12_1$	C2
Cell dimensions				
a, b, c (Å)	141.6 102.8, 59.2	141.6, 102.6, 60.0	84.5, 87.4, 185.5	141.6, 102.9, 59.1
α, β, γ (°)	90, 112.4, 90	90, 112.8, 90	90, 90, 90	90, 112.6, 90
Resolution (Å)	40.0/1.9 (2.0/1.9)*	40.0/ 2.3 (2.4/ 2.3)*	30.00/ 3.1 (3.2/3.1)*	40.0/ 1.9 (2.0/ 1.9)*
R_{merge}	0.1 (0.3)*	0.1 (0.4)*	0.1 (0.5)*	0.1 (0.4)*
$I / \sigma I$	12.2 (3.2)*	18.4 (3.8)*	11.8 (2.6)*	9.6 (5.4)*
Completeness (%)	90.1 (92.6)*	100 (99.9)*	99.3 (99.2)*	100 (99.7)*
Redundancy	3.0 (2.8)*	8.1 (7.8)*	7.1 (7.0)*	5.7 (5.7)*
Refinement				
Resolution (Å)	40.0/1.9	40.0/ 2.3	30.0/ 3.1	40.0/ 1.9
No. reflections	52,728	33,294	24,221	58,385
R_{work} / R_{free}	0.19/0.21	0.19/ 0.23	0.22/ 0.29	0.18/ 0.19
No. atoms	4863	4936	9174	5008
Protein	4502	4502	9031	4504
Ligand/ion	106	249	143	139
Water	255	185	0	365
B-wilson	19.0	35.1	63.4	14.6

	Structure 1	Structure 2	Structure 3	Structure 4
B factors				
Overall	18.6	22.5	43.5	14.6
Main chain	17.6	20.1	43.3	13.0
Side chains	19.6	24.7	43.7	16.1
R.m.s deviations				
Bond lengths (Å)	0.008	0.011	0.009	0.007
Bond angles (°)	1.064	1.302	1.164	0.978
Model quality				
Ramachandran plot				
Most favoured	91.4%	91%	86.3	92.6
Additional allowed	8.4%	9.0%	13.5	7.2
Generously allowed	0.2%	0%	0.3	0.2

Table 4: Crystallographic data collection and refinement statistics (* Values in parentheses refer to the highest resolution shell)
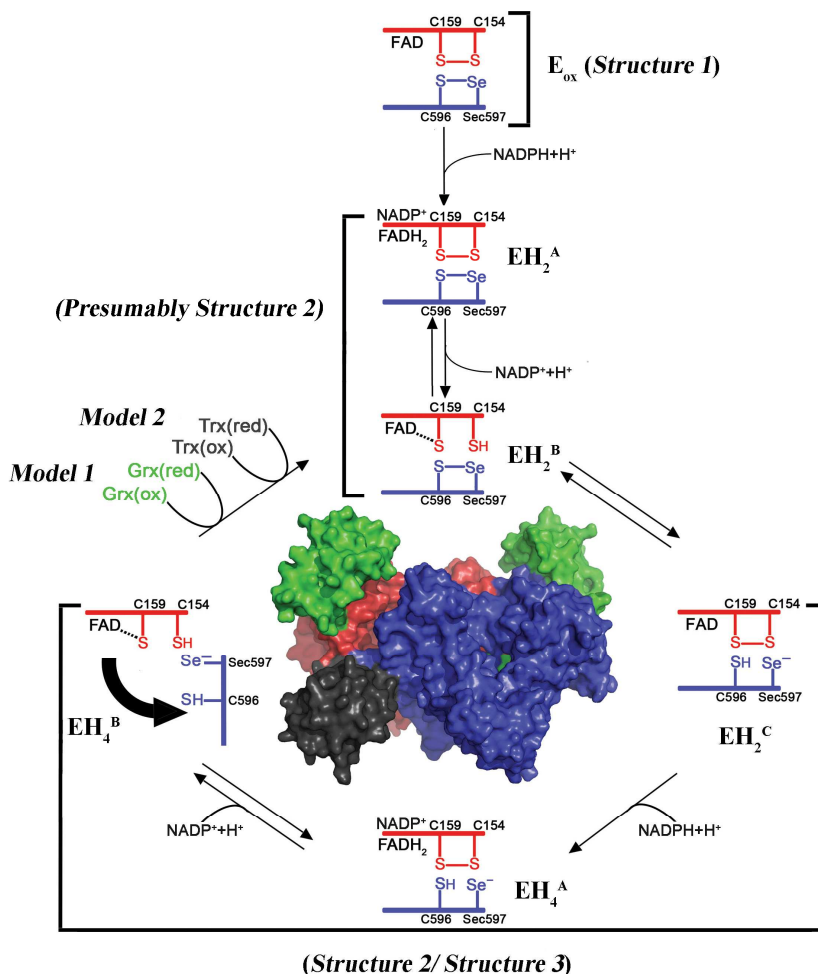
(*Structure 2/ Structure 3*)

Fig. 22: Electron transfer in and out of the TR domain of SmTGR. When NADPH binds to the oxidized state of the enzyme (*Structure 1*), electrons are transferred from the nicotinamide ring to the FAD; reduced FADH$_2$ shuttles electrons to Cys154-Cys159 couple (in red) close to the isoalloxazine ring of FAD (as observed in *Structure 2*), and finally electrons reach the Cys596-Sec597 redox couple on the C-terminal segment of the other subunit (in blue, as observed in *Structure 3*). The C-terminus acts as a flexible arm, which might donate electrons either internally to the Cys28-Cys31 active couple on the oxidized Grx

domain (in green) or externally to various oxidized substrates such as SmTrx (in dark grey). SmTGR redox species populated during the catalytic cycle are shown, from the fully oxidized enzyme (E_{ox}) to the two-electrons reduced forms (EH_2^A, EH_2^B, EH_2^C), to the final four-electrons reduced species (EH_4^A, EH_4^B).

### 4.4.1 The oxidized form of SmTGR (*Structure 1*)

Overall structure: fusion of thioredoxin reductase (TR) and glutaredoxin (Grx) domains

In order to obtain the fully oxidized enzyme, crystals of the U597C mutant of SmTGR were incubated for 48h with a 2mM solution of copper sulphate (see Math&Meth). The resulting oxidized SmTGR represents the first step of the catalytic cycle and is able to accept reducing equivalents from the NADPH donor (*Structure 1,* Fig. 22). The structure was solved at 1.9 Å resolution and the map gave the possibility to fit residues from 6 to 593. The refined model consists of one monomer *per* asymmetric unit. Since the enzyme in solution is a dimer as demonstrated by high resolution gel-permeation (HPLC, result not shown), the crystallographic dimer generated by reflection on the twofold symmetry axis is the biological unit (Fig. 23A-23B).

The overall structure of the enzyme reveals that each monomer results from the unusual fusion of two domains: a smaller Grx domain, ranging from residues 1 to 106 (green in Fig. 23), and a larger TR domain, including residues 107–598 (red and blue in Fig. 23). The Grx domain shows a typical thioredoxin/glutaredoxin fold. The secondary structure of this region, in fact, comprises a central four-stranded β-sheet (the first two β-strands are parallel and the other two are antiparallel) and five surrounding α-helices (Fig. 24). The same fold has been already detected in several isoforms of Grx from eukaryotes, having either a monomeric or dimeric arrangement (PDBcodes: 1Z7R [120], 2HT9, 3C1R [121], 3CTF, 3L4N [122]). The loop comprising residues 103-108 connects the Grx domain of SmTGR, located at the N-terminal portion of the protein, to the large TR domain. The overall fold of the TR domain is typical of a member of the pyridine nucleotide-disulphide oxidoreductase family, thus very similar to the general folding of TR and GR

enzymes. As already discussed for the 3D organization of mammalian TR and GR [117, 118], enzymes belonging to the above-mentioned family usually assemble as functional homodimers, and in each monomer three sub-domains can be recognized: (a) an N-terminal FAD binding domain, (b) a central domain for NADPH-binding, and (c) a C-terminal interface domain. A superposition between rat TR (rTR, PDBcode: 1H6V, [117]) and the oxidized form of SmTGR (*Structure 1*) allowed the identification in the TR portion of the worm enzyme of the corresponding sub-domains, comprised between the following residue ranges: (a) 105-259 and 397-466 (red in Fig. 25), (b) 260-396 (yellow in Fig. 25) (c) 467-593 (cyan in Fig. 25). The first two sub-domains are variants of a Rossmann fold, being composed of a larger five-stranded parallel β-sheet flanked by a smaller three-stranded β-sheet on the one side and a different number of α-helices on the other side (Fig. 25-26). The secondary structure of the third sub-domain shows a central five-stranded antiparallel β-sheet, with four flanking α-helices (Fig. 25-26). The binding site of NADPH and its interaction with the residues surrounding the FAD cleft will be discussed in section 4.4.2, while the monomer-monomer interface will be described in details below.
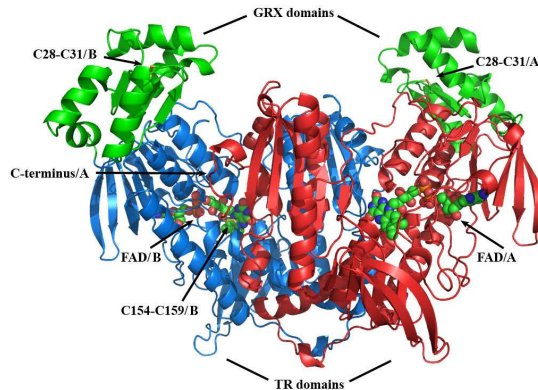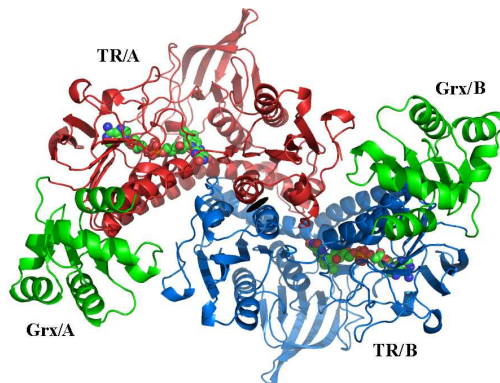
Fig. 23 Panel A: *Structure 1*, SmTGR in its oxidized state. Green: Grx domains; Blue and red: TR domains. The FAD cofactors, one for each monomer, are bound in close proximity of the C-terminal segment of the protein and are shown as spheres. Two redox centers of SmTGR are shown, with the sulphur groups of the reactive cysteine couples (C28-31, C154-159) represented as orange sticks. The third reactive cys couple (C596-C597) is not visible in the electron density map, but the position of the C-terminal arm of monomer A is pointed by an arrow. **Panel B**: same structure as in panel A but the view is from the top, looking down the twofold dimerization axis, shown in black.
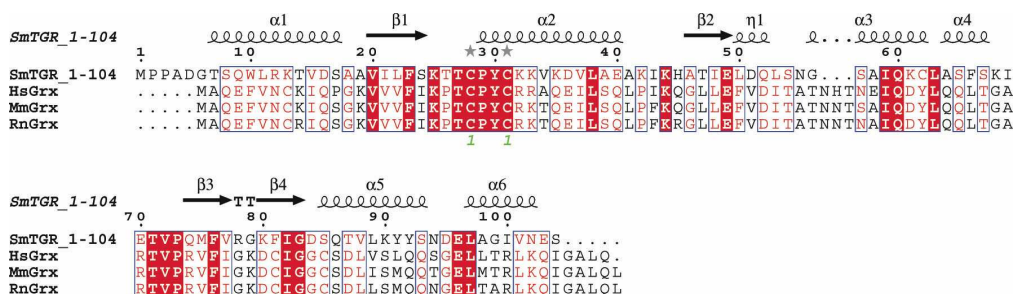
Fig. 24: Sequence alignment between the Grx domain of SmTGR (residues 1-104) and Grx proteins from different organisms: Homo sapiens (Hs), Mus musculus (Mm), and Rattus norvegicus (Rn). The alignment files obtained with ClustalW have been visualized with ESPript. The secondary structure of the Grx domain of SmTGR is shown in the top line. Identical residues are boxed in red, similar residues in red, non-conserved residues in black.
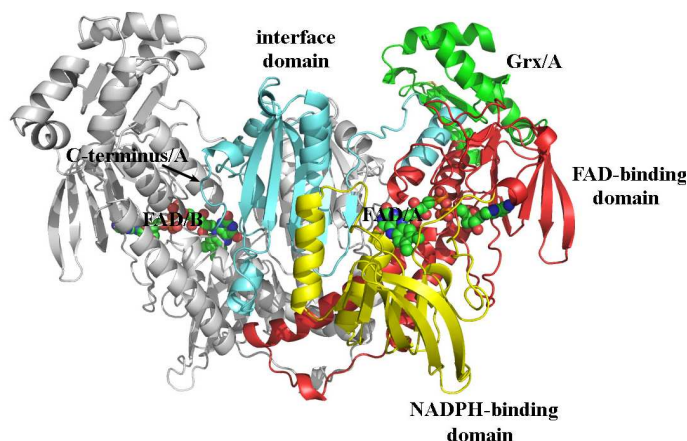

Fig. 25: Localization of the three sub-domains comprised in one monomer (A) of SmTGR. Red: FAD binding domain; yellow: NADPH-binding domain; cyan: interface domain. The adjacent monomer of SmTGR is shown in light grey. The position of the C-terminal segment of monomer A (close to the FAD binding site of monomer B) is pointed with an arrow.

Fig. 26: Sequence alignment between SmTGR and TGR, TR and GR from different organisms. Hs= Homo sapiens; Mm= Mus musculus; Rn= Rattus norvegicus. The alignment files obtained with ClustalW have been visualized with ESPript. The secondary structure of SmTGR is shown in the top line. Identical residues are boxed in red, similar residues in red, non-conserved residues in black.

A structural superposition between a monomer of U597C oxidized SmTGR and those of both human GR (hGR, PDBcode: 3DJG) and the U498C mutant of human TR (hTR, PDBcode: 2ZZ0) shows that some structural features make SmTGR more similar to TRs than to GRs (Fig. 27). In common with TR, SmTGR presents 16 extra residues (carrying the Gly-Cys-Sec-Gly consensus sequence) at the C-terminus, which is absent in GR. Moreover two insertions in the schistosoma enzyme (residues 139–149, and residues 238–245) can be exactly superimposed to analogue sequences in hTR but do not have an equivalent portion in hGR (Fig. 27). The same features are evident from a superposition of SmTGR with rTR (1H6V) (results not shown). The two loops resulting form these insertions seem to shield the adenine of the FAD, which is more buried in TGR and TR if compared with GR enzymes [117]. A unique feature in the structure of SmTGR, absent in other members of the GR family, is an extended and solvent accessible mobile loop (residues 359–364), constituted by a group of polar residues (D-T-E-N-N-K), positioned at the bottom of the structure under the FAD binding site. This loop lies below two β-strands (residues 347-356 and 367-375) belonging to the NADPH binding domain (Fig. 27).
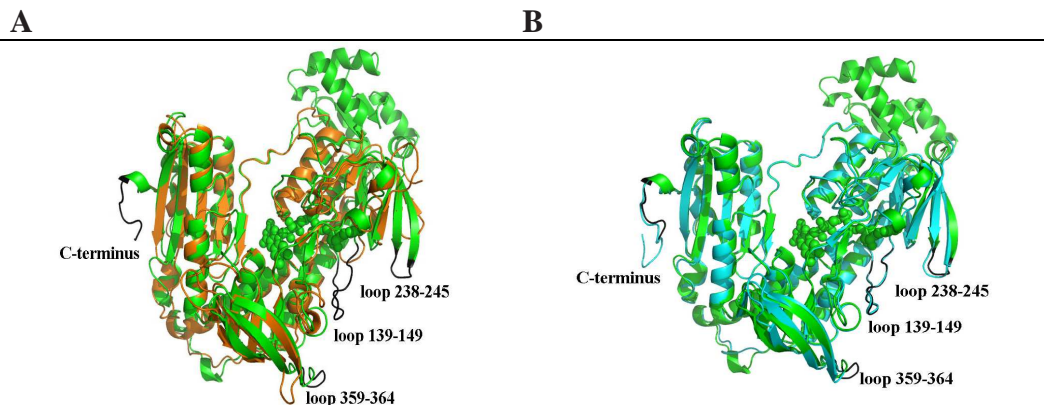

Fig. 27: Superposition of the 3D structure of monomer B of oxidized SmTGR with either one monomer of hTR (Panel A) or hGR (Panel B). Green: SmTGR; orange: hGR; cyan: hTR. In black are shown the

regions of the worm enzyme which makes it more similar to TR than to GR enzymes.

The dimer interface

Dimerization in SmTGR occurs through the larger TR domains and results in a distorted ''W'' structure, with the two Grx domains positioned at the top of each outer arm of the W (Fig. 23A). The monomer–monomer contact area is composed of an antiparallel five stranded β-sheet, flanked on each side by two α-helices (α16–α17 on one side and α18-α19 on the opposite side) and a 3_{10} helix (η6 on one side and η7 on the other). For the sake of clarity the nomenclature of the secondary structure elements is the same shown in the sequence alignment in Fig 26.

The total surface area buried in the dimer interface (4120 Å^2) is mostly due to complementarity of residues within the helices α18 of both monomers, with a central role played by a network of Van der Waals interactions, mainly involving residues G550, Y551, V553, A554 and I555 from each monomer. A series of symmetric polar contacts participate also to the dimerization of the protein, and engage the following couples of residues: E546-S575/N (2.9 Å), Q549-E576/N (3.6 Å), Q549-I570/N (2.8 Å), where the former residue belongs to one monomer and the latter comes from the adjacent monomer. Moreover E509 forms also a polar contact with K163 of the FAD binding domain of the adjacent monomer (2.9 Å). Most of these residues are conserved in TRs (Fig. 26).

Just at the bottom of the interface region carrying the above residue couples, there is an additional contact area between the monomers that worth to be mentioned, because it has been demonstrated to be involved in the binding of noncompetitive inhibitors in hGR (PDB code: 1XAN, [123]). It is a large cavity, leaned by couples of hydrophobic residues coming from both monomers (F78, V74, L438, W70, Y407 in hGR). This cavity is present also in SmTGR, but it is coated by more polar residues (A174, L170, P542, H166, E509) and these residues are highly conserved between SmTGR and hTR. Thus it can be summed up that the sequence identity of the dimer-dimer interface of SmTGR is higher with TR than with GR,

even if the interface region is similar among the three enzymes, given that the largest contact area is due to α18 helices from each monomer.

The FAD binding site

Each TR domain of SmTGR contains a large cleft which hosts the FAD cofactor. The two symmetric FAD binding sites are both located at the interface and each noncovalently bound cofactor interacts with residues from both TR domains (Fig. 23A-28), as typical of TRs and GRs [117, 118]. Like in other FAD-disulfide oxidoreductases, the FAD is bound in an extended conformation and most of the neighboring residues are conserved in the GR superfamily. The adenine is bound in a polar pocket closed on the top by a salt link between K399 and E140 (NZ/K399-OE1/E140 = 2.7 Å). The isoalloxazine ring is sandwiched between Y296 (on-face OH-N10 distance of 3.4 Å) and the couple C154-C159 (C159 SG-N1 distance of 3.2 Å), which is oxidized in this structure (Fig. 28). Y296 and the Cys couple are invariant in GR and TR enzymes (Fig. 26).
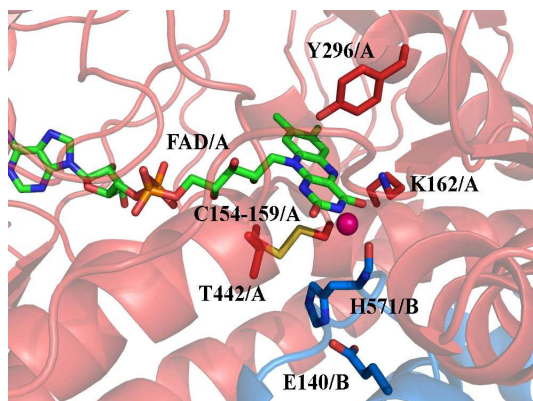

Fig. 28: FAD binding site in the oxidized SmTGR. The FAD cofactor bound to monomer A (red) is here shown. The surrounding residues mainly involved in the formation of H-bonds with the cofactor are shown in sticks. The pink ball represents the water molecule which mediates the contact between O2 of the flavin and the peptidyl N of H571/A.

The FAD ring is firmly kept in place by a network of H-bonds, with residues coming from both monomers. In particular, O4 of FAD/A is at 2.8 Å distance from NZ of K162/A, on the same side of the S-S bridge formed by C154-C159/A. N3 is at 2.7 Å from the mainchain O of H571 of the other monomer (B), and O2 contacts the peptidyl N of H571/B via a water molecule (O2-HOH71 = 2.6 Å; HOH71-N/H571 = 3.0 Å); O2 is also at H-bond distance (3.0 Å) from N of T442/A (Fig. 28). This architecture leaves atoms N1 and N5 of the FAD cofactor free to react respectively with C159, on one side, and the nicotinamide ring on the other, the latter only after displacement of Y296 (see section 4.4.2). Furthermore, the side chain of H571/B is oriented between the carboxyl group of E576 of the same monomer and the S-S bridge of the adjacent monomer (Fig. 28). H571 may be important for the S-S bridge reactivity, because its stereochemistry and the spherical shape of its electron density suggest a torsion movement, which could bring ND1 alternatively toward E576 and C154.

The redox centers

The enzymatic activity of SmTGR, aimed to transfer reducing equivalents form NADPH through the enzyme and then to the SmTGR oxidized substrates, basically involves a series of disulphide exchange reactions. Thus the cysteine residues of the protein play a crucial role in the catalysis. SmTGR contains 15 Cys *per* monomer, three of them located in the Grx domain and 12 in the TR one, including the C-terminal Sec597, which is mutated in Cys in the enzyme here described. At least six of these Cys are conserved in couples and are known to change their oxidation state during the catalytic cycle: (i) C154 and C159 located directly on top of the FAD cofactor (Fig. 23A-28); (ii) C596 and Sec597 at the C-terminal end of the polipeptidic chain; (iii) C28 and C31 placed in the Grx domain (Fig. 23A). In this structure of the U597C mutant the redox couple C28-C32 of the Grx domain and the C154-C159 couple of the TR domain are both fully oxidized, the distances between the two sulphurs being 2.1 Å in both cases. The position of Y296 is also consistent with this state, the aromatic ring being perpendicular with the isoalloxazine ring of FAD.

4.4.2 The complex SmTGR-NADPH (*Structure 2*)

With the aim to determine the structural changes associated with the binding of NADPH to SmTGR in the first step of the catalytic cycle, when a NADPH molecule transfers reducing equivalents to the oxidized enzyme, the U597C mutant of SmTGR has been crystallized in the presence of NADPH. The structure of the complex has been determined at 2.3 Å resolution (*Structure 2*, Fig. 22). Because of the presence of reduced glutathione (GSH) in the crystallization buffer also this reductant could be detected in the electron density maps, hence the whole refined model consists of one monomer per asymmetric unit, plus one FAD, one NADPH and two GSH molecules.

By and large *Structure 2* differs from *Structure 1* mainly for the oxidation state of the redox site onto the Grx domain and for slight side chain movements of some residues in the FAD and NADPH binding pockets. The C28-C31 couple in fact is here reduced, probably as a consequence of an excess of GSH present in the crystallization buffer; while C154 and C159, the two active residues on the *si-face* of the isoalloxazine ring of FAD, are found in both redox states. In this respect Cys154 appears in a double conformation (each with 0.5 occupancy), while C159 maintains the same position shown in *Structure 1*. Thus the distance between the two sulphur groups is 3.1 Å in the reduced state and 2.1 Å in the oxidized one. Moreover, C159 is at 3.2 Å from C4 and C10 of the isoalloxazine ring of FAD and might be implicated in a charge transfer complex, as already observed in human GR (pdb code: 3djg, [118]). The reduced C154 forms a H-bond with a water molecule (2.7 Å), kept in place by H571 of the adjacent monomer (Fig. 29A). H571 might have a role in the stabilization of the FAD-thiolate charge transfer complex, as it has been already hypothesized for the corresponding Hys residue in TR from *Drosophila melanogaster* crystallized in the presence of excess NADPH [124].

The NADPH binding site is mainly composed by three loops involving residues 292-297, 317-324, and 391-393. NADPH binds on the *re-face* of FAD (*si-face* and *re-face* of FAD are assigned following the rules of Hanson K.R. [125]), and is stabilized by the following electrostatic interactions: a cation-π bond between

R317 and the adenine; a salt bridge between R322 and the phosphate on ribose C2; and two H-bonds between S295-NADPH(AO2) and S318- NADPH(AOP2). The nicotinamide ring of NADPH is sandwiched between the isoalloxazine ring of FAD (at a distance of 3.8 Å) and the aromatic ring of Y296 (3.6 Å) (Fig. 29A). Y296 swings upon NADPH binding, and is stabilized in this new position by hydrophobic contacts between the phenol ring and the side chains of P324 and V473 (as also reported for human TR, [117]).

GSH has been detected in two distinct sites of the structure. The first one lies in the Grx domain and will be described below in *Structure 4* (see section 4.4.4). The second GSH is found in the TR domain, in a pocket formed by one α-helix (L397-T404), a β-strand (K227-L230) and the nucleotide moiety of the FAD. The Cys of GSH is engaged in a disulfide bond with C402 (2.1 Å). The rest of the molecule is stabilized by polar contacts with K227, G228, R229 and L230. Moreover the carboxylate group of the γ-glutaminyl end is at 2.9 Å from FAD adenine amine group (Fig. 29B). The binding of one GSH molecule in the TR domain is accompanied by a change in the conformation of the region in between residues 397-404, if compared to the unliganded structure (PDB code: 2v6o, [75]) (Fig. 29B). The presence of GSH forces the loop 397-404 to turn around two pivot residues (L397 and T404) and to acquire a 2-turn α-helix structure. As a result, the hydrophobic side chains of V400 and L401 are exposed to the solvent and GSH takes the place previously occupied by the loop (Fig. 29B). The presence of NADPH/NADP$^+$ in its binding site might be somehow correlated with the glutathionylation of C402, given that (i) attempts to co-crystallize the enzyme with NADPH in the absence of GSH were always unsuccessful; (ii) the change in conformation of the above mentioned loop is close to the gate of the NADPH binding site (Fig. 29B). At the moment we are unable to propose a rationale to the concomitant presence of the two ligands, especially in view of the fact that C402 is not a member of a redox cys couple.
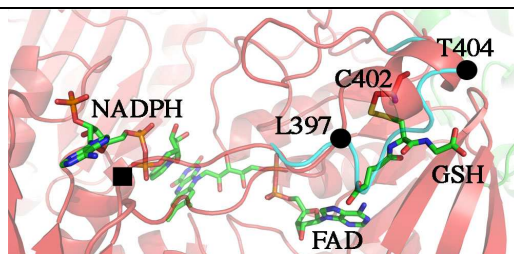
A
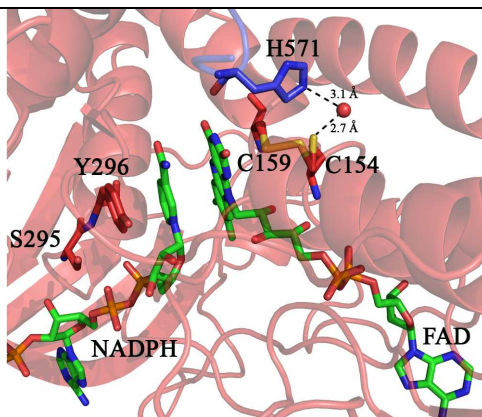
B

Fig. 29: NADPH and GSH binding sites in *Structure 2*. **Panel A.** Zoom in the FAD active site. The NADPH and FAD are shown in green sticks, Y296, S295, C154, C159 in red sticks, while H571 of the partner subunit is shown in blue sticks. Upon NADPH binding, the loop 292-297 changes conformation re-orienting the side chains of S295 and Y296 with respect to *Structure 1* in order to make room for the reductant. The C159-C154 couple is partially reduced and accordingly C154 is found in a double conformation. In the reduced conformation (50% occupancy) the sulphur of C154 points towards the solvent and is in contact with a water molecule (2.7 Å, shown as red ball), which is kept in place by H571. **Panel B**. The GSH binding site on TR domain of *Structure 2*. The GSH (in green sticks) is found in a position that in other TGR structures is usually occupied by the loop 397-404 (in cyan ribbon). The ligand is found in a pocket formed by one α-helix (L397-T404), a β-strand (K227-L230) and the nucleotide moiety of the FAD. GSH makes a mixed disulphide with C402 and forces the loop 397-404 to adopt a α-helical secondary structure (in red ribbon) by turning around two pivot residues L397 and T404 (shown as full black circles). One of the gates of the NADPH binding site (black square) is four residues upstream of L397.

4.4.3 The C-terminal reduced form of SmTGR (*Structure 3*)

The structure of the U597C mutant of SmTGR showing its C-terminal segment in the fully reduced state (*Structure 3*), solved at 3.1 Å resolution, is unique among the four structures here reported in that it presents a $P2_12_12_1$ space group. The main differences between this structure and the others reported so far (pdb codes: 2v6o, 3h4k, *Structure 1*, and *Structure 2*) are the presence of the physiological dimer in the asymmetric unit and the structuring of the C-terminal arm, whose density is visible in one of the two monomers.

The low resolution did not permit an accurate estimate of the redox state of the cysteine couple at the FAD active site (C154-C159) and at the Grx redox site (C28-C31), because (i) the slight configurational change of C154 with respect to C159 upon reduction (~ 1.0 Å. see *Structure 2*) would be hard to detect , also in view of the fact that the electron pair is shared between the FAD and the C154-C159 couple, leading to the latter being only partially reduced, as in *Structure 2* (consistent with the rapid kinetic experiments, see section 4.5.2); and (ii) both the Grx domains are characterized by high mobility indicated by the high B factors. In fact too weak electron density did not permit the assignment of the first five residues at the N-terminus of both monomers, as well as of the last five residues at the C-terminal portion of monomer A. On the contrary a stronger electron density allowed the building of the entire C-terminal segment of monomer B, implying a structural asymmetry in the organization of the two monomers. A second evidence of this asymmetry comes from the different thermal factors of the two Grx domains (residues 7-104): the Grx portion of monomer A being rather less mobile (overall $<B> = 57.0$ Å^2) than the Grx domain of monomer B (overall $<B> = 88.6$ Å^2).

The terminal tetrapeptide G-C-C-G, as it appears in the electron density map, is fully reduced, the two cysteine residues (C596-C597) being in a trans position with respect to the main chain and pointing their sulphur atoms toward the solvent (Fig. 30). The positioning of the C-terminus is permitted by a kink centered on residue K586. This conformation is stabilized by several H-bonds and salt bridges (listed in Tab. 5), mostly with residues of the B monomer. Hence the C-terminus of

the B monomer lies in the central cavity of SmTGR W-shaped homodimer, with the terminal tetrapeptide, containing the catalytic cysteines, located at only 13 Å from the C154-C159 redox couple of the FAD catalytic site of monomer A, a distance compatible with the reducing activity of the C-terminus (Fig. 30).

4.4.4 The complex SmTGR-GSH (*Structure 4*)

In the absence of NADPH, only one molecule of GSH *per* monomer was found in the electron density map. It is located at the redox site on the Grx domain, as already quoted for *Structure 2*. The 3D structure of U597C SmTGR in complex with GSH was determined at 1.9 Å resolution (*Structure 4*), the refined model consisting of one monomer per asymmetric unit, with residues ranging from 6 to 593, as in the previous structures here presented.

Electron density of the GSH molecule was detected in the proximity of C28, the redox active site of the Grx domain (Fig. 31). The distance between the sulphur atoms of C31 and C28 is 3.2 Å, suggesting that these Cys are reduced, as expected, given the high GSH concentration present in the crystallization conditions. As observed in *Structure 2* the C154-159 couple is partially reduced, probably as a result of the reversible electron transfer between $FADH_2$ and the close cys couple. The average B-factor of the GSH ligand is slightly higher (by ~5 $Å^2$) than that of its surrounding residues. The GSH is kept in place by the following H-bonds established with the surrounding residues: (i) S85 binds the γ-glutamyl moiety (OG/S85-O12/GSH = 2.5 Å; N/S85- O11/GSH = 2.9 Å); (ii) V72 forms two H-bonds with the central region of GSH (O/V72-N2GSH = 3.0 Å; N/V72-O2/GSH = 2.8 Å) orienting the sulphur atom towards the redox active site of the Grx domain (3.4 Å is the distance between the sulphur of GSH and the sulphur of C28); and (iii) Q60 and K25 bind the glycine moiety of the ligand (NZ/K25-O32/GSH = 2.8 Å; NE2/Q60-O31/GSH = 2.9 Å) (Fig. 31).
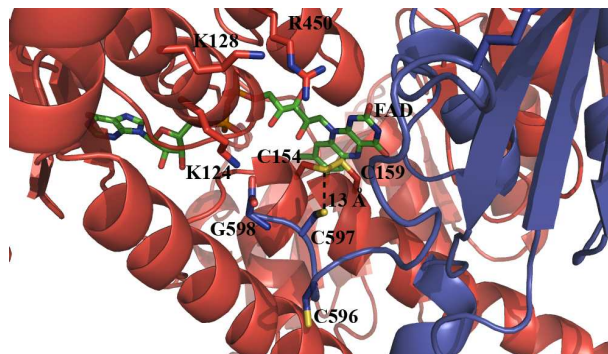
Fig. 30: Ribbon representation of the C-terminal region of monomer B in *Structure 3*. The two catalytic Cys belonging to the C-terminal arm (C596, C597), shown in blue sticks, are both reduced; C597 is located about 13 Å from C154-C159 couple (see text). The positively charged residues K124, K128 and R450 of the adjacent monomer involved in the stabilization of the C-terminal arm are shown in red sticks.

C-terminal residue (monomer B)	Residues from monomer A	Residues from monomer B	Distance (Å)
V583(O)		H502(N)	3.0
T584(OG)		S587(OG)	2.9
K585(N)		V500(O)	2.9
K585(O)		G588(N)	2.8
K585(NZ)		E327(OE1)	2.8
K585(NZ)		Q327(OE1)	2.8
P591(N)		N504(O)	3.3
V593(N)		N518(OD1)	2.7
G598(O)	K124(NZ)		2.4

Table 5: Polar contacts between the C-terminal arm and the TR domain of SmTGR accordingly to *Structure 3*.
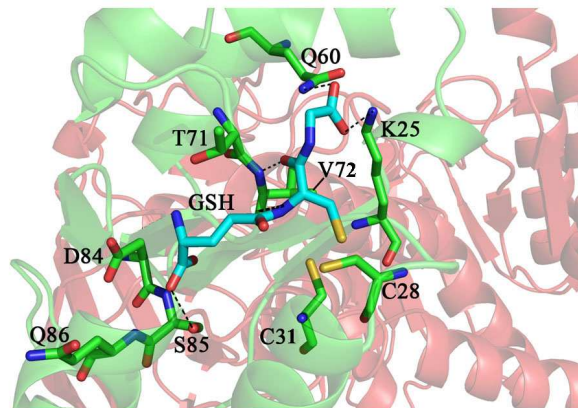
Fig. 31: The GSH binding site on the Grx domain in *Structure 2* and *4*. GSH (in cyan sticks) is in a pocket above the redox site of the Grx domain (C28-C31, in green sticks). Residue surrounding the ligand are shown in stick and polar contacts are represented by dotted lines. The GSH sulphur points towards C28 and its position is stabilized by contacts with V72. The carboxylate of the glutamic acid of GSH is H-bonded to Q60 and K25.

4.5 Functional studies on SmTGR

With the aim to assess the ability of the U597C SmTGR mutant used in our crystallographic studies to reduce its physiological substrates, a functional characterization of the enzyme has been carried out. Both stopped-flow and spectrophotometric experiments are described in the following sections. A comparison with the activities of the truncated SmTGR, lacking the C-terminal tetrapeptide (SmTGRtr), and those of the wild-type SeCys-containing enzyme (SmTGRwt) are also presented, in order to clarify the role played by the C-terminus in SmTGR catalyzed reactions.

4.5.1 Enzymatic activities of U597C SmTGR

The reducing activity of the enzyme has been tested towards various substrates, i.e.: (i) DTNB and Trx, to assess the functionality of the TR domain; (ii) the mixed disulphide formed by hydroxyethil-disulfide (HED) and GSH in the

presence of yeast GR, to evaluate the Grx activity of the enzyme; and (iii) the oxidized glutathione (GSSG) to measure the GR activity (see Chapter 3).

	DTNB reduction	Trx reduction	Grx (+yeastGR)	GR
[§]SmTGRwt	114	6.37	1867	71.5
SmTGRtr	710	N.D.	220	205
U597C SmTGR	90	202	430	N.D.

Table 6: Km (μM) for different enzymatic reactions
[§] values taken from Kuntz et al. [29]

	DTNB reduction	Trx reduction	Grx (+yeastGR)	GR
[§]SmTGRwt	16	30	17.8	21.7
SmTGRtr	1.2	N.D.	6.44	0.19
U597C SmTGR	0.98	0.085	6.0	N.D.

Table 7: kcat (s^{-1}) for different enzymatic reactions
[§] values taken from Kuntz et al. [29]

Relatively to DTNB reduction and Grx activity, the U597C SmTGR behaves like SmTGRtr, having similar steady state parameters (Tab. 6-7). However differently from the Sec-containing enzyme, in both mutants the Grx activity is detectable only if external GR is added (data not shown). Taken together these results prove that the U597C mutant has both functional FAD active site and Grx domain, but the U597C mutation prevents the internal transfer of reducing equivalents from the C-terminus to the Grx domain. Moreover U597C SmTGR is able to reduce SmTrx in the insulin assay (see Chapter 3), contrary to the truncated form, even if the enzyme turnover is low if compared with the wild-type enzyme (Tab. 7). This datum indicates that the C-terminus of the crystallized U597C mutant is functional, but confirms the hypothesized role of Sec in improving the catalytic efficiency of the enzyme [117]. Finally U597C SmTGR does not present a detectable activity (up to 4 μM enzyme) in reducing GSSG (GR activity), as opposite to the wt enzyme [29] and to the truncated enzyme [75] (Tab. 6-7). Although at the moment it is not possible to formulate an obvious explanation to this observation, some hypothesis may be advanced. On the one hand the fact that the Cys mutant does not retain any GR activity, with respect to the truncated form of the enzyme, could be explained recalling the hypothesis that the entire C-terminal arm of the enzyme may hinder the entrance of GSSG in its reducing site giving their structural resemblance [117]. On the other hand the behaviour of the U597C mutant in comparison with the wt enzyme suggests that Sec has a central role in the reduction of GSSG onto the Grx domain. In this respect the substitution Sec to Cys (Sec pK_a= 5.2; Cys pK_a= 8.5; [126]) determines a different net charge on the C-terminal arm, which might hinder its movement towards the Grx domain. In conclusion, the following hypotheses may be proposed: (i) the GR activity of the wild type SmTGR is mainly due to the reduction of GSSG by the Grx domain, which in turn is internally reduced by electron transfer from the $FADH_2$, *via* the C154-C159 couple and the C-terminal arm. (ii) The GR activity of the truncated SmTGR is GR-like, i.e. is due to the binding of GSSG in proximity of the C154-C159 couple on the TR domain. (iii) In the mutant U597C the GR activity is

undetectable because the internal reduction of the Grx domain is inefficient, due to the mutation, and because the C596-C597 couple on the C terminal arm competes with GSSG for binding to the C154-C159 couple.

4.5.2 Reductive and oxidative half reactions of U597C SmTGR

The reduction of U597C SmTGR by NADPH and the further oxidation of the reduced enzyme by its physiological substrate SmTrx has been studied by mean of time resolved spectroscopy and the results are reported below. Both processes are referred to as "half-reactions" being representative of the electron entry into and exit from SmTGR respectively.

The former reaction was followed in a stopped-flow experiment in which the concentrations of both the enzyme and NADPH were systematically varied, in order to determine the order of the reaction and the kinetic constants (see Chapter 3). Since the two reagents (NADPH and SmTGR) are required, the process is expected to be a second order bimolecular reaction. Fig. 32A shows the absorption spectra of U597 SmTGR, recorded as a function of time, after the addition of NADPH. The wavelengths of 460 and 560 nm have been selected for further analysis, being representative of the spectral changes of the FAD cofactor (the absorption at 460 is due to the oxidized flavin) and of the charge transfer complex formed between FAD and the C154-C159 couple (detected at 560 nm) [127]. The time course recorded at 460 nm (Fig. 32B), corresponding to the experiment reported in panel A, is biphasic and may be fitted to a two step pseudo-first order sequential mechanism, using the integrated equation developed by Bateman [128]. The rate constants obtained are both second order, with values of 4×10^6 and 1×10^6 $M^{-1}s^{-1}$, for the first and second step of the reaction respectively (Fig. 32B).

The time resolved spectra and the overall behavior of the reaction resembles those recorded under similar experimental conditions for TR from *Drosophila melanogaster* (DmTR) [127]. The main difference between DmTR and SmTGR behavior may be detected in the spectral region around 680 nm, where in DmTR a change in absorbance during the reduction reaction is ascribed to the formation of a

transient charge-transfer complex between $FADH_2$ and $NADP^+$. No spectral changes could be visualized around 680 nm for the schistosoma enzyme, probably indicating that the charge-transfer complex does not accumulate in the reaction.

By means of absorbance spectroscopy, the re-oxidation of SmTGR (reduced by stoichiometric amounts of NADPH) by the physiological substrate SmTrx has been also followed. This reaction is accompanied by a decrease of absorbance at 550 nm and an increase of the peak at 460 nm, as a result of the progressive oxidation of the flavin (Fig. 32C). The time course at 460 nm is shown in Fig. 32D, and is well described by a second order rate constant of 0.8×10^4 $M^{-1}s^{-1}$. This value is approximately two orders of magnitude lower than that reported by Kuntz *et al.* for the wild type enzyme [29], consistent with the important role played by Sec in the reduction of the physiological substrate.

In conclusion both the reduction and oxidation half cycles of SmTGR are rate limited by second order kinetic processes, and accumulation of a Michaelis type complex does not occur at the concentration used.
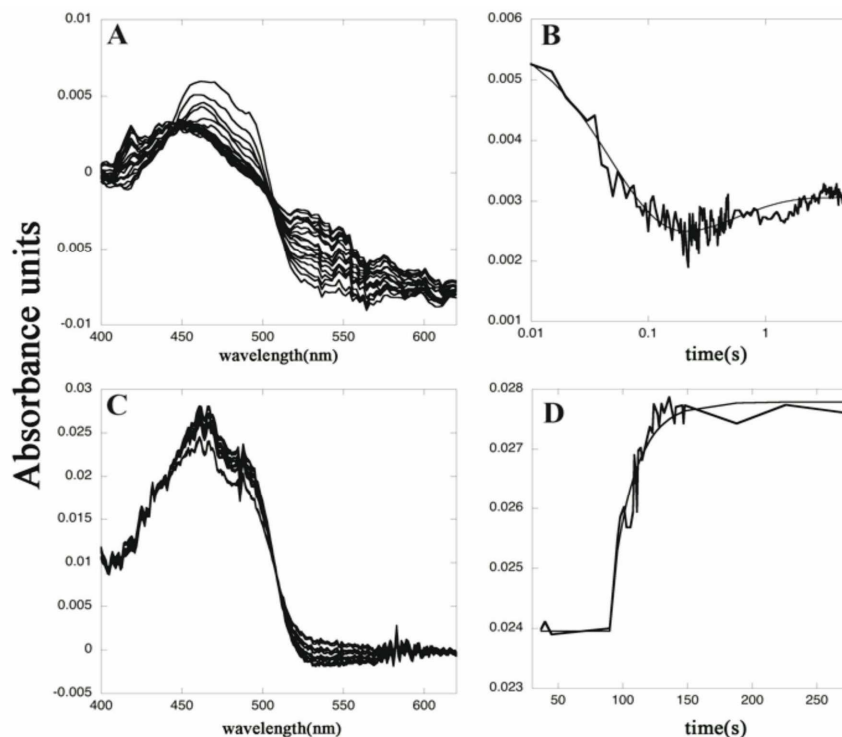
Fig. 32: Reductive and oxidative half reactions of U597C SmTGR, spectrophotometric experiments. **Panel A**. Spectra of 3.5μM U597C SmTGR reduced with 5μM NADPH recorded in a stopped-flow apparatus. The decrease of the FAD peak at 460 nm and the increase of the absorbance around 550 nm due to the formation of the charge transfer complex are shown. Spectra were recorded every 5ms from 5 to 500 ms and then every 50 ms up to 5500 ms. **Panel B**. Time course recorded at 460 nm relative to the experiment reported in Panel A fitted with a double exponential. The first process is assigned to the reduction of the FAD by NADPH ($k = 4x10^6 \, M^{-1}s^{-1}$) to form the two electrons reduced species EH_2; the second one is the perturbation of the cofactor spectrum due to the formation of the EH_4 species ($k = 1x10^6 \, M^{-1}s^{-1}$). **Panel C**. Spectra of reduced U597C SmTGR (3.0μM) oxidized by SmTrx (7 μM) recorded in a spectrophotometer apparatus. The decrease of absorbance of the charge transfer complex around 550 nm and the increase of the FAD peak at 460 nm are shown. **Panel D**. Time course at 460 nm relative to the experiment reported in Panel C fitted to a single exponential. The second order process is assigned to the oxidation of the $FADH_2$ of SmTGR by SmTrx ($k = 0.8x10^4 \, M^{-1}s^{-1}$).

87

4.6 Modeling of the complexes mediating the electron-transfer from SmTGR to both Grx domain and SmTrx

Unfortunately, the observations coming from X-ray crystallography presented above lack details about the last steps of the catalytic cycle of SmTGR, i.e. the transfer of reducing equivalents from the C-terminus of the enzyme to either the Grx domain or the SmTrx. Hence two models are proposed below for both the interaction of the C-terminal arm with the Grx domain (*Model 1*) and the complex formed between SmTGR and SmTrx (*Model 2*). *Structure 3* and *Structure 4* of U597C SmTGR and the structure of oxidized SmTrx (PDB code: 2XBI) have been used in the modeling. A brief description of the 3D organization of SmTrx, which has not been presented in the preceding sections, is summarized below.

SmTrx presents the typical thioredoxin fold, made up by a five-stranded β sheet ($\beta1-5$) capped on each side by two α helices ($\alpha1,3$ and $\alpha2,4$) [112] (Fig. 33). The conserved active site amino acids W33–C34–G35–P36–C37 link the strand $\beta2$ to helix $\alpha2$, and are arranged in a $\beta-$turn shape. The redox site formed by C34 and C37 is oxidized, the distance between the two sulphurs being 2.1 Å. This cysteine pair is shielded from the solvent by the C-terminal portion of helix $\alpha2$ and by the loop between $\alpha3$ and $\beta4$ and by the active site loop itself. As a result of this architecture, C34 works as the nucleophilic cysteine towards its substrates, being more exposed to the solvent, while C37 is buried and could act as the resolving cysteine [129]. Both the aspartate (D28) and the H-bonded water molecule (D28(OD1)-O = 2.7 Å) responsible for the deprotonation of the resolving cysteine (C37) during the redox cycle, are present (Fig. 33).
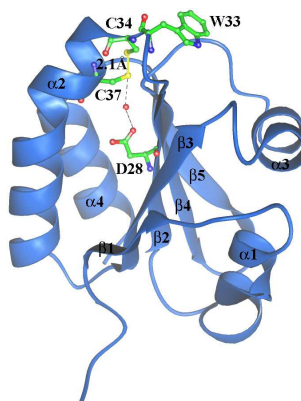
Fig. 33: Cartoon representation of the 3D structure of the oxidized form of SmTrx, showing the typical thioredoxin fold. Residues known to be relevant for the catalysis are represented in sticks.

4.6.1 Model 1. The C-terminus of SmTGR onto the Grx domain

The starting point for this model is represented by the superposition of the two C-terminal residues (C597 and G598), visible in *Structure 4* of U597C SmTGR, to the analogue residues (Cys and Gly) of the GSH molecule bound onto the Grx domain in *Structure 4* of the same enzyme (see Chapter 3). After the structural superposition, using K586 as pivot residue, a simple rotation on the psi angle of K586 of monomer B (in blue in Fig. 34A-34B) brings the C-terminal arm onto the redox site of the Grx domain of the adjacent monomer A (in red in Fig. 34A-34B).

The model clarifies the functional role of the TGR dimer. Indeed, the dimerization is made necessary by the fact that the Grx domain of each monomer is much closer to the C-terminal arm of the opposite monomer (~ 20 Å) than to the C-terminal arm of the same monomer (~ 65 Å); distances were measured between C28 of both monomers and K586 of monomer B as found in *Structure 3*.
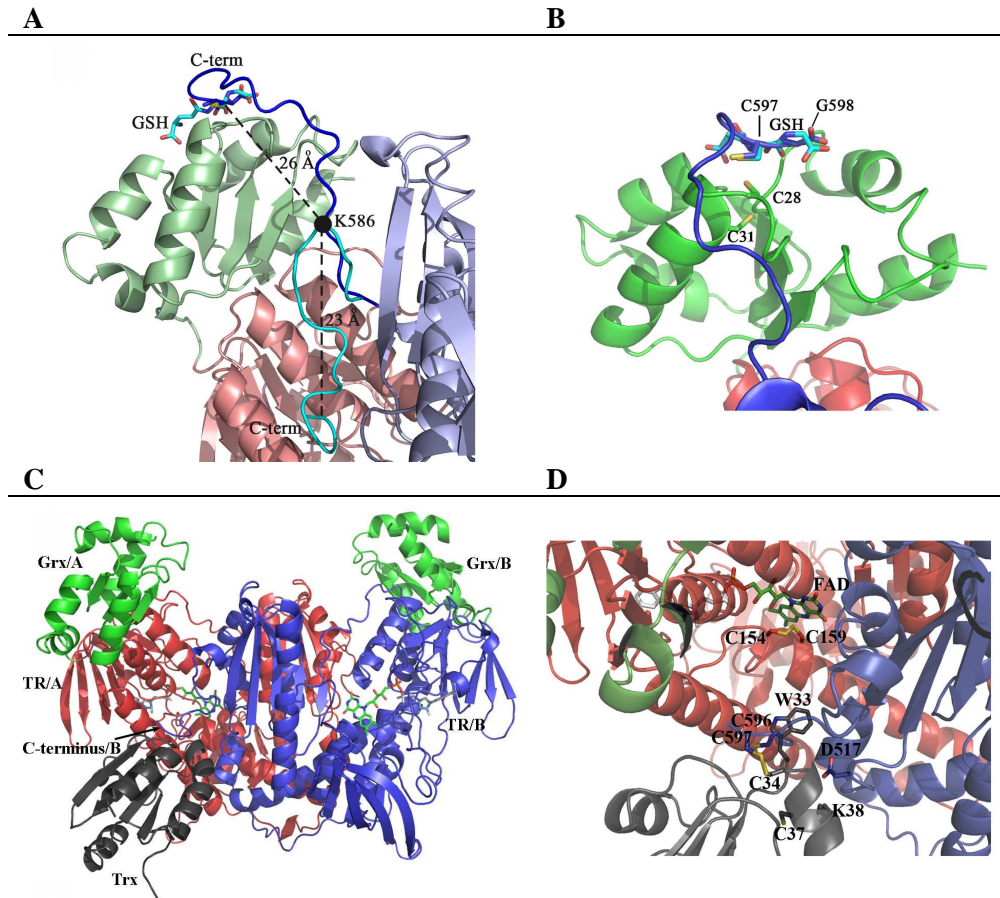
Fig 34: Model of the interaction between the C-terminus of SmTGR and the Grx domain. **Panel A**: Superposition between *Structure 3* and *Model 1*. A rotation on the pivot residue K586/A (visualized as a full black circle) brings the C-terminus of monomer B from the position found in *Structure 3* (in cyan) to the Grx domain of monomer A (from *Model 1*, in blue). The superposition between the last two residues of the C-terminus (C597-G598 in blue sticks) and the analogue residues of GSH (in cyan sticks, as bound in *Structure 4*) is also shown. The distances between Cα of K586 and Cα of C597 and between the former and the Cα of the GSH Cys are shown. **Panel B**: Zoom of the superposition between C597-G598 (blue sticks) of the C-terminal arm and the GSH (cyan sticks)

onto the Grx redox site (green sticks). **Panel C:** *Model 2*. The relative location of SmTrx and SmTGR in the modelled complex is shown (SmTrx in grey; subunit A in red and subunit B of SmTGR in blue; Grx domains in green. **Panel D:** The SmTrx binding site on SmTGR in *Model 2*. The magnification allows to visualize the redox sites of both enzymes. The main side chains involved in the contact between SmTrx and SmTGR are shown in sticks.

4.6.2 Model 2. The complex between SmTGR and SmTrx

With the aim to find a docking surface for the external substrate SmTrx, a surface complementarity search between the two proteins was carried out, followed by automated cycles of restrained refinement in order to minimize the energy and regularize the geometry, avoiding possible clashes (see Chapter 3). SmTrx can be docked onto U597C SmTGR in a surface cleft at the bottom of the TR domain, opposite to the Grx domain (Fig. 34C-34D). This cleft, formed by residues belonging to the C-terminus of monomer B and to the FAD binding site of subunit A, has a complementary surface to the stretch from W33 to K38 of SmTrx, which contains the active site couple C34-C37. In particular, W33 of SmTrx fits into a hydrophobic pocket formed by residues of monomer A of SmTGR (V155, I160, L164, L208); K38 of SmTrx is engaged in a salt bridge with D517 of the subunit B of SmTGR; and C34 (the most external of the active site Cys couple) ends up at 2.0 Å distance from C597 of SmTGR subunit B (Fig. 34C-34D). The geometry of this mixed disulfide bond is superimposable to the mixed S-S bond found in the crystallographic complex of *E. coli* TR-Trx (PDB code: 1F6M, [130]), supporting the plausibility of this model. Another independent support to the model comes from the structures of Trx from other species, which show that the Trp adjacent to the catalytic site is engaged in hydrophobic contacts upon dimerization [129].

4.7 The catalytic mechanism of SmTGR

By combining the structural and functional data presented above (see sections 4.4-4.6) an hypothesis of the catalytic mechanism of SmTGR may be formulated (Fig. 22). It may be assumed that the mechanism below described for the Sec-Cys mutant of the worm enzyme is plausible and consistent with the Sec-containing wild-type enzyme, as a consequence of the following observations: (i) the only

structure of a Sec-containing rat TR shows the stereochemistry of the C-terminal arm to be very similar to that seen in *Structure 3* [131]; and (ii) the functional characterization of U597C SmTGR indicates that the enzyme has fully functional FAD and Grx redox sites and an active C-terminal arm (see section 4.5.1).

For the sake of clarity the enzymatic process has been divided into two half-processes, comprising the transfer of reducing equivalents inside the TR domain of SmTGR (from NADPH to the C-terminus) and the exchange of electrons between the reduced C-terminal arm and its substrates outside the TR domain, represented by either the Grx domain or the external SmTrx.

4.7.1 Electron flow within the TR domain: from NADPH to the C-terminus

The catalytic cycle starts with the transfer of two electrons from NADPH to the primary redox center (constituted by FAD and the couple C154-C159) of the oxidized enzyme (*Structure 1*, E_{ox}). The product of this reaction is the EH_2^A species, where the FAD cofactor has been reduced to $FADH_2$ (Fig. 22). The kinetic experiments (see section 4.5.2) proved that this step is rate limited by the formation of the complex $FADH_2$-$NADP^+$ and hence second order.

Since the primary redox center of the enzyme has the ability to accept four electrons, rather than two, a charge transfer state is populated as the product, in which electrons move back and forth between the flavin and the Cys couple (EH_2^B). This mixed valency state exchanges electrons with the C-terminal redox center, comprising residues C596-C597 (EH_2^C).

Those enzyme molecules in which the primary redox centre is fully oxidized because of this internal electron transfer are thus able to accept two more electrons coming from a new molecule of NADPH (EH_4^A). This is the second reaction step and implies little further reduction of the FAD, since it mainly occurs on those enzyme molecules in which the cofactor has been reoxidized. In those molecules in which the C-terminal redox center has been already reduced, the second couple of electrons may be exchanged between the FAD and the C154-C159 couple (EH_4^B),

leading to a partial re-oxidation of the FAD cofactor, which can be seen in the time absorbtion spectra at 460 nm at longer times (Fig. 32B).

Structure 2 and *Structure 4*, which have been obtained in the presence of excess reductants (NADPH and GSH), probably are representative of the species called EH_4, having two electrons stored on the FAD/C154-C159 redox center and two additional electrons localized on the C-terminal C597-C598 couple. However the two structures are also compatible with the EH_2 reduced form, bearing the reducing equivalents on the FAD/C154-C159 site, because of the fact that the C-terminal segment is not visible in the 3D structure and it is a reasonable assumption that the overall structure of SmTGR is not affected by the redox state of the disordered C-terminal residues. Finally *Structure 3*, which clearly shows one ordered C-terminus per dimer, carrying the C596-C597 couple fully reduced, may be assigned either to the EH_4 reduced form or to the minor fraction of EH_2 species in which the electrons have been internally transferred from the FAD/C154-C159 to the C-terminal redox center (EH_2^C), in view of the fact that the resolution of the structure does not allow the detection of the redox state of the C154-C159 couple. In agreement with Bauer and co-workers [127], *Structure 3* is supposed to be ready to transfer reducing equivalents to its substrates, such as Trx and/or the Grx domain.

4.7.2 Electrons exit from the TR domain: from the C-terminus to either SmTrx or the Grx domain

Once the reductive half-reaction is finished with the formation of the EH_4^B species, the oxidative half-reaction may start. A mixed disulphide is formed between the C-terminal sulphur groups of SmTGR and the catalytic C34-C37 couple of SmTrx. The reduced SmTrx is released and SmTGR is recycled back to the EH_2^B form (Fig. 22). Looking at *Structure 3*, the C-terminal arm is solvent exposed and ~13 Å apart from the isoalloxazine ring, in a position suitable to supply reducing equivalents to SmTrx (Fig. 30). The C-terminal arm is probably quite mobile in solution and one can assume that only a further slight movement is sufficient to shuttle electrons from C154-C159 to Trx. Electrostatic interactions between the C-

terminal arm of one subunit and a positive surface on the symmetric subunit (contributed by K124, K128 and R450, see Fig. 30) may suggest a mechanism whereby the motion of the former depends on its oxidation state. It may be hypothesized that the C-terminus contacts the external surface of enzyme when reduced, while it slides back into the FAD binding site upon oxidation (the net charge of the C-terminus dropping from -2 to -1, Sec being completely ionized at physiological pH).

The C-terminal arm of SmTGR is also involved in the reduction of the Grx domain and thus in the Grx activity of the enzyme, as demonstrated by experiments on TGR from different organisms [48, 78, 132]. Structural motions compatible with internal electron transfer are required in order to bring the mobile C-terminus onto the Grx redox site and *Structure 4* and *Model 1* give some hints on this movement. Indeed in *Structure 4* the GSH molecule is bound to the active site of the Grx domain, with its sulphurs group 3.1 Å far from C28 of the protein (Fig. 31). Moreover, as shown in *Model 1*, by means of a rotation of the C-terminus of *Structure 4* around the Cα-C bond of K586, the C597-G598 pair of subunit B superimposes to GSH bound to the Grx domain of subunit A (Fig. 34A-34B). This motion is made possible by the fact that, from K586 onwards, the C-terminus is unstructured and anchored by only a few contacts with the rest of the protein (as seen in *Structure 3*). Two more structural features need to be pointed out: (i) the last two residues of SmTGR, i.e. Sec-Gly, resemble the Cys-Gly moiety of GSH (except for the selenium atom, Fig. 34A-34B); and that (ii) the distance between Cα of K586/B and C597/B (~ 23 Å) is comparable with that between Cα of K586/B and the sulphurs group of GSH bound onto the Grx domain of monomer A (~ 26 Å, Fig. 34A). Based on these observations, a rigid body rotation on the pivot residue K586 is sufficient to bring the C-terminus of monomer B onto the GSH binding site on the Grx domain of monomer A (Fig. 34A-34B). Hence, it can be hypothesized that the C-terminal arm, once reduced, mimics free GSH by acting as a reducing agent on the Grx domain of the adjacent subunit of SmTGR.

5. CONCLUDING REMARKS

The research project developed within this thesis is focused on the characterization of two proteins from the parasite *Schistosoma mansoni*, one of the three major species of the blood fluke Schistosoma infecting humans. The two enzymes here presented, i.e.: glutathione peroxidase (SmGpx) and thioredoxin glutathione reductase (SmTGR), have been chosen among the enzymatic components of the worm "detoxification pathway" (Fig. 7 pages 18-19). This system plays a key role in the protection of the worm from reactive oxygen species, thus guarantying its life-maintenance inside the human host. Indeed, on the one hand, SmGpx action is aimed to preserve the membrane lipids from oxidation, being the enzyme associated to the membranes and localized mainly in the worm tegument, at the host-parasite interface [69]. On the other hand TGR is the hub enzyme of the parasite detoxification pathway, hence it controls the whole transfer of reducing equivalents from NADPH either to the thioredoxin or glutathione systems, through intermediate enzymatic (Trx, Gpx, Tpx, Prx) and not-enzymatic partners (GSH/GSSG) [39]. A better understanding of the structure and mechanism of action of each component of this metabolic pathway may give new hints towards the finding of valid alternatives to the current treatment of the Schistosoma infection, which lacks an effective vaccine and is based on a main single drug since the mid-1970s [23].

The first crystal structure at 1.0 and 1.7 Å resolution of two recombinant SmGpxs, carrying the active site mutations U43C and U43S respectively, has been presented in this work (Fig. 17A page 52). The Schistosoma enzyme, belonging to the monomeric class 4 (phospholipid hydroperoxide) Gpx, has been compared with the structurally characterized Sec-Cys mutant of the human homologue (HsGpx4) [63] and a peculiar reactivity of SmGpx has been detected. Indeed the structural superposition between SmGpx and HsGpx4 reveals that the two enzymes have a very similar 3D organization (RMSD$_{overall}$=0.68 Å), with the exception of the redox state of the catalytic cysteine, which is irreversibly oxidized to sulphonic acid (SO_3^{3-})

in SmGpx, while fully reduced and active in the human enzyme (Fig. 17B page 52). The geometry of the active site is conserved in SmGpx with respect to HsGpx4 and within the Gpx family, being the residues Q78, W132, and N133 placed at H-bond distance from Ocs43, but the over-oxidation of the cys residue fully compromised its catalytic activity against the substrates tested. This is quite expected if we consider that the catalytic cycle of selenium-containing Gpx_s requires the enzyme to shuttle between two redox states; i.e.: an oxidized form (R-SeOH) and a reduced form (R-Se⁻). Once reduced after the binding of the glutathione (GSH), Gpx is able to act on inorganic peroxides and lipid hydroperoxides, transforming them to hydroxides and recycling itself to the oxidized species, ready to start the cycle again (Fig. 9 page 22). The over-oxidation of C43 of SmGpx to sulphonic acid is irreversible and thus prevents the enzyme even to enter the cycle. It has been recently suggested that selenocysteine (Sec) has a lower tendency to oxidation if compared with Cys, hence selenoenzymes (such as TR) are less prone to oxidation and consequent inactivation, even under conditions of oxidative stress [133, 134]. This could be the case of SmGpx: the Sec-containing wild-type enzyme should not undergo the spontaneous over-oxidation observed for the recombinant Cys mutant, thus preserving the glutathione peroxidase activity of the parasite inside the human host.

The greater tendency to auto-oxidation of C43 in SmGpx with respect to C46 of HsGpx4 may be justified by slight differences between the catalytic sites of the two enzymes. Indeed, in the SmGpx, the surface pocket hosting the catalytic cys presents on the one hand an increased accessibility to the solvent if compared with the human enzyme (being area and volume of the pocket $140Å^2$/ $94Å^3$ for U43C SmGpx and $93Å^2$/ $72Å^3$ for HsGpx4 respectively), and on the other hand it has a greater polarity, which might promote the entrance of water molecules and metal ions favoring the oxidation of C43 to sulphonic acid (Fig. 18A-18B page 56).

The pocket hosting C43 in SmGpx may be divided in two half-clefts, namely "active-site cleft" and "secondary cleft", and C43 seems to act as a flexible barrier in between (Fig. 18C page 56). The two half-clefts were identified through both a static (CASTp algorithm) and dynamic (MD simulations) analysis, and the latter proved

that their volume distribution is subjected to dynamic fluctuations during the catalytic cycle of the enzyme, probably allowing these clefts to host specific substrates such as GSH and phospholipid hydroperoxides. It is difficult to establish which one of the two half-clefts is mainly involved in the binding of either one or the other substrate, because of the lack of a structure of SmGpx in its ligated form. However, some observations need to be pointed out: (i) the secondary cleft may be easily superimposed to the GSH binding site already suggested for bovine Gpx [62], (ii) the high concentration of positive charges in the secondary cleft is compatible with the binding of glutathione; and (ii) both half-clefts may contribute to the binding of the phospholipids hydroperoxides, whose negatively-charged head may be placed in a positive region of the secondary cleft (hosting a sulphate anion in the crystallographic structure), and the hydrophobic tails layered over an extended hydrophobic surface on the top of the active site cleft (Fig. 18D page 56).

In conclusion, by combining static crystallography with molecular dynamics simulations, a hypothesis for the substrate binding sites on SmGpx has been proposed. Moreover it is known that the particular tissue distribution of SmGpx at the host-parasite interface has made it a candidate of choice for the design of a vaccine against schistosomiasis, like other schistosome antioxidant enzymes (SmSOD and SmGST) [20, 69]. In this respect the availability of an atomic resolution structure of this enzyme, though in an inactive state, may represent a useful first step toward the localization of its epitopes.

While SmGpx seems more suitable as a vaccine candidate, SmTGR, the second enzyme here described, has been demonstrated to be a target of choice for old and new antischistosomal drugs [29]. In fact, with respect to its mammalian counterparts (TR, thioredoxin reductase, and GR, glutathione reductase), the worm TGR exhibits a peculiar 3D organization and mechanism of action, both investigated in this work. More in detail the catalytic cycle of SmTGR has been mapped through the structural characterization of the Sec597Cys mutant in different redox states, i.e.: the oxidized form (at 1.9 Å resolution); the NADPH- and GSH-bound forms (2.3 Å

and 1.9 Å, respectively); and the partially reduced enzyme (3.1 Å), showing the physiological dimer and the entire C-terminus of one subunit.

SmTGR is a homodimeric flavoprotein. As it appears from the crystallographic structures here presented, the enzyme results from the fusion of a larger TR domain with a smaller Grx domain, and presents one molecule of FAD non-covalently bound to each TR domain (Fig. 23A and 25, pages 69 and 70 respectively). This unusual architecture reflects the peculiar reactivity of the parasite SmTGR, which is able to exploit three different catalytic activities, i.e.: thioredoxin reductase, glutathione reductase, and glutaredoxin activity, thus fully replacing TR, GR and Grx of the human host.

The whole redox activity of the wild type SmTGR derives from the contribute of three main active centers: (i) the FAD redox site with the near-by C154-C159 couple, (ii) the C-terminal U596-C597 redox couple, and (iii) the Grx redox site hosting the C28-C31 active residues (Fig. 23A page 69). The C-terminal segment of each monomer is an unstructured region, which may undergo motions in order to reach and transfer electrons to the FAD active site of the adjacent monomer, thus making the enzyme a functional dimer. The *Structure 3* here presented, showing the C-terminal cys couple of one monomer located at 13Å distance from the C154-C159 couple of the adjacent monomer, supports this statement (Fig. 30 page 81).

In order to enter the catalytic cycle the oxidized SmTGR accepts reducing equivalents by NADPH. The NADPH molecule binds on the *re-face* of the FAD cofactor and is sandwiched between the isoalloxazine ring of FAD and the aromatic ring of Y296. As also observed for human TR and GR, Y296, which points towards the flavin in the oxidized form of the enzyme (E_{ox}, *Structure 1*, Fig. 28 page 74), swings upon NADPH binding in a stacked position with the nicotinamide ring of NADPH and the isoalloxazine ring of FAD (*Structure 2,* Fig. 29 page 78). Electrons flow from NADPH to the cofactor, and then to the C154-C159 active couple. The C-terminus carrying the residues C596-C597 is able to pick up electrons from the C154-C159 redox site, leading to the formation of the partially reduced form of the enzyme observed in *Structure 3* (Fig. 30 page 81). Once the first couple of electrons

has reached the C-terminus, the FAD active site is ready to accept a second couple of electrons from NADPH, thus generating the four electrons reduced form of SmTGR. Two kinetic constants have been assigned to both the first reduction step, which forms the two electrons reduced species EH_2 ($k = 4x10^6$ $M^{-1}s^{-1}$); and to the second reduction step, which leads to the formation of the EH_4 species ($k = 1x10^6$ $M^{-1}s^{-1}$).

Once fully reduced, the C-terminal arm should transfer reducing equivalents either to the Grx domain of the enzyme, or to the external substrate SmTrx. In this respect is important to point out that the C-terminal segment of SmTGR appears from *Structure 3* to be solvent exposed and quite mobile, above all in view of the fact that from K586 onwards it is unstructured and anchored by only a few contacts with the rest of the protein. SmTrx can be placed in a surface cleft of SmTGR, formed by residues belonging to the C-terminus of one monomer and to the FAD binding site of the adjacent monomer, at the bottom of the TR domain in *Structure 3*, and a mixed disulphide may be formed between the active site C34 of SmTrx and the C597 of SmTGR, located at 2.0 Å distance from each other (Fig. 34C-34D page 90). The geometry of the resulting disulphide bond is superimposable to the mixed S-S bond already found in the crystallographic complex of *E. coli* TR-Trx, thus proving the plausibility of the model [130]. Moreover, looking at *Structure 4*, which shows a GSH binding site on the Grx domain of SmTGR and taking into account that the C-terminal tetrapeptide (G-C-U-C) may mimic the GSH moiety, a model for the contact between the C-terminus and the Grx redox site may be built after a motion around the pivot residue K586 (Fig. 34A-34B page 90). Hence the mechanism here proposed assume that the C-terminus may deliver electrons selectively to different acceptors shuttling between two alternative positions: (i) it may be located in close proximity to the FAD redox site of the adjacent monomer (as observed in *Structure 3*) where it can both pick up electrons from the C154-C159 couple and transfer them to the oxidized SmTrx, as has been observed in TR enzymes, or (ii) it may internally transfer reducing equivalents to the Grx domain by

occupying the region which is involved in the binding of GSH (as observed in *Structure 4*).

In conclusion the structural analysis of SmTGR here presented, combined with the suggested models, gives some hints toward the understanding of the mechanism of action of the enzyme. The complex structural organization is aimed to make the parasite enzyme able to fulfill a complex function, i.e.: linking the two principal antioxidant detoxification pathways (GSH and Trx pathways), which are distinct in the human host. A recent paper [47] reports the presence of TGR only in parasitic flatworms but not in the free-living species of the same phylum, where separated GR and TR exist similarly to mammals. Hence SmTGR should guarantee selective advantages to the parasites. The internal reduction of the Grx domain in TGR enzymes could be vital for parasites, which spend all their life in the host organism under constant oxidative attack [78]. Under these conditions, sudden fluctuations of the GSH concentration may impair Grx activity and increase the percentage of protein glutathionylation, thus compromising some vital activities of the parasite [46, 135]. The peculiar intramolecular electron pathway of TGR, which carries reducing equivalents from NADPH to the internal Grx domain through the C-terminus, may assure deglutathionylation of target proteins independently of GSH, hence helping the parasites to survive into the human body by circumventing the host-induced oxidative stress.

6. BIBLIOGRAPHY

1.   King, C.H., *Toward the elimination of schistosomiasis.* N Engl J Med, 2009. **360**(2): p. 106-9.
2.   Engels, D., et al., *The global epidemiological situation of schistosomiasis and new approaches to control and research.* Acta Trop, 2002. **82**(2): p. 139-46.
3.   Taylor, M., *Global trends in schistosomiasis control.* Bull World Health Organ, 2008. **86**(10): p. 738.
4.   Fenwick, A., *Waterborne infectious diseases--could they be consigned to history?* Science, 2006. **313**(5790): p. 1077-81.
5.   King, C.H., *Parasites and poverty: the case of schistosomiasis.* Acta Trop, 2010. **113**(2): p. 95-104.
6.   Burke, M.L., et al., *Immunopathogenesis of human schistosomiasis.* Parasite Immunol, 2009. **31**(4): p. 163-76.
7.   Pearce, E.J. and A.S. MacDonald, *The immunobiology of schistosomiasis.* Nat Rev Immunol, 2002. **2**(7): p. 499-511.
8.   Caldas, I.R., et al., *Human schistosomiasis mansoni: immune responses during acute and chronic phases of the infection.* Acta Trop, 2008. **108**(2-3): p. 109-17.
9.   Ferrari, T.C., G. Gazzinelli, and R. Correa-Oliveira, *Immune response and pathogenesis of neuroschistosomiasis mansoni.* Acta Trop, 2008. **108**(2-3): p. 83-8.
10.   Sturrock, R.F., *Schistosomiasis epidemiology and control: how did we get here and where should we go?* Mem Inst Oswaldo Cruz, 2001. **96 Suppl**: p. 17-27.
11.   Han, Z.G., et al., *Schistosoma genomics: new perspectives on schistosome biology and host-parasite interaction.* Annu Rev Genomics Hum Genet, 2009. **10**: p. 211-40.
12.   Yazdanbakhsh, M. and D.L. Sacks, *Why does immunity to parasites take so long to develop?* Nat Rev Immunol. **10**(2): p. 80-1.
13.   Siddiqui, A.A., et al., *Experimental vaccines in animal models for schistosomiasis.* Parasitol Res, 2008. **102**(5): p. 825-33.
14.   Capron, A., et al., *Schistosomes: the road from host-parasite interactions to vaccines in clinical trials.* Trends Parasitol, 2005. **21**(3): p. 143-9.
15.   Gobert, G.N. and D.P. McManus, *Update on paramyosin in parasitic worms.*

Parasitol Int, 2005. **54**(2): p. 101-7.

16. Zhu, Y., et al., *Synergistic enhancement of immunogenicity and protection in mice against Schistosoma japonicum with codon optimization and electroporation delivery of SjTPI DNA vaccines.* Vaccine, 2010. **28**(32): p. 5347-55.

17. Wei, F., et al., *IL-18 enhances protective effect in mice immunized with a Schistosoma japonicum FABP DNA vaccine.* Acta Trop, 2009. **111**(3): p. 284-8.

18. Da'dara, A.A., et al., *Immunization with plasmid DNA encoding the integral membrane protein, Sm23, elicits a protective immune response against schistosome infection in mice.* Vaccine, 2001. **20**(3-4): p. 359-69.

19. Argiro, L., et al., *Induction of a protection against S. mansoni with a MAP containing epitopes of Sm37-GAPDH and Sm10-DLC. Effect of coadsorption with GM-CSF on alum.* Vaccine, 2000. **18**(19): p. 2033-8.

20. LoVerde, P.T., C. Carvalho-Queiroz, and R. Cook, *Vaccination with antioxidant enzymes confers protective immunity against challenge infection with Schistosoma mansoni.* Mem Inst Oswaldo Cruz, 2004. **99**(5 Suppl 1): p. 37-43.

21. Cook, R.M., et al., *Nucleic acid vaccination with Schistosoma mansoni antioxidant enzyme cytosolic superoxide dismutase and the structural protein filamin confers protection against the adult worm stage.* Infect Immun, 2004. **72**(10): p. 6112-24.

22. Abdul-Ghani, R., et al., *Current chemotherapy arsenal for schistosomiasis mansoni: alternatives and challenges.* Parasitol Res, 2009. **104**(5): p. 955-65.

23. Cioli, D., L. Pica-Mattoccia, and S. Archer, *Antischistosomal drugs: past, present ... and future?* Pharmacol Ther, 1995. **68**(1): p. 35-85.

24. Pica-Mattoccia, L., et al., *The schistosome enzyme that activates oxamniquine has the characteristics of a sulfotransferase.* Mem Inst Oswaldo Cruz, 2006. **101 Suppl 1**: p. 307-12.

25. Utzinger, J., et al., *The potential of artemether for the control of schistosomiasis.* Int J Parasitol, 2001. **31**(14): p. 1549-62.

26. Angelucci, F., et al., *The anti-schistosomal drug praziquantel is an adenosine antagonist.* Parasitology, 2007. **134**(Pt 9): p. 1215-21.

27. Melman, S.D., et al., *Reduced susceptibility to praziquantel among naturally occurring Kenyan isolates of Schistosoma mansoni.* PLoS Negl Trop Dis, 2009. **3**(8): p. e504.

28. Sayed, A.A., et al., *Identification of oxadiazoles as new drug leads for the control of*

schistosomiasis. Nat Med, 2008. **14**(4): p. 407-12.

29.   Kuntz, A.N., et al., *Thioredoxin glutathione reductase from Schistosoma mansoni: an essential parasite enzyme and a key drug target.* PLoS Med, 2007. **4**(6): p. e206.

30.   Chong, C.R. and D.J. Sullivan, Jr., *New uses for old drugs.* Nature, 2007. **448**(7154): p. 645-6.

31.   Kasny, M., et al., *Chapter 4. Peptidases of trematodes.* Adv Parasitol, 2009. **69**: p. 205-97.

32.   Donnelly, S., et al., *Helminth cysteine proteases inhibit TRIF-dependent activation of macrophages via degradation of TLR3.* J Biol Chem. **285**(5): p. 3383-92.

33.   Fitzpatrick, J.M., et al., *Schistosome egg production is dependent upon the activities of two developmentally regulated tyrosinases.* FASEB J, 2007. **21**(3): p. 823-35.

34.   Swierczewski, B.E. and S.J. Davies, *A schistosome cAMP-dependent protein kinase catalytic subunit is essential for parasite viability.* PLoS Negl Trop Dis, 2009. **3**(8): p. e505.

35.   Gourlay, L.J., et al., *The three-dimensional structure of two redox states of cyclophilin A from Schistosoma mansoni. Evidence for redox regulation of peptidyl-prolyl cis-trans isomerase activity.* J Biol Chem, 2007. **282**(34): p. 24851-7.

36.   Bobbala, D., et al., *Effect of cyclosporine on parasitemia and survival of Plasmodium berghei infected mice.* Biochem Biophys Res Commun, 2008. **376**(3): p. 494-8.

37.   Kohn, A.B., et al., *Schistosome calcium channel beta subunits. Unusual modulatory effects and potential role in the action of the antischistosomal drug praziquantel.* J Biol Chem, 2001. **276**(40): p. 36873-6.

38.   Mulvenna, J., et al., *Exposed proteins of the Schistosoma japonicum tegument.* Int J Parasitol, 2010. **40**(5): p. 543-54.

39.   Salinas, G., et al., *Linked thioredoxin-glutathione systems in platyhelminths.* Trends Parasitol, 2004. **20**(7): p. 340-6.

40.   Chiumiento, L. and F. Bruschi, *Enzymatic antioxidant systems in helminth parasites.* Parasitol Res, 2009. **105**(3): p. 593-603.

41.   Cioli, D., et al., *Will new antischistosomal drugs finally emerge?* Trends Parasitol, 2008. **24**(9): p. 379-82.

42.   Nordberg, J. and E.S. Arner, *Reactive oxygen species, antioxidants, and the mammalian thioredoxin system.* Free Radic Biol Med, 2001. **31**(11): p. 1287-312.

43. Arner, E.S., *Focus on mammalian thioredoxin reductases--important selenoproteins with versatile functions.* Biochim Biophys Acta, 2009. **1790**(6): p. 495-526.

44. Fritz-Wolf, K., S. Urig, and K. Becker, *The structure of human thioredoxin reductase 1 provides insights into C-terminal rearrangements during catalysis.* J Mol Biol, 2007. **370**(1): p. 116-27.

45. Winyard, P.G., C.J. Moody, and C. Jacob, *Oxidative activation of antioxidant defence.* Trends Biochem Sci, 2005. **30**(8): p. 453-61.

46. Johansson, C., C.H. Lillig, and A. Holmgren, *Human mitochondrial glutaredoxin reduces S-glutathionylated proteins with high affinity accepting electrons from either glutathione or thioredoxin reductase.* J Biol Chem, 2004. **279**(9): p. 7537-43.

47. Otero, L., et al., *Thioredoxin and glutathione systems differ in parasitic and free-living platyhelminths.* BMC Genomics, 2010. **11**: p. 237.

48. Alger, H.M. and D.L. Williams, *The disulfide redox system of Schistosoma mansoni and the importance of a multifunctional enzyme, thioredoxin glutathione reductase.* Mol Biochem Parasitol, 2002. **121**(1): p. 129-39.

49. Alger, H.M., et al., *Molecular and enzymatic characterisation of Schistosoma mansoni thioredoxin.* Int J Parasitol, 2002. **32**(10): p. 1285-92.

50. Thomas, J.P., et al., *Protective action of phospholipid hydroperoxide glutathione peroxidase against membrane-damaging lipid peroxidation. In situ reduction of phospholipid and cholesterol hydroperoxides.* J Biol Chem, 1990. **265**(1): p. 454-61.

51. Maiorino, M., et al., *A selenium-containing phospholipid-hydroperoxide glutathione peroxidase in Schistosoma mansoni.* Eur J Biochem, 1996. **238**(3): p. 838-44.

52. Sayed, A.A. and D.L. Williams, *Biochemical characterization of 2-Cys peroxiredoxins from Schistosoma mansoni.* J Biol Chem, 2004. **279**(25): p. 26159-66.

53. Sayed, A.A., S.K. Cook, and D.L. Williams, *Redox balance mechanisms in Schistosoma mansoni rely on peroxiredoxins and albumin and implicate peroxiredoxins as novel drug targets.* J Biol Chem, 2006. **281**(25): p. 17001-10.

54. Margis, R., et al., *Glutathione peroxidase family - an evolutionary overview.* FEBS J, 2008. **275**(15): p. 3959-70.

55. Herbette, S., P. Roeckel-Drevet, and J.R. Drevet, *Seleno-independent glutathione peroxidases. More than simple antioxidant scavengers.* FEBS J, 2007. **274**(9): p.

2163-80.

56. Toppo, S., et al., *Evolutionary and structural insights into the multifaceted glutathione peroxidase (Gpx) superfamily.* Antioxid Redox Signal, 2008. **10**(9): p. 1501-14.

57. Lu, J. and A. Holmgren, *Selenoproteins.* J Biol Chem, 2009. **284**(2): p. 723-7.

58. Papp, L.V., et al., *From selenium to selenoproteins: synthesis, identity, and their role in human health.* Antioxid Redox Signal, 2007. **9**(7): p. 775-806.

59. Squires, J.E. and M.J. Berry, *Eukaryotic selenoprotein synthesis: mechanistic insight incorporating new factors and new functions for old factors.* IUBMB Life, 2008. **60**(4): p. 232-5.

60. Maiorino, M., et al., *Probing the presumed catalytic triad of a selenium-containing peroxidase by mutational analysis.* Z Ernahrungswiss, 1998. **37 Suppl 1**: p. 118-21.

61. Zuberbuehler, C.A., et al., *Effects of selenium depletion and selenium repletion by choice feeding on selenium status of young and old laying hens.* Physiol Behav, 2006. **87**(2): p. 430-40.

62. Epp, O., R. Ladenstein, and A. Wendel, *The refined structure of the selenoenzyme glutathione peroxidase at 0.2-nm resolution.* Eur J Biochem, 1983. **133**(1): p. 51-69.

63. Scheerer, P., et al., *Structural basis for catalytic activity and enzyme polymerization of phospholipid hydroperoxide glutathione peroxidase-4 (GPx4).* Biochemistry, 2007. **46**(31): p. 9041-9.

64. Ren, B., et al., *The crystal structure of seleno-glutathione peroxidase from human plasma at 2.9 A resolution.* J Mol Biol, 1997. **268**(5): p. 869-85.

65. Prabhakar, R., et al., *Elucidation of the mechanism of selenoprotein glutathione peroxidase (GPx)-catalyzed hydrogen peroxide reduction by two glutathione molecules: a density functional study.* Biochemistry, 2005. **44**(35): p. 11864-71.

66. Tosatto, S.C., et al., *The catalytic site of glutathione peroxidases.* Antioxid Redox Signal, 2008. **10**(9): p. 1515-26.

67. Roche, C., et al., *Cloning and characterization of the gene encoding Schistosoma mansoni glutathione peroxidase.* Gene, 1994. **138**(1-2): p. 149-52.

68. Williams, D.L., et al., *Molecular cloning and sequencing of glutathione peroxidase from Schistosoma mansoni.* Mol Biochem Parasitol, 1992. **52**(1): p. 127-30.

69. Mei, H., et al., *Expression and characterization of glutathione peroxidase activity in the human blood fluke Schistosoma mansoni.* Infect Immun, 1996. **64**(10): p. 4299-

306.

70.   Su, D., et al., *Mammalian selenoprotein thioredoxin-glutathione reductase. Roles in disulfide bond formation and sperm maturation.* J Biol Chem, 2005. **280**(28): p. 26491-8.

71.   Rendon, J.L., et al., *Purification, characterization and kinetic properties of the multifunctional thioredoxin-glutathione reductase from Taenia crassiceps metacestode (cysticerci).* Mol Biochem Parasitol, 2004. **133**(1): p. 61-9.

72.   Agorio, A., et al., *Alternative mRNAs arising from trans-splicing code for mitochondrial and cytosolic variants of Echinococcus granulosus thioredoxin Glutathione reductase.* J Biol Chem, 2003. **278**(15): p. 12920-8.

73.   Sun, Q.A., et al., *Reaction mechanism and regulation of mammalian thioredoxin/glutathione reductase.* Biochemistry, 2005. **44**(44): p. 14528-37.

74.   Sharma, M., et al., *Comparative modeling of thioredoxin glutathione reductase from Schistosoma mansoni: a multifunctional target for antischistosomal therapy.* J Mol Graph Model, 2009. **27**(6): p. 665-75.

75.   Angelucci, F., et al., *Glutathione reductase and thioredoxin reductase at the crossroad: the structure of Schistosoma mansoni thioredoxin glutathione reductase.* Proteins, 2008. **72**(3): p. 936-45.

76.   Angelucci, F., et al., *Mapping the catalytic cycle of Schistosoma mansoni thioredoxin glutathione reductase by X-ray crystallography.* J Biol Chem, 2010. **285**(42): p. 32557-67.

77.   Simeonov, A., et al., *Quantitative high-throughput screen identifies inhibitors of the Schistosoma mansoni redox cascade.* PLoS Negl Trop Dis, 2008. **2**(1): p. e127.

78.   Bonilla, M., et al., *Platyhelminth mitochondrial and cytosolic redox homeostasis is controlled by a single thioredoxin glutathione reductase and dependent on selenium and glutathione.* J Biol Chem, 2008. **283**(26): p. 17898-907.

79.   Gromer, S., et al., *Human placenta thioredoxin reductase. Isolation of the selenoenzyme, steady state kinetics, and inhibition by therapeutic gold compounds.* J Biol Chem, 1998. **273**(32): p. 20096-101.

80.   Angelucci, F., et al., *Inhibition of Schistosoma mansoni thioredoxin-glutathione reductase by auranofin: structural and kinetic aspects.* J Biol Chem, 2009. **284**(42): p. 28977-85.

81.   *The CCP4 suite: programs for protein crystallography.* Acta Crystallogr D Biol

Crystallogr, 1994. **50**(Pt 5): p. 760-3.

82. Emsley, P. and K. Cowtan, *Coot: model-building tools for molecular graphics.* Acta Crystallogr D Biol Crystallogr, 2004. **60**(Pt 12 Pt 1): p. 2126-32.

83. Potterton, L., et al., *Developments in the CCP4 molecular-graphics project.* Acta Crystallogr D Biol Crystallogr, 2004. **60**(Pt 12 Pt 1): p. 2288-94.

84. Davis, I.W., et al., *MolProbity: all-atom contacts and structure validation for proteins and nucleic acids.* Nucleic Acids Res, 2007. **35**(Web Server issue): p. W375-83.

85. Laskowski, R.A., et al., *PROCHECK: a program to check the stereochemical quality of protein structures.* J. Appl. Cryst., 1993. **26**: p. 283-291.

86. Larkin, M.A., et al., *Clustal W and Clustal X version 2.0.* Bioinformatics, 2007. **23**(21): p. 2947-8.

87. Gouet, P., et al., *ESPript: analysis of multiple sequence alignments in PostScript.* Bioinformatics, 1999. **15**(4): p. 305-8.

88. Baker, N.A., et al., *Electrostatics of nanosystems: application to microtubules and the ribosome.* Proc Natl Acad Sci U S A, 2001. **98**(18): p. 10037-41.

89. Dolinsky, T.J., et al., *PDB2PQR: an automated pipeline for the setup of Poisson-Boltzmann electrostatics calculations.* Nucleic Acids Res, 2004. **32**(Web Server issue): p. W665-7.

90. DeLano, W.L., *The PyMOL Molecular Graphics System.* DeLano Scientific, San Carlos, CA, USA, 2002.

91. Schneidman-Duhovny, D., et al., *PatchDock and SymmDock: servers for rigid and symmetric docking.* Nucleic Acids Res, 2005. **33**(Web Server issue): p. W363-7.

92. Becke, A.D., *Density-functional thermochemistry. III. The role of exact exchange.* J Chem Phys, 1993. **98**: p. 5648-52.

93. Lee, C., W. Yang, and R.G. Parr, *Development of the Colle-Salvetti correlation-energy formula into a functional of the electron density.* Phys Rev B Condens Matter, 1988. **37**(2): p. 785-789.

94. Schaefer, A., H. Horn, and R. Ahlrichs, *Fully optimized contracted Gaussian basis sets for atoms lithium to krypton* J Chem Phys, 1992. **97**: p. 2571-77.

95. Schmidt, M.W., et al., *General atomic and molecular electronic structure system.* J Comput Chem, 1993. **14**: p. 1347-63.

96. Breneman, C.M. and K.B. Wiberg, *Determining atom-centered monopoles from*

molecular electrostatic potentials. The need for high sampling density in formamide conformational analysis. J Comput Chem, 1990. **11**: p. 361-73.

97. Allinger, N.L., J.A. Allinger, and L.Q. Yan, *Molecular mechanics (MM2) calculations on organo selenium and tellurium compounds.* J Mol Struct 1989. **201**(363-69).

98. Berendsen, H.J.C., et al., *Interaction models for water in relation to protein hydration.* Intermolecular forces. Dordrecht, The Netherlands: D Reidel Publishing Company, 1981: p. 331-342.

99. Berendsen, H.J.C., D. Van Der Spoel, and R. Van Drunen, *GROMACS: a message-passing parallel molecular dynamics implementation.* Comput Phys Commun, 1995(91): p. 43-56.

100. Van Gunsteren, W.F., et al., *Biomolecular simulations: the GROMOS96 manual and user guide.* Zurich, Groningen: BIOMOS b.v, 1996.

101. Hess, B., et al., *LINCS: a linear constraint solver for molecular simulations.* J Comput Chem, 1997. **18**: p. 1463-72.

102. Amadei, A., A.B. Linssen, and H.J. Berendsen, *Essential dynamics of proteins.* Proteins, 1993. **17**: p. 412-25.

103. Evans, D.J. and G.P. Morriss, *Statistical mechanics of nonequilibrium liquids.* London: Academic Press, 1990.

104. Essmann, U., et al., *A smooth particle mesh Ewald method.* J Chem Phys, 1995. **103**: p. 8577-93.

105. Laskowski, R., A. , *SURFNET: a program for visualizing molecular surfaces, cavities, and intermolecular interactions.* J Mol Graph, 1995. **13**: p. 323-30.

106. Otwinowski, Z. and W. Minor, *Macromolecular crystallography.* Methods Enzymol, 1997. **276**: p. 307-26.

107. Summa, C.M. and M. Levitt, *Near-native structure refinement using in vacuo energy minimization.* Proc Natl Acad Sci U S A, 2007. **104**(9): p. 3177-82.

108. Holmgren, A. and M. Bjornstedt, *Thioredoxin and thioredoxin reductase.* Methods Enzymol, 1995. **252**: p. 199-208.

109. Holmgren, A., *Thioredoxin catalyzes the reduction of insulin disulfides by dithiothreitol and dihydrolipoamide.* J Biol Chem, 1979. **254**(19): p. 9627-32.

110. Carlberg, I. and B. Mannervik, *Glutathione reductase.* Methods Enzymol, 1985. **113**: p. 484-90.

111. Holmgren, A. and F. Aslund, *Glutaredoxin.* Methods Enzymol, 1995. **252**: p. 283-92.
112. Martin, J.L., *Thioredoxin--a fold for all reasons.* Structure, 1995. **3**(3): p. 245-50.
113. Brouwers, J.F., et al., *The incorporation, modification and turnover of fatty acids in adult Schistosoma mansoni.* Mol Biochem Parasitol, 1997. **88**(1-2): p. 175-85.
114. Porter, N.A., S.E. Caldwell, and K.A. Mills, *Mechanisms of free radical oxidation of unsaturated lipids.* Lipids, 1995. **30**(4): p. 277-90.
115. Buettner, G.R., *The pecking order of free radicals and antioxidants: lipid peroxidation, alpha-tocopherol, and ascorbate.* Arch Biochem Biophys, 1993. **300**(2): p. 535-43.
116. Biterova, E.I., et al., *Crystal structures of oxidized and reduced mitochondrial thioredoxin reductase provide molecular details of the reaction mechanism.* Proc Natl Acad Sci U S A, 2005. **102**(42): p. 15018-23.
117. Sandalova, T., et al., *Three-dimensional structure of a mammalian thioredoxin reductase: implications for mechanism and evolution of a selenocysteine-dependent enzyme.* Proc Natl Acad Sci U S A, 2001. **98**(17): p. 9533-8.
118. Berkholz, D.S., et al., *Catalytic cycle of human glutathione reductase near 1 A resolution.* J Mol Biol, 2008. **382**(2): p. 371-84.
119. Martinez-Gonzalez, J.J., et al., *In vitro killing action of auranofin on Taenia crassiceps metacestode (cysticerci) and inactivation of thioredoxin-glutathione reductase (TGR).* Parasitol Res. **107**(1): p. 227-31.
120. Feng, Y., et al., *Structural insight into poplar glutaredoxin C1 with a bridging iron-sulfur cluster at the active site.* Biochemistry, 2006. **45**(26): p. 7998-8008.
121. Yu, J., et al., *Glutathionylation-triggered conformational changes of glutaredoxin Grx1 from the yeast Saccharomyces cerevisiae.* Proteins, 2008. **72**(3): p. 1077-83.
122. Luo, M., et al., *Structural and biochemical characterization of yeast monothiol glutaredoxin Grx6.* J Mol Biol. **398**(4): p. 614-22.
123. Savvides, S.N. and P.A. Karplus, *Kinetics and crystallographic analysis of human glutathione reductase in complex with a xanthene inhibitor.* J Biol Chem, 1996. **271**(14): p. 8101-7.
124. Huang, H.H., et al., *Acid-base catalysis in the mechanism of thioredoxin reductase from Drosophila melanogaster.* Biochemistry, 2008. **47**(6): p. 1721-31.
125. Hanson, K.R., *Applications of the Sequence Rule. I. Naming the Paired Ligands g,g*

at a Tetrahedral Atom Xggij. II. Naming the Two Faces of a Trigonal Atom Yghi. Journal of th american chemical society, 1966. **88**: p. 2731-42.

126. Arner, E.S., *Selenoproteins-What unique properties can arise with selenocysteine in place of cysteine?* Exp Cell Res, 2010. **316**(8): p. 1296-303.

127. Bauer, H., et al., *The mechanism of high Mr thioredoxin reductase from Drosophila melanogaster.* J Biol Chem, 2003. **278**(35): p. 33020-8.

128. Bateman, H., *The solution of a system of differential equations occurring in the theory of radio-active transformations.* Proc. Cambridge Philos. Soc., 1910. **15**: p. 423-27.

129. Wahl, M.C., et al., *Comparative structural analysis of oxidized and reduced thioredoxin from Drosophila melanogaster.* J Mol Biol, 2005. **345**(5): p. 1119-30.

130. Lennon, B.W., C.H. Williams, Jr., and M.L. Ludwig, *Twists in catalysis: alternating conformations of Escherichia coli thioredoxin reductase.* Science, 2000. **289**(5482): p. 1190-4.

131. Cheng, Q., et al., *Crystal structure and catalysis of the selenoprotein thioredoxin reductase 1.* J Biol Chem, 2009. **284**(6): p. 3998-4008.

132. Rai, G., et al., *Structure mechanism insights and the role of nitric oxide donation guide the development of oxadiazole-2-oxides as therapeutic agents against schistosomiasis.* J Med Chem, 2009. **52**(20): p. 6474-83.

133. Hondal, R.J. and E.L. Ruggles, *Differing views of the role of selenium in thioredoxin reductase.* Amino Acids.

134. Snider, G., et al., *Methaneseleninic Acid Is a Substrate for Truncated Mammalian Thioredoxin Reductase: Implications for the Catalytic Mechanism and Redox Signaling.* Biochemistry.

135. Grant, C.M., *Role of the glutathione/glutaredoxin and thioredoxin systems in yeast growth and response to stress conditions.* Mol Microbiol, 2001. **39**(3): p. 533-41.

136. Khan, A., *A liquid water model: density variation from supercooled to superheated states, prediction of H-bonds, and temperature limits.* J Phys Chem, 2000. **104**: p. 11268-274.

PROTEINS

Combining crystallography and molecular dynamics: The case of *Schistosoma mansoni* phospholipid glutathione peroxidase

Daniela Dimastrogiovanni,[1] Massimiliano Anselmi,[2] Adriana Erica Miele,[1] Giovanna Boumis,[1] Linn Petersson,[1] Francesco Angelucci,[1] Alfredo Di Nola,[2] Maurizio Brunori,[1] and Andrea Bellelli[1*]

[1] Dipartimento di Scienze Biochimiche A. Rossi Fanelli and Istituto Pasteur, Fondazione Cenci Bolognetti, "Sapienza" University of Rome, Rome, Italy

[2] Dipartimento di Chimica, "Sapienza" University of Rome, Rome, Italy

ABSTRACT

Oxidative stress is a widespread challenge for living organisms, and especially so for parasitic ones, given the fact that their hosts can produce reactive oxygen species (ROS) as a mechanism of defense. Thus, long lived parasites, such as the flatworm Schistosomes, have evolved refined enzymatic systems capable of detoxifying ROS. Among these, glutathione peroxidases (Gpx) are a family of sulfur or selenium-dependent isozymes sharing the ability to reduce peroxides using the reducing equivalents provided by glutathione or possibly small proteins such as thioredoxin. As for other frontline antioxidant enzymatic systems, Gpxs are localized in the tegument of the Schistosomes, the outermost defense layer. In this article, we present the first crystal structure at 1.0 and 1.7 Å resolution of two recombinant SmGpxs, carrying the active site mutations Sec43Cys and Sec43Ser, respectively. The structures confirm that this enzyme belongs to the monomeric class 4 (phospholipid hydroperoxide) Gpx. In the case of the Sec to Cys mutant, the catalytic Cys residue is oxidized to sulfonic acid. By combining static crystallography with molecular dynamics simulations, we obtained insight into the substrate binding sites and the conformational changes relevant to catalysis, proposing a role for the unusual reactivity of the catalytic residue.

INTRODUCTION

Aerobic organisms have evolved various nonenzymatic and enzymatic systems to detoxify reactive oxygen species (ROS), thereby limiting the adverse effects of these damaging compounds. Among the enzymes involved in the cellular response to oxidative stress are several glutathione-dependent enzymes, like glutaredoxins (Grx), glutathione peroxidases (Gpx), thioredoxin reductases (TR), and glutathione reductases (GR).

Gpxs represent a family of enzymes with complex evolutionary relationships and characterized by various activities, reducing partners and cellular localizations.[1] Some Gpxs are selenoproteins[2] using glutathione (GSH) to catalyze the reduction of H_2O_2 and organic hydroperoxides, but recently several nonselenium Gpx with cellular activities different from their canonical antioxidant role have been identified.[3]

Selenium-containing Gpxs have a functionally relevant residue of Selenium Cysteine (Sec), encoded by a TGA codon,[4,5] in the active site. Sec is required for full catalytic efficiency, as shown by point mutation or *in vivo* Se depletion[6]; and the Sec to Cys mutant Gpxs studied so far present a variable degree of functional impairment with respect to their wild type counterparts.[7] The presence of Sec has aroused interest on Gpx, due to the *in vivo* relevance of selenoproteins[8]; however, the known difficulties in heterologous expression of native selenoenzymes represent a practical problem.[9]

Although the classification of Gpxs is complex and has been repeatedly revised, it seems that seleno Gpxs may still be classified into four

Mapping the Catalytic Cycle of *Schistosoma mansoni* Thioredoxin Glutathione Reductase by X-ray Crystallography[*][S]

Francesco Angelucci[1], Daniela Dimastrogiovanni[1], Giovanna Boumis, Maurizio Brunori, Adriana E. Miele, Fulvio Saccoccia, and Andrea Bellelli[2]

From the Department of Biochemical Sciences "A. Rossi Fanelli," CNR Institute of Molecular Biology and Pathology and Istituto Pasteur-Fondazione Cenci Bolognetti, Sapienza University of Rome, P.le Aldo Moro 5, 00185 Rome, Italy

Schistosomiasis is the second most widespread human parasitic disease. It is principally treated with one drug, praziquantel, that is administered to 100 million people each year; less sensitive strains of schistosomes are emerging. One of the most appealing drug targets against schistosomiasis is thioredoxin glutathione reductase (TGR). This natural chimeric enzyme is a peculiar fusion of a glutaredoxin domain with a thioredoxin selenocysteine (U)-containing reductase domain. Selenocysteine is located on a flexible C-terminal arm that is usually disordered in the available structures of the protein and is essential for the full catalytic activity of TGR. In this study, we dissect the catalytic cycle of *Schistosoma mansoni* TGR by structural and functional analysis of the U597C mutant. The crystallographic data presented herein include the following: the oxidized form (at 1.9 Å resolution); the NADPH- and GSH-bound forms (2.3 and 1.9 Å, respectively); and a different crystal form of the (partially) reduced enzyme (3.1 Å), showing the physiological dimer and the entire C terminus of one subunit. Whenever possible, we determined the rate constants for the interconversion between the different oxidation states of TGR by kinetic methods. By combining the crystallographic analysis with computer modeling, we were able to throw further light on the mechanism of action of *S. mansoni* TGR. In particular, we hereby propose the putative functionally relevant conformational change of the C terminus after the transfer of reducing equivalents from NADPH to the redox sites of the enzyme.

Schistosomes are human platyhelminth parasites causing Schistosomiasis, a severe disease still classified among the major causes of mortality in tropical and subtropical countries, affecting more than 200 million people (1). The only drug employed to fight the disease is praziquantel, whose efficacy is restricted to the adult stages of the parasite and whose mechanism of action is still incompletely clarified (2, 3). Because this drug is administered to 100 million people every year, some less sensitive strains have already been isolated, and given the massive drug administration, resistance might become a serious problem (3).

Because of this, the search for a new drug against Schistosomiasis is a necessity and a priority according to the World Health Organization (4). The main evidence suggesting that targeting the thiol redox pathway of the parasite may represent a profitable starting point for rational drug design is as follows: (i) schistosomes, living in the human bloodstream, are subjected not only to endogenous reactive oxygen species but are also exposed to radicals produced by the host immune response; and (ii) the thiol redox pathway employed by the worms for the enzymatic reduction of the reactive oxygen species is different from its human counterpart (5, 6).

In mammals, two proteins belonging to the pyridine nucleotide disulfide oxidoreductase family, thioredoxin reductase (TR)[3] and glutathione reductase (GR), are the head antioxidant enzymes shuttling electrons through the thioredoxin (Trx) and the GSH systems, respectively (5). Trx peroxidases in addition to Trxs are the other components of the Trx system; the GSH system involves GSH peroxidase (Gpx) and glutaredoxin (Grx), an oxidoreductase acting on S-glutathionylated substrates (7, 8). TRs and GRs are homodimeric NADPH-dependent flavoproteins that are structurally highly similar. The two proteins share the main fold and the architecture of the binding sites for NADPH and FAD. However, TRs differ from GRs because of the presence of a selenocysteine residue (Sec, U) located in a GCUG tetrapeptide at the C terminus of the protein. This additional C-terminal extension is required for the full catalytic activity of the enzyme (9–11). Thioredoxin glutathione reductase (TGR) is another selenoprotein belonging to the abovementioned family of oxidoreductases. Characterization of mouse TGR demonstrated that the enzyme can reduce components of both mammalian Trx and GSH systems. In mammals, TGR exerts a wide range of catalytic activities though its selective overexpression in testis after puberty suggests its involvement in very specific functions related with sperm maturation (12).

[3] The abbreviations used are: TR, thioredoxin reductase; TGR, thioredoxin glutathione reductase; SmTGRfl, S. mansoni TGR full length (U597C mutant); SmTrx, *S. mansoni* thioredoxin; GR, glutathione reductase; Grx, glutaredoxin; PDB, Protein Data Bank; Sec, selenocysteine.

Glutathione reductase and thioredoxin reductase at the crossroad: The structure of *Schistosoma mansoni* thioredoxin glutathione reductase

Francesco Angelucci, Adriana E. Miele, Giovanna Boumis, Daniela Dimastrogiovanni, Maurizio Brunori, and Andrea Bellelli*

Istituto Pasteur Fondazione Cenci–Bolognetti and CNR Institute of Molecular Biology and Pathology, Department of Biochemical Sciences "A. Rossi Fanelli", "Sapienza" University of Rome, Piazzale Aldo Moro 5, 00185 Rome, Italy

ABSTRACT

Thioredoxin glutathione reductase (TGR) is a key flavoenzyme expressed by schistosomes that bridges two detoxification pathways crucial for the parasite survival in the host's organism. In this article we report the crystal structure (at 2.2 Å resolution) of TGR from Schistosoma mansoni (SmTGR), deleted in the last two residues. The structure reveals the peculiar architecture of this chimeric enzyme: the small Glutaredoxin (Grx) domain at the N-terminus is joined to the large thioredoxin reductase (TR) one via an extended complementary surface, involving residues not conserved in the Grx superfamily; the TR domain interacts with an identical partner via its C-terminal domain, forming a dimer with a twisted "W" shape. Although lacking the penultimate Selenocysteine residue (Sec), the enzyme is still able to reduce oxidized glutathione. These data update the interpretation of the interdomain communication in TGR enzymes. The possible function of this enzyme in pathogenic parasites is discussed.

INTRODUCTION

Schistosomiasis is a severe parasitic disease, affecting 200 million people in tropical and subtropical areas. It is caused by platyhelminths of the gender *Schistosoma*, whose complex life cycle involves two hosts and several life stages.[1] The cure relies on one single drug, praziquantel, effective only against the adult stage of the parasite and administered to 100 million people yearly. Therapies based on a single compound are risky, given the high probability to cause resistance. Indeed, schistosome strains displaying low praziquantel susceptibility have already been detected.[2]

We focused our attention to the detoxification pathway, since the parasite is subjected to a high oxidative stress, mainly because of the host's immune response.[3] Hence, interfering with this pathway may help in the search of new therapies. Very recently, an enzyme of this metabolism proved to be very promising[4]: Thioredoxin glutathione reductase from *S. mansoni* (SmTGR), that was demonstrated to be the target of two previously used schistomicidials (oltipraz and antimonium salts). RNA interference and exposure to SmTGR inhibitors kill *S. mansoni* in few hours *in vitro*, and substantially reduce worm burden in animal models. Moreover, inhibition of the enzyme activity is also effective against the schistosome's juvenile stages.[4] A biochemical explanation of these data may be found in the peculiar detoxification pathway of schistosomes compared to mammals.

In animal cells, redox regulation is provided by the Thioredoxin (Trx) and Glutathione (GSH/GSSG) systems, which are reduced by NADPH via specific flavine-oxidoreductases. Electrons are then shuttled to proteins and other compounds through reversible thiol oxidoreduction. The Trx and GSH/GSSG systems provide reducing equivalents for several processes like DNA biosynthesis and redox control of cell growth and death.[5,6]

The animal GSH/GSSG system consists of (i) GSSG reductase (GR), a member of the pyridine nucleotide disulfide oxidoreductase family (GR family);

113

Inhibition of *Schistosoma mansoni* Thioredoxin-glutathione Reductase by Auranofin
STRUCTURAL AND KINETIC ASPECTS[*]

Francesco Angelucci[‡1], Ahmed A. Sayed[§1,2], David L. Williams[¶], Giovanna Boumis[‡], Maurizio Brunori[‡], Daniela Dimastrogiovanni[‡], Adriana E. Miele[‡], Frida Pauly[‡], and Andrea Bellelli[‡3]

From the [‡]Department of Biochemical Sciences "A. Rossi Fanelli," "Sapienza" University of Rome and Istituto Pasteur-Fondazione Cenci Bolognetti, P. Le Aldo Moro 5, 00185 Rome, Italy, the [§]Department of Biological Sciences, Illinois State University, Normal, Illinois 61790, and the [¶]Department of Immunology/Microbiology, Rush University Medical Center, Chicago, Illinois 60302

Schistosomiasis is a parasitic disease affecting over 200 million people currently treated with one drug, praziquantel. A possible drug target is the seleno-protein thioredoxin-glutathione reductase (TGR), a key enzyme in the pathway of the parasite for detoxification of reactive oxygen species. The enzyme is a unique fusion of a glutaredoxin domain with a thioredoxin reductase domain, which contains a selenocysteine (Sec) as the penultimate amino acid. Auranofin (AF), a gold-containing compound already in clinical use as an anti-arthritic drug, has been shown to inhibit TGR and to substantially reduce worm burden in mice. Using x-ray crystallography we solved (at 2.5 Å resolution) the structure of wild type TGR incubated with AF. The electron density maps show that the actual inhibitor is gold, released from AF. Gold is bound at three different sites not directly involving the C-terminal Sec residue; however, because the C terminus in the electron density maps is disordered, we cannot exclude the possibility that gold may also bind to Sec. To investigate the possible role of Sec in the inactivation kinetics, we tested the effect of AF on a model enzyme of the same superfamily, *i.e.* the naturally Sec-lacking glutathione reductase, and on truncated TGR. We demonstrate that the role of selenium in the onset of inhibition by AF is catalytic and can be mimicked by an external source of selenium (benzeneselenol). Therefore, we propose that Sec mediates the transfer of gold from its ligands in AF to the redox-active Cys couples of TGR.

Schistosomiasis is one of the most important human parasitic infections in the world, affecting over 200 million people in developing countries with 280,000 deaths/year in sub-Saharan

Africa alone (1). The therapy for schistosomiasis is based on a single drug, praziquantel, that is administered to millions of people yearly (2, 3). A reliable alternative to praziquantel does not exist at the moment. Oxamniquine, the only other drug commercially available, is expensive and is active against only one of the three schistosome species capable of infecting humans, namely *Schistosoma mansoni*. Artemisinins, although safe, are active only against the immature stages of the parasites. A treatment strategy that relies on just a single drug is at risk given the high probability that drug-resistant parasites will emerge (4).

Recently, a possible solution to this urgent problem has been proposed, *i.e.* targeting the antioxidant pathway of the parasite. In platyhelminths, like *Schistosoma* and *Echinococcus*, thiol redox homeostasis is completely dependent on the enzyme thioredoxin-glutathione reductase (TGR),[4] which directs the NADPH reducing equivalents to both GSH and thioredoxin (4–6). On the other hand, in humans and other vertebrates the same function is fulfilled by two distinct enzymes that initiate two parallel pathways, namely thioredoxin reductase (TR) and glutathione reductase (GR).

TGR is a natural chimeric flavo-enzyme whose structure results from the fusion of a TR domain with a glutaredoxin domain (7–9). We recently solved the crystal structure of TGR from *S. mansoni* (10). The redox activity of the enzyme relies on at least three redox sites communicating with one another: (i) the FAD site, composed by the isoalloxazine ring of the flavin and the Cys^{154}–Cys^{159} couple (characteristic of all the enzymes of the TR/GR family); (ii) the C terminus, constituted by the Gly-Cys-Sec-Gly sequence shared with the majority of TRs but not with GRs; and (iii) the glutaredoxin redox site represented by Cys^{28}–Cys^{31} at the N-terminal portion of the protein.

The presence of this peculiar enzyme in schistosomes was exploited in the search of new schistosomicidal drugs (11, 12). The significance of *S. mansoni* (Sm)TGR as a putative drug target was first demonstrated using an RNA interference approach, which killed 90% of treated parasites *in vitro*. Moreover, it was demonstrated that SmTGR activity is inhibited by

---

The Mechanism of Inhibition of TGR by Auranofin

SCHEME 1. **Possible reaction path for AF and SmTGR.** One molecule of AF reacts with wild type reduced SmTGR (species 1) to yield a transient intermediate bearing an Au(I) coordinated with Sec^{597} and triethylphosphine (species 2); we hypothesize that acetoxythioglucose is released first (see text). The intermediate species releases triethylphosphine to form a Sec-gold-Cys complex with any of the available cysteinyl residues; three reaction products are possible (species 3, 4, and 6). The chemical species in which the C-terminal arm is cross-linked via the gold ion to a distant Cys residue (species 4 and 6) may rearrange to yield the more stable short distance Cys-gold-Cys complexes (species 5 and 7). When equilibrium is reached, a mixture of species 3, 5, and 7 is expected to be present, dynamically interchanging via the less stable intermediates 4 and 6. Additional molecules of AF may be introduced, leading to SmTGR molecules bearing two or three gold ions. The gold-binding site 3, in which the metal ion is not coordinated by Cys or Sec, is not considered in the scheme.

two schistosomicidal drugs used in the past to fight the infection, antimonyl potassium tartrate and oltipraz, suggesting that the enzyme is the main target of these compounds (6). Based on these promising results, a quantitative high throughput screening of ~71000 compounds was carried out to isolate new leads targeting the *S. mansoni* redox pathway (13).

A potentially interesting inhibitor of TGR is auranofin (AF; Au(I); 3,4,5-triacetyloxy-6-(acetyloxymethyl) oxane-2-thiolate; triethyl phosphanium; $C_{20}H_{34}O_9S$-gold-$P(C_2H_5)_3$; see the formula in Scheme 1). *In vitro*, 10 μM AF causes unpairing of male and female worms after 1 h and results in 100% mortality after 9 h of exposure (6). In the same study it

was found that TR and GR activities of TGR in worm homogenates were nearly 100% inhibited after 1 h and that the GSH:GSSG ratio decreased from 18:1 in control worms to 2.6:1 (85% decrease) after 6 h of treatment. Larval, juvenile, and adult stages of the parasite are killed by 5 μM AF in 24 h, which acquires significance given that this concentration of the drug is well tolerated by mammalian cells. Indeed, in preliminary experiments, AF administered to infected mice at dosages well tolerated by the host killed 60% of adult schistosomes. This reduction of worm burden would lead to a significant decrease in the pathology and morbidity associated with schistosomiasis (6). Moreover, it has recently been

115

demonstrated that AF also inhibits the TGRs from the related parasites *Echinococcus granulosus* (14) and *Taenia crassiceps* (15).

Compared with other newly identified leads (11), AF has an important advantage as a schistosomicidal drug, because it has been in clinical use to cure rheumatoid arthritis for 25 years and thus presents a well known and quite safe toxicity profile (16, 17). Finding new uses for clinically established drugs represents a clever strategy of drug discovery, considering the drastic reduction of time and cost relative to developing novel drugs (18). These considerations are of extreme importance for neglected diseases, such as schistosomiasis, which are not of primary interest to the pharmaceutical industry.

AF has been demonstrated to be a nanomolar inhibitor of Sec-containing enzymes such as TR and TGR (6), whereas 1000-fold higher concentrations appear to be required to inhibit GR, which lacks the C-terminal Sec (19). These observations suggest that Sec is either the binding site of AF or is essential in displacing the gold from its ligands given that its nucleophilic power is greater than sulfur. Other gold(I) compounds are known to irreversibly inhibit human glutathione reductase by the formation of a covalent adduct between catalytic cysteines and the metal (Cys-gold-Cys); a similar mechanism for AF has been previously hypothesized but not proven. It was suggested that AF might lose both the thioglucose and the triethylphosphine ligands by sequential exchange reactions with cellular thiols, leading to final gold-protein thiol adducts similar to those produced with gold compounds in GR (20).

Using x-ray crystallography, we hereby demonstrate for the first time the formation of Cys-gold-Cys adducts in two different sites of the three-dimensional structure of wild type SmTGR incubated with AF. Unfortunately we cannot determine the exact position of the C terminus in any of the solved structures, and therefore we do not know whether it is bound to AF derivatives or gold. We have also determined the effect of AF on the activity of yeast GR (a protein lacking Sec) and on a Sec-lacking truncated form of SmTGR. Interestingly we found that the addition of benzeneselenol increases considerably the velocity of inactivation of GR by AF. Taken together, kinetic and structural data allow us to assign a catalytic role to the C-terminal Sec, suggesting a possible mechanism whereby AF inhibits TGRs and TRs.

EXPERIMENTAL PROCEDURES

Cloning, Expression, and Purification of SmTGR Forms—The truncated SmTGR lacking the last two amino acids, *i.e.* Sec[597] and Gly[598], and the Sec-containing form of SmTGR were prepared as described previously (6, 10).

Crystallization—9 μM wild type SmTGR, reduced with a saturating amount of NADPH (300 μM) was stirred overnight in 50 mM Tris, pH 7.4, 100 mM NaCl at 4 °C in presence of 100 μM auranofin. AF was kindly provided by Dr. Frank Shaw (Normal, IL). The mixture was then dialyzed (1:27000) against 20 mM Tris, pH 7.4, 100 mM NaCl and reconcentrated to 5 mg/ml before crystallization trials were set up. The protein solution was mixed with an equal amount of the reservoir solution containing 0.1 M Hepes at pH 7.0, 20% polyethylene glycol 3350, 0.2 M potassium iodide, and 5 mM GSH. Crystals grew in 3–4 weeks

TABLE 1

Summary of crystallographic data

	Wild type SmTGR
Data collection	
Space group	C2
Cell dimensions	
a, b, c (Å)	147.51, 102.16, 60.57
α, β, γ (°)	90.00, 114.15, 90.00
Resolution (Å)	40.0-2.55 (2.59-2.55)[a]
R_{merge}	0.12 (0.48)
$I/\sigma I$	14.7 (2.4)
Completeness (%)	99.7% (99.9%)
Redundancy	5.2 (5.2)
Refinement	
Resolution (Å)	40.0-2.55
No. reflections	25562
R_{work}/R_{free}	0.231/0.256
No. of atoms (1 subunit/au)	4745
Protein	4540
Ligand/ion	104
Water	101
B-factors (overall)	35.42
Root mean square deviations	
Bond lengths (Å)	0.006
Bond angles (°)	0.91
Ramachandran plot	
Most preferred	90.4%
Allowed	9.2%
Generously allowed	0.4%

[a] Highest resolution shell is shown in parentheses.

to $0.4 \times 0.2 \times 0.2$ mm^3 and were cryoprotected with the same reservoir solution plus 30% polyethylene glycol 200.

X-ray Data Collection—The data were collected at 100 K. The best data set has been collected as 1.0° oscillation frames using the MAR CCD detector on the BL14-1 Beamline at BESSY (Berlin, Germany) at a wavelength of 0.98 Å. Data analysis performed with HKL2000 (21) indicated that the crystals belongs to the C2 space group with the following unit cell dimensions: *a* = 147.51 Å; *b* = 102.16 Å; *c* = 60.57 Å; and β = 114.51°. The data were scaled and are 99.7% complete at 2.55 Å resolution, with an R_{merge} of 12% and a χ^2 of 1.2. The crystal contains 1 subunit/asymmetric unit, with a V_M of 3.2 Å^3 Da^{-1} and a solvent content of 61.3%.

Structure Refinement and Analysis—The structure was solved by molecular replacement using the program PHASER (22) and the structure of truncated SmTGR (Protein Data Bank code 2v6o) as the search model. Refinement of the atomic coordinates and displacement parameters was carried out by means of Refmac5 (23). Model building was performed using the program package COOT (24). The structure of the complex was refined to 2.55 Å resolution with an overall temperature factor of 35.4 Å^2 (for other data collection and refinement statistics, see Table 1). The configuration was verified by PROCHECK (25). The locations of gold atoms were defined using the anomalous Fourier maps. Atomic coordinates and structure factors have been deposited in the Protein Data Bank with the accession code 3H4K.

GR Activity Assay—Glutathione reductase from baker's yeast (Sigma-Aldrich) was washed four times at $3500 \times g$ with 50 mM Tris/HCl, 0.1 M NaCl, pH 7.4, using Amicon Ultra 15 centrifugal filter devices (Millipore, Cork, Ireland) with a molecular mass cut-off of 30 kDa to change buffer and remove trace amounts of dithiothreitol. GR activity was assayed as a NADPH-dependent reduction of GSSG (26). In all of the assays described

The Mechanism of Inhibition of TGR by Auranofin

below, 0.5-ml reaction mixtures contained 30 μl of the stock GR solution (0.5 μM, final concentration 30 nM) plus 200 μM NADPH and 500 μM GSSG.

To assess the effect of AF on GR, incubation mixtures were prepared containing 0.5 μM GR and 1, 4, 10, and 50 μM AF, all containing 100 μM NADPH in 50 mM Tris, pH 7.4, and 100 mM NaCl. The measurements were performed at 0, 15, 30, 60, 120, and 240 min after the aerobic incubation was started. The reaction was initiated by the addition of 500 μM GSSG and followed by the decrease in absorbance at 340 nm. Controls containing no AF were measured at each time point, and the activity was expressed as a percentage of each sample against the control.

SmTGR Inhibition Assay—To assess the effect of AF on truncated TGR, incubation mixtures were prepared containing 3.0 μM SmTGR (truncated form, lacking the last two amino acids) with and without 8 μM AF, eventually with 3 μM BzSe. All of the samples, under aerobic conditions, contained 100 μM NADPH in 50 mM Tris, pH 7.4, and 100 mM NaCl. Aliquots of 85 μl were tested for activity by the 5,5'-dithiobis-(2-nitrobenzoic acid) (DTNB) assay in a 0.5-ml cuvette. The measurements were performed at 0, 30, 60, 120, and 240 min after the incubation was started. The reaction was initiated by the addition of 1 mM DTNB and followed by the increase in absorbance at 412 nm. Controls containing no AF were measured at each time point, and the activity was expressed as a percentage of each sample against the control.

RESULTS

Structural Analysis—The structure of wild type SmTGR treated with AF was solved by molecular replacement. After the refinement processes and geometry optimization of the model, an anomalous difference Fourier map was calculated from 40 to 2.5 Å and contoured at 8 σ. Its superimposition on the difference density map $(F_o - F_c)$ contoured at the same σ and calculated on the refined SmTGR structure without the metal (10), clearly shows the position of the gold atoms in the asymmetric unit. AF itself was never detected in our structures, but three gold-binding sites were identified in each subunit, as shown in Fig. 1A. As already reported for the truncated form of the enzyme (10), the C terminus was not visible in the electron density maps.

Site 1—The metal is bound between the catalytic cysteines (Cys^{154}–Cys^{159}) over the FAD-binding site. The geometry of the Cys-gold-Cys array is linear, and the distance between the sulfurs and the gold is 2.3 Å. The metal occupancy is ~50%. Cys^{154} is found in double conformation (Fig. 1B); in the gold-containing site, this residue coordinated to the metal points toward Cys^{159}, whereas in the gold-free site Cys^{154} is not involved in a disulfide bridge with Cys^{159} and points away from the FAD and Cys^{159}. At this resolution, the orientation of Cys^{159} is almost independent of the presence of gold.

Site 2—Also in this case, the gold was found between two cysteines, namely Cys^{520} and Cys^{574}, with an occupancy of ~50%. As in site 1, the geometry is linear, but the sulfur-gold distances are longer than the canonical values (Fig. 1, C and D); this might indicate a fluxional behavior of the gold between the two cysteines (27). Thus the geometry calculated from the electron density maps should be taken as an average.
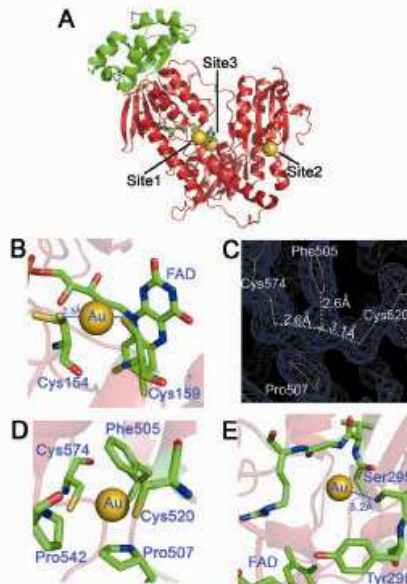

FIGURE 1. **The three gold-binding sites of wild type SmTGR.** A, the three-dimensional model of one subunit is shown with the three gold-binding sites. Site 1 shows the gold in between Cys^{154} and Cys^{159}; site 2 shows the gold in between Cys^{520} and Cys^{574}; site 3 shows the gold in the putative NADPH-binding pocket. The glutaredoxin domain of TGR is shown in green, whereas the thioredoxin domain is shown in red. The bound flavin is also highlighted. B, site 1. The linear geometry of the Cys^{154}-gold-Cys^{159} adduct is shown. The occupancy of the gold atom is about 50%. Both distances of the sulfur-gold bond are 2.3 Å, as expected for this type of coordination moiety. C, site 2. The electron density map $(2F_o - F_c)$ contoured at 1 σ shows the possible charge transfer complex between the gold and Phe^{505}. D, site 2. The gold atom between Cys^{574} and Cys^{520} is shown together with the other residues that surround the metal, i.e. Phe^{505}, Pro^{507}, and Pro^{542}. E, site 3. Gold in the putative NADPH-binding site of SmTGR. Tyr^{296} is known to swing upon NADPH binding in thiol reductase enzymes (30). Ser^{295} is the residue closest to the gold (Ser^{295}(OG)-gold: 3.2 Å). Other van der Waals' contacts are with the main chain atoms of the polypeptide (Ala^{100}, Val^{331}, Gly^{332}, and Arg^{395}).

The gold atom in site 2 is surrounded by hydrophobic residues, i.e. Phe^{505}, Pro^{507}, and Pro^{542} (Fig. 1, C and D). The aromatic ring of Phe^{505} is 2.6 Å away from the gold atom (Fig. 1D), this distance being smaller than the sum of the van der Waals' radii of the sp^2 carbon and the metal. It is known from gas phase studies that benzene and gold(I) interact to form a charge transfer complex (28). The stability of the complex was calculated to be 70 kcal/mol, in the range of a covalent bond (29). Therefore, the position of the gold atom between Cys^{520} and Cys^{574} might be also stabilized by a charge transfer complex that forces the metal into a peculiar position.

Because no functional role has been assigned as yet to the couple Cys^{520}–Cys^{574}, we cannot infer the role of site 2 in the
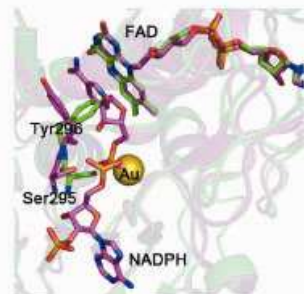
117

FIGURE 2. **The SmTGR crystal structure in complex with gold ions (in green) is superimposed to the mouse TR with NADPH bound (in *magenta*; Protein Data Bank code 1zdl (30)).** The root mean square deviation is 0.82 Å over the 462 aligned residues. The residues surrounding NADPH in mouse TR are conserved in SmTGR (sequence alignment not shown). The structural comparison shows the change in conformation of the loop 293–296 and in particular of Tyr[296] and Ser[295], highlighted for the two enzymes as balls and sticks (the other amino acid side chains are omitted for clarity). The OG atom of Ser[295] is the closest contact with the gold ion in the SmTGR crystal structure (see "Results" and Fig. 1). In the mouse TR structure, Ser[295] shifts in position to make room for the bound NADPH; the clash between the metal in site 3 and the phosphate of the cofactor in SmTGR is self-evident.

inhibition of TGR by AF, but we point out that: (i) site 2 is invariant in all the TGRs and mammalian TRs that have a Sec at the penultimate position, whereas it is absent in GRs or in TRs lacking the penultimate Sec (sequence alignment not shown); and (ii) site 2 of one subunit is in close proximity to the C terminus of the same subunit and to the FAD-binding site of the other subunit ($Cys^{574}/SG-Cys^{154}/SG = 14.5$ Å).

Site 3—The third gold atom is located in a pocket on the side of the FAD opposite to $Cys^{154}-Cys^{159}$, with an occupancy of ~40% (Fig. 1E). The cavity is surrounded by the amino acid side chains of Ser^{295}, Tyr^{296}, and Val^{297} and the main chains of Ala^{390}, Val^{391}, Gly^{392}, and Arg^{393}. No atoms have the correct distance to form coordination bonds, the closest atom being the oxygen of the Ser^{296} at 3.2 Å; however, all of the above residues can be engaged in van der Waals' contacts. Superposition of the structures of SmTGR and mouse TR bound to NADPH (Protein Data Bank code 1zdl) (30) suggests that site 3 may correspond to the NADPH-binding site (Fig. 2), and thus it might be relevant to the mechanism of inactivation by AF.

Reaction of a Sec-lacking, Truncated SmTGR Variant with AF—Because AF behaves as a gold carrier and the final complex contains the bare metal bound either to Cys residues or to a hydrophobic pocket (site 3), we decided to test whether Sec is indeed essential for inactivation of TGR by AF, as is usually thought. X-ray diffraction maps were thus collected for a Sec-lacking artificial variant of the enzyme, namely the truncated SmTGR, a construct lacking the last two C-terminal residues, Sec^{597} and Gly^{598} (10). This variant, when crystallized in the presence of a slight molar excess of AF (2–3-fold) plus a catalytic source of selenium (see below), incorporates gold at sites 1 and 3 (results not shown); we are at present unable to explain why no gold was observed in site 2. The time courses of inacti-

The Mechanism of Inhibition of TGR by Auranofin

vation of truncated and wild type SmTGR by AF are reported in Fig. 3C. The Sec-lacking variant, which is 15-fold less active than the wild type in the DTNB assay (10), is inhibited by AF 200-fold more slowly than the wild type enzyme (which is inactivated with a rate constant of 0.21/min).

GR Inactivation Assays—The observation that the gold-binding sites identified by x-ray crystallography do not involve the penultimate Sec challenges the currently accepted mechanism of inhibition of TGR/TR by AF (14, 19). To investigate this point, we carried out functional experiments using GR as a model enzyme. GR has three crucial features that make it suitable for this purpose: (i) it lacks the Sec residue and the C-terminal tail, thus serving as a negative control for the role of selenium; (ii) it has only one of the gold-binding sites identified in SmTGR, i.e. that homologous to site 1 (20) (the Cys couple of site 2 of TGRs and TRs is lacking, and most of the side chains that surround the gold in site 3 are not conserved, e.g. Ser^{295} is replaced by a Gly in the baker's yeast GR; sequence alignment not shown); and (iii) it has much higher catalytic activity than truncated SmTGR, thus simplifying the assays. A spectrophotometric enzymatic assay was carried out using 0.5 μM GR incubated with 1, 4, 10, and 50 μM AF over a period of 4 h; activity was followed as the NADPH-dependent (200 μM) reduction of GSSG (500 μM), monitoring the reaction at 340 nm (26). When GR was incubated with AF in the absence of NADPH, no inhibition was detected, a finding consistent with the entrapment of gold between cysteines (as for site 1, a reaction dependent on the enzyme being reduced). The concentrations of GR, NADPH, and AF in the assay mixture were chosen following Gromer *et al.* (19). The results of these experiments (Fig. 3A) show that AF inactivates GR at every concentration from 1 to 50 μM, the time course being in all cases complex and the rate slowing down progressively. The experiment shows that AF is capable of inhibiting an enzyme that lacks Sec, as expected on the basis of the structural considerations made on SmTGR (see above).

Given the complex time course and the very slow inactivation rate, quantitative analysis is not easy, and thus we resorted to estimate the initial rate of inactivation of GR by AF, at the different concentrations. Initial first order rate constants plotted as a function of AF concentration, reported in Fig. 4, shows that inactivation rate is AF concentration-dependent but tends to a plateau. Nevertheless we have direct evidence that the inactivation is faster at higher AF concentrations and that the reaction is essentially irreversible (because activity is not recovered even after long dialysis). This is consistent with the high stability of the sulfur-gold-sulfur complex observed in site 1 of SmTGR and presumably formed also in the homologous site of GR.

The Role of Selenium—The limited level of inhibition of GR by AF reported in the literature (19) is most probably due to the insufficient time allowed for complex formation (i.e. ≤20 min); the more effective inhibition seen with TR/TGR may be due to the faster reactivity of Sec-containing reductases rather than to higher affinity for AF or gold. To test this hypothesis, GR was incubated with AF in the presence of an external source of selenium, BzSe. Because BzSe is unstable, being easily oxidized to diphenyl diselenide, it was reduced with NaBH$_4$ before use;
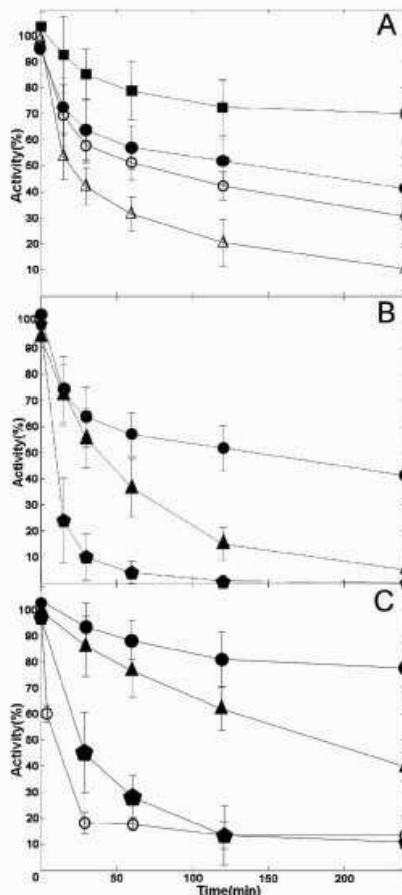
The Mechanism of Inhibition of TGR by Auranofin

FIGURE 4. **Rate constant of inactivation (min^{-1}) of yeast GR (0.5 μM) as a function of AF concentration (1, 4, 10, and 50 μM), as derived from linearization of the first points of the time courses reported for Fig. 3A.**

consequently, the concentrations reported in our experiments are probably overestimated, the actual concentration of the reduced form probably falling under aerobic conditions. The assay was performed on aliquots of an incubation mixture containing 0.5 μM GR, 4 μM AF, and 2 μM BzSe. Parallel control experiments (not shown) demonstrated that in the absence of AF, BzSe is not an inhibitor of GR, at least in the low micromolar concentration range. Moreover, a third condition was tested, where AF and BzSe were preincubated at 25 °C for 2 h before the addition of the enzyme. The results in Fig. 3B show that the kinetics of inhibition by AF is significantly affected by the addition 2 μM BzSe to the assay mixtures, the onset of inactivaion being clearly accelerated. GR approaches 0% activity within 4 h, whereas the addition of 4 μM AF alone yields only 50% inhibition over the same time interval. Fig. 3B also shows that incubating AF and BzSe together before addition to the assay mixtures increases substantially the rate of the reaction. These experiments confirm that although selenium is not absolutely required for inactivation of the enzyme by AF, it has a significant effect on the rate of onset of inactivation.

The effect of the external source of selenium was also tested for the truncated SmTGR variant that lacks the last two amino acids (Sec-Gly). Also in this case the onset of enzyme inactivation is accelerated in the presence of BzSe (Fig. 3C).

DISCUSSION

Structural Basis of the Inhibition of Thiol-dependent Reductases by Gold—Despite the extensive use of AF as an antiarthritic drug, the rationale for its mechanism of action in relation with its chemistry is not yet established. In general, gold-containing compounds are thiol/selenol reactive species; indeed AF and other gold compounds are strong inhibitors of mammalian TR and GR.

Our data indicate that the actual inhibitor is gold(I) rather than the whole AF molecule. The phosphine and thioglucose ligands cannot be seen in any of our electron density maps, confirming that AF is actually a pro-drug whose function is to carry and deliver gold to its final target(s) with the metal bound in between Cys couples of the enzyme.

As to the geometry and the presumable relative affinities of the gold-binding sites observed in our maps, we note that in site

FIGURE 3. *A,* baker's yeast GR is inactivated by AF: time courses obtained at concentrations of 1 μM (squares), 4 μM (closed circles), 10 μM (open circles), and 50 μM (open triangles). *B,* effect of BzSe on baker's yeast GR inactivation by AF. Time course in the presence of 4 μM AF (circles) or 4 μM AF plus 2 μM BzSe (triangles). GR exposed to a mixture in which AF 4 μM and BzSe 2 μM were preincubated for 2 h before the assay (pentagons). *C,* inactivation by AF of truncated SmTGR and wild type SmTGR, and the effect of BzSe. Time courses of truncated SmTGR in the presence of 8 μM AF (circles) or 8 μM AF plus 3 μM BzSe (triangles). Truncated SmTGR exposed to a mixture in which AF 8 μM and BzSe 3 μM were preincubated for 2 h before the assay (pentagons); time course of wild type SmTGR 20 nM incubated with 50 nM AF (open circles).
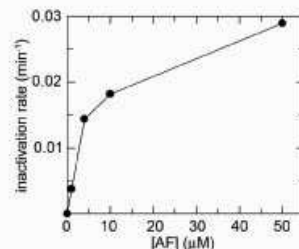
119

1 the gold atom is bound between the catalytic cysteines Cys^{154}–Cys^{159} in a linear two-coordination geometry, typical of the gold(I)-sulfur complexes (Fig. 1). Site 2 also shows the gold bound with an almost linear geometry between two cysteines, Cys^{520}–Cys^{574}, close to the C terminus of the same subunit and the FAD-binding site of the other subunit (Fig. 1); a charge transfer complex with Phe^{505} is probably also involved. Because the functional role of this site is not clear, the consequences of gold binding to Cys^{520}–Cys^{574} are at present uncertain. Site 3 is different from the other two because it contains no Cys, the metal being located in a cavity with no atoms at the correct distance to form coordination bonds (Fig. 1); however, it probably overlaps with the NADPH-binding site (Fig. 2).

Our results suggest a possible mechanism of inhibition of thiol-dependent reductases by AF, namely the transfer of gold(I) to one or more redox-active Cys (or Sec-Cys) couples of the enzyme (Scheme 1 and below). Our proposal is consistent with what is known about the electron flow in TR and GR (29, 30); the FAD cofactor is reduced by NADPH and donates its electrons to the first Cys couple (Cys^{154}–Cys^{159} in SmTGR). Reduction of GSSG in GR is presumed to occur at this site. In TRs and TGRs the path of electrons is more complex, because they are transferred from the first Cys couple to the C-terminal Cys^{596}–Sec^{597} couple and from here to thioredoxin, or, in the case of TGR, to the additional Grx domain. TRs and TGRs possess an additional conserved Cys couple (Cys^{520}–Cys^{574} in SmTGR), whose functional role is unknown.

We observe gold binding to two of these redox sites (sites 1 and 2), plus to the putative NADPH-binding site (site 3), and a further site may be present at the C terminus (Cys^{596}–Sec^{597}) that is disordered in our structures. Because binding to any of these may in principle be sufficient to inhibit the enzyme, one may ask which is the most relevant binding site *in vivo*. We assume that gold is redistributed at equilibrium among the three redox couples of SmTGR (Scheme 1) and that in the presence of enough AF all the three redox couples would be fully occupied, provided that enough time is allowed and that the enzyme is kept reduced. Based on what is known about TRs and TGRs (31), we also assume that any derivative of SmTGR bearing gold at the C-terminal binding site would be incapable of reducing thioredoxin or the glutaredoxin domain, whereas any species bearing gold at site 1 would be inactive toward any substrate, including the artificial DTNB. Site 2 participates in this exchange of gold, but its functional role is unclear, whereas site 3 is probably relevant to the inhibition of SmTGR (see above), but we cannot see how it could participate to the gold exchange with the other sites.

Our hypothesis is consistent with data by other researchers; *e.g.* irreversible inhibition of human GR by gold (released by GoPi) has been shown by x-ray crystallography to be due to the formation of a Cys-gold-Cys adduct with the Cys couple lying over the FAD (Cys^{58} and Cys^{63}, homologous to Cys^{154}–Cys^{159} in SmTGR) (20, 32). Moreover, the clinically used plasma levels of AF are in the order of 20 μM (19); these values are similar to our reaction conditions that require 10 μM SmTGR and 100 μM AF (*i.e.* a stoichiometric excess of only 2–3-fold, assuming four binding sites/enzyme subunit); thus significant occupancy of all

the binding sites of SmTGR may be expected if AF therapy of schistosomiasis were to become a standard practice.

Affinity of the Sulfur-Gold-Sulfur Complex—The gold-enzyme complex has very high affinity, because inhibition is insensitive to both dilution in the final assay mixture and extensive dialysis. An adduct analogous to that observed for site 1 of SmTGR has been found in human GR treated with the gold compound GoPi (20), and also in this case the inhibition was demonstrated to be irreversible. What is the affinity of GR or TGR for gold? Our experiments demonstrate that complete inhibition is obtained using micromolar concentrations of AF, provided that enough time is allowed for the reaction to go to completion; in our hands, complete inhibition of GR and truncated SmTGR is only achieved when BzSe is added to accelerate the reaction. Thus our best estimate suggests $IC_{50} < 10^{-7}$ M, consistent with our previous estimate of $IC_{50} \sim 10^{-8}$ M for wild type SmTGR (6) and much lower than the concentrations needed to kill the worms "*in vitro*" (10 μM).

This estimate must be taken with caution, because in such a complex reaction as that depicted in Scheme 1, the affinity of the enzyme for its inhibitor (the gold(I) ion) must be considered from at least two different view points, *i.e.* the true thermodynamic reversibility and the (possible) release of free gold. If the mechanism of inhibition is transfer of gold from AF to a Cys couple, as revealed by x-ray crystallography, true thermodynamic reversibility would imply not only the dissociation of the metal from the enzyme but simultaneous resynthesis of AF from gold, phosphine, and thioglucose. Resynthesis of AF, besides being unlikely, has a paradoxical consequence: given the stoichiometry of the reaction (TGR-gold + ATG + P(Et)$_3$ ↔ TGR + AF, where ATG stands for acetoxy-thioglucose, and P(Et)$_3$ stands for triethylphosphine), dilution is expected to increase inhibition, rather than vice versa. Moreover, free triethyl-phosphine in solution is prone to oxidation; thus its concentration decreases with time (16) and makes it impossible to accurately determine a precise value of K_i. For all practical purposes, the true IC_{50} of AF must be indistinguishable from zero, and enzyme activity may probably be restored only by the addition of compounds capable of chelating gold with affinity higher than Cys couples (*e.g.* 2,3 dimercapto-propanol; see Ref. 19).

If, on the other hand, one considers the affinity of gold for its binding sites in GR, TR, or TGR (*i.e.* the tendency of the complex to dissociate releasing the free metal ion, rather than AF), we may only recall that the energy of the gold-sulfur bond has been estimated at ~ 55 kcal/mol (33).

Given such a high affinity of gold for sulfur pairs, the incomplete (50%) occupancy of sites 1 and 2 in our structures is puzzling, and we can offer two, nonmutually alternative hypotheses, whose testing requires further experimental work. Incomplete occupancy of sites 1 and 2 might be due to the slow redistribution of gold between its protein-binding sites (see Scheme 1). Moreover, negative kinetic cooperativity between the two subunits of the dimer or between the two sites of the same protomer cannot be excluded; binding of gold to one site could slow down the reaction at the other.

Because the same Cys couple exists in TR, TGR, and GR and because binding of gold to this couple is essentially irreversible,

The Mechanism of Inhibition of TGR by Auranofin

the 1000-fold lower apparent affinity of AF for GRs reported by Gromer *et al.* (19) seemed puzzling. Our data solve this issue by demonstrating that the incubation of GR with AF in these experiments (20 min) was too short to allow the formation of the GR-gold complex. Indeed if we analyze the time courses of Fig. 3A up to 15 min., we reproduce similar results of Gromer *et al.* (19).

The time courses of inactivation indicate a complex reaction mechanism whose order decreases from 2 at low concentration of AF to lower values. This behavior (Fig. 4), which is typical of reactions in which an intermediate populated in the course of a bimolecular reaction decays monomolecularly to more stable chemical species, is not inconsistent with the first two reactions of Scheme 1 (*i.e.* the bimolecular formation of the Cys- or Sec-gold-Pt(Et)3 complex, followed by the irreversible monomolecular entrapment of the metal in the Cys-gold-Cys complex).

Selectivity of AF for TR/TGR: the Role of Selenium—Two strongly correlated issues remain to be discussed, namely the kinetics of gold incorporation and the possible reason for the strong preference of AF for TRs and TGRs over GRs. Our data show that Sec is not the only binding site of the drug, and indeed we demonstrate that (i) GR and Sec-free SmTGR are significantly inhibited by the addition of AF stoichiometric with Cys couples, provided enough time is allowed for the slow transfer of gold to the protein, and (ii) external selenium (in the form of benzeneselenol) plays a significant and in some way surprising catalytic role and facilitates the transfer of gold from AF to the redox active Cys couples, both in GR and in truncated SmTGR.

If we accept that TRs/TGRs and GRs all have very high affinity for gold, our best hypothesis to explain the selectivity of AF for the former is that TRs and TGRs react faster. Indeed we demonstrated in this paper that yeast GR reacts slowly with AF and that the incubation times used in previous experiments (*e.g.* 19) were too short to allow extensive inactivation, resulting in an overestimate of the K_i (in the micromolar range). Our data demonstrate that (i) wild type SmTGR is inactivated by AF faster than both its truncated (*i.e.* Sec lacking) variant and yeast GR and (ii) an external source of selenium greatly speeds up the reactivity of Sec-free thiol reductases. These observations point to a catalytic role of Sec that would promote the displacement of the first gold ligand of AF, probably thioglucose (in analogy with the reaction of AF with the human serum albumin) (16) (Scheme 1). The intermediate adduct Sec-gold-triethylphosphine thus formed would transfer the metal to its final protein ligands. We hypothesize that BzSe is able to accelerate the rate of inhibition of GR or Sec-free TGR with AF because it displaces thioglucose and helps transfer of the metal to Cys residues. This ability would be due to the fact that BzSe shares some properties of Sec, *e.g.* it has a similar pK_a (4.6 for BzSe *versus* 5.2 for Sec (5, 34)) and has high nucleophilic character when ionized.

There are two possible and mutually nonexclusive reasons why Sec reacts with and activates AF faster than the Cys residues, *i.e.* (i) a more reactive electronic structure and (ii) a better exposure to the solvent of the C terminus that by-passes the slow diffusion to site 1 of the bulky molecule of AF. The first point is in apparent contrast with the fact that selenium has a greater affinity than sulfur for gold (16). Nevertheless, studies

have shown that derivatives of AF in which the thioglucose moiety has been substituted by a selenol glucose or a cyanide ion (both high affinity ligands for gold) are more apt to loose the $P(Et)_3$ ligand when they react with human albumin (16, 35). The labilization of phosphine in the albumin sulfur-gold-PEt3 adduct is attributed to a strong trans-effect of the albumin thiolate of Cys^{34} (36). In TGRs or TRs, this first labilization of the gold-P(Et)3 bond is probably followed by the formation of the Sec-gold-Cys species (see Scheme 1). In turn, this adduct could be easily transformed into the final Cys-gold-Cys given that Sec or in general selenium compounds (*e.g.* BzSe) are better leaving groups than sulfur (Ref. 37 and Scheme 1). The second hypothesis, which considers a steric effect, is consistent with the crystal structures of TRs and SmTGR in which it is clear that the C terminus is more exposed to the solvent than the buried FAD catalytic site (10, 30).

Consistent with the literature and based on our own results, the mechanism of action of AF is envisaged as a series of ligand displacement reactions (Scheme 1). Indeed it is known that when administered *in vivo*, AF partially releases the gold atom to protein thiols and to free thiols; through ligand displacement reactions, gold is then transferred from serum albumin (16) to other proteins or thiols in the body, until it reaches a final acceptor that traps the gold in a stable linear two-coordination geometry (20, 38). The peculiarity of TRs and TGRs would be their own ability to carry out the undressing and stable coordination of gold without the help of other proteins or free thiols, because of the C-terminal Sec. This reaction intermediate would further transfer the gold atom to its final acceptor within the same polypeptide chain (Scheme 1). This mechanism is similar to that proposed for mercuric ion reductase, a homodimeric enzyme belonging to the same family as TGR (39).

REFERENCES

1. Hotez, P. J., Molyneux, D. H., Fenwick, A., Kumaresan, J., Sachs, S. E., Sachs, J. D., and Savioli, L. (2007) *N. Engl. J. Med.* **357**, 1018–1027
2. Doenhoff, M. J., Kusel, J. R., Coles, G. C., and Cioli, D. (2002) *Trans. R. Soc. Trop. Med. Hyg.* **96**, 465–469
3. Angelucci, F., Basso, A., Bellelli, A., Brunori, M., Pica-Mattoccia, L., and Valle, C. (2007) *Parasitology* **134**, 1215–1221
4. Cioli, D., Valle, C., Angelucci, F., and Miele, A. E. (2008) *Trends Parasitol.* **24**, 379–382
5. Salinas, G., Selkirk, M. E., Chalar, C., Maizels, R. M., and Fernández, C. (2004) *Trends Parasitol.* **20**, 340–346
6. Kuntz, A. N., Davioud-Charvet, E., Sayed, A. A., Califf, L. L., Dessolin, J., Arnér, E. S., and Williams, D. L. (2007) *PLoS Med.* **4**, e206
7. Sun, Q. A., Kirnarsky, L., Sherman, S., and Gladyshev, V. N. (2001) *Proc. Natl. Acad. Sci. U.S.A.* **98**, 3673–3678
8. Alger, H. M., and Williams, D. L. (2002) *Mol. Biochem. Parasitol.* **121**, 129–139
9. Sharma, M., Khanna, S., Bulusu, G., and Mitra, A. (2009) *J. Mol. Graph. Model* **27**, 665–675

121

The Mechanism of Inhibition of TGR by Auranofin

10. Angelucci, F., Miele, A. E., Boumis, G., Dimastrogiovanni, D., Brunori, M., and Bellelli, A. (2008) *Proteins* **72**, 936–945
11. Sayed, A. A., Simeonov, A., Thomas, C. J., Inglese, J., Austin, C. P., and Williams, D. L. (2008) *Nat. Med.* **14**, 407–412
12. Loukas, A., and Bethony, J. M. (2008) *Nat. Med.* **14**, 365–367
13. Simeonov, A., Jadhav, A., Sayed, A. A., Wang, Y., Nelson, M. E., Thomas, C. J., Inglese, J., Williams, D. L., and Austin, C. P. (2008) *PLoS Negl. Trop. Dis.* **2**, e127
14. Bonilla, M., Denicola, A., Novoselov, S. V., Turanov, A. A., Protasio, A., Izmendi, D., Gladyshev, V. N., and Salinas, G. (2008) *J. Biol. Chem.* **283**, 17898–17902
15. Rendón, J. L., del Arenal, I. P., Guevara-Flores, A., Uribe, A., Plancarte, A., and Mendoza-Hernández, G. (2004) *Mol. Biochem. Parasitol.* **133**, 61–69
16. Shaw, C. F., 3rd (1999). *Chem. Rev.* **99**, 2589–2600
17. Becker, K., Gromer, S., Schirmer, R. H., and Müller, S. (2000) *Eur. J. Biochem.* **267**, 6118–6125
18. Chong, C. R., and Sullivan, D. J., Jr. (2007) *Nature* **448**, 645–646
19. Gromer, S., Arscott, L. D., Williams, C. H., Jr., Schirmer, R. H., and Becker, K. (1998). *J. Biol. Chem.* **273**, 20096–20101
20. Urig, S., Fritz-Wolf, K., Réau, R., Herold-Mende, C., Tóth, K., Davioud-Charvet, E., and Becker, K. (2006). *Angew. Chem. Int. Ed.* **45**, 1881–1886
21. Otwinowski, Z., and Minor, W. (1997) *Methods Enzymol.* **276**, 307–326
22. Read, R. J. (2001) *Acta Crystallogr. Sect. D Biol. Crystallogr.* **57**, 1373–1382
23. Murshudov, G. N., Vagin, A. A., Lebedev, A., Wilson, K. S., and Dodson, E. J. (1999). *Acta Crystallogr. Sect. D Biol. Crystallogr.* **55**, 247–255
24. Emsley, P., and Cowtan, K. (2004) *Acta Crystallogr. Sect. D Biol. Crystallogr.* **60**, 2126–2132
25. Laskowski, R. A., MacArthur, M. W., Moss, D. S., and Thornton, J. (1993)

26. Carlberg, I., and Mannervik, B. (1985) *Methods Enzymol.* **113**, 484–490
27. Mézailles, N., Avarvari, N., Maigrot, N., Ricard, L., Mathey, F., Le Floch, P., Cataldo, L., Berclaz, T., and Geoffroy, M. (1999). *Angew. Chem. Int. Ed. Engl.* **38**, 3194–3197
28. Ho, Y.-P., and Dunbar, R. C. (1999) *Int. J. Mass Spectrosc.* **182–183**, 175–184
29. Schröder, D., Hrušák, J., Hertwig, R. H., Wolfram, K., Schwerdtfeger, P., and Schwarz, H. (1995) *Organometallics* **14**, 312–316
30. Biterova, E. I., Turanov, A. A., Gladyshev, V. N., and Barycki, J. J. (2005) *Proc. Natl. Acad. Sci. U.S.A.* **102**, 15018–15023
31. Arnér, E. S. (2009) *Biochim. Biophys. Acta* **1790**, 495–526
32. Deponte, M., Urig, S., Arscott, L. D., Fritz-Wolf, K. R. R., Herold-Mende, C., Koncarevic, S., Meyer, M., Davioud-Charvet, E., Ballou, D. P., Williams, C. H., Jr., and Becker, K. (2005). *J. Biol. Chem.* **280**, 20628–20637
33. Schröder, D., Schwarz, H., Hrušák, J., and Pyykkö, P. (1998) *Inorg. Chem.* **37**, 624–632
34. Filipovska, A., Kelso, G. F., Brown, S. E., Beer, S. M., Smith, R. A., and Murphy, M. P. (2005) *J. Biol. Chem.* **280**, 24113–24126
35. Isab, A. A., Hormann, A. L., Coffer, M. T., and Shaw, C. F. (1988) *J. Am. Chem. Soc.* **110**, 3278–3284
36. Coffer, M. T., Shaw, C. F., 3rd, Hormann, A. L., Mirabelli, C. K., and Crooke, S. T. (1987) *J. Inorg. Biochem.* **30**, 177–187
37. Lothrop, A. P., Ruggles, E. L., and Hondal, R. J. (2009) *Biochemistry* **48**, 6213–6223
38. Viry, E., Battaglia, E., Deborde, V., Müller, T., Réau, R., Davioud-Charvet, E., and Bagrel, D. (2008) *ChemMedChem* **3**, 1667–1670
39. Engst, S., and Müller, S. M. (1999) *Biochemistry* **38**, 3519–3529

J. Appl. Crystallogr. **26**, 283–291